REDUCING IRON ON A KNIFE'S EDGE – GENOMIC AND MECHANISTIC STUDIES OF (HYPER)THERMOPHILIC DISSIMILATORY IRON-REDUCING BACTERIA AND ARCHAEA

By

MICHAEL P. MANZELLA

A DISSERTATION

Submitted to
Michigan State University
in partial fulfillment of the requirements
for the degree of

Microbiology and Molecular Genetics – Doctor of Philosophy

2015

PUBLIC ABSTRACT

REDUCING IRON ON A KNIFE'S EDGE – GENOMIC AND MECHANISTIC STUDIES OF (HYPER)THERMOPHILIC DISSIMILATORY IRON-REDUCING BACTERIA AND ARCHAEA

By

MICHAEL P. MANZELLA

The majority of life on our planet is thanks to the sun. From trees to microscopic algae, all of these rely on sunlight to make energy. These organisms are termed "primary producers" because they are at the base of the food chain. As you proceed up the food chain life does not rely directly on the sun and instead feeds off of these primary producers. Yet, sites exist on our planet where life exists without any influence from the sun. Deep-sea environments, called hydrothermal vents, are one such example. At these sites, Earth's hot inner core bubbles up to the sea floor and supports a community of microbes and larger organisms, some of which can grow at extremely high temperatures. These communities are often found thousands of meters below the ocean surface, and they too rely on primary producers. These primary producers do not rely on the sun and instead get food and energy from the fluids that come out of the vents. The microorganisms at these sites are thought to be ancient, and thus studying them can help us understand how life originated on our planet. I chose one microorganism from each of the other major branches on our "tree of life" of which we, being from the *Eukarya*, do not belong – the *Bacteria* and the *Archaea*. I sequenced their DNA and searched for tools they use to survive at these high temperature sites. I was particularly interested in finding tools that they use to 'breathe' insoluble iron oxides, rust. This rust is a challenge to breathe, as it cannot enter their cells like oxygen can. Fortunately, I found a number of tools which could allow them to use iron for growth. Most interestingly among the tools I found were microscopic hairs on the outside of the cell that work like metal wires and allow the cells to pass electricity to the iron, thereby breathing it at a distance. This is the first time these 'nanowires' have been found in organisms growing at high temperatures and within the *Archaea*.

ABSTRACT

REDUCING IRON ON A KNIFE'S EDGE – GENOMIC AND MECHANISTIC STUDIES OF (HYPER)THERMOPHILIC DISSIMILATORY IRON-REDUCING BACTERIA AND ARCHAEA

By

MICHAEL P. MANZELLA

Some members of the *Bacteria* and the *Archaea* have the rare ability to transfer electrons beyond the surface of their cells. This extracellular electron transfer permits the reduction of otherwise inaccessible electron acceptors such as insoluble Fe(III) oxides. The mechanisms that enable this ability have direct implications for geochemical cycles today and for life on early Earth. The physical settings present on early Earth, hot and influenced primarily by hydrothermal activity, can be found in rare sites on modern Earth. These sites most often surround deep-sea hydrothermal vents. Organisms present at these sites thrive, in most cases, absent of the sun's influence. Instead of primary production from photosynthetic microorganisms, these communities rest on the shoulders of chemoautolithotrophic bacteria and archaea. Two of these organisms, the thermophilic bacterium *Geothermobacter ehrlichii* and the hyperthermophilic archaeon *Geoglobus ahangari* were selected to undergo genome and physiological characterization to determine how they interact with the abundant insoluble Fe(III) oxides found at hydrothermal vents. Both genomes were sequenced and, while only the genome of *G. ahangari* was complete, this permitted identification of critical components for iron respiration. In addition, mechanistic studies were performed on *G. ahangari* to elucidate a direct-contact mechanism of iron reduction. Finally, the extracellular filaments from these microorganisms were characterized and the more abundant filaments, in both organisms, were found to be conductive. These are the first examples of nanowires discovered outside of the mesophilic bacteria. In addition, the phylogenetic and geographic diversity between these isolates suggests that microbial nanowires are more widespread than previously thought.

This dissertation is dedicated to my family. My mother, Lynn, for always being there and making sure I was “alive and well.” My father, David, and his wife, Mary, for always asking “when are you going be done” and for being an inspiration (especially towards the end) to never give up. My sister, Jennifer, whose constant worrying (about everything) ensured that I never had, or wanted to. And last but not least, my brother, Kevin, for never ceasing to be a wise-[guy] and making sure I never took myself too seriously.

Dad, I will miss you for the rest of my life. It isn’t fair that you were taken from this world so early. I’m glad you were still around to say you were proud of me finishing my Ph.D., it meant the world to me. I love you dad.

ACKOWLEDGEMENTS

I would like to first thank both Dr. Gemma Reguera and Dr. Kazem Kashefi for the advice and support I have received while at Michigan State University. I was taken on as your first “hybrid” graduate student and, while there were some growing pains on all of our parts, I have benefited a great deal from having not one, but two wonderful mentors. The flow of the project did not proceed as any of us imagined at the start, but in the end I believe we ended up exactly where it needed to. Thank you both, for everything you have done.

I gratefully acknowledge all of the resources at Michigan State University. The support I received from Dr. Tracy K. Teal was essential to my success with the genome work (Chapters 2 and 3) and it could not have been done without the support from the Research Technology Support Facility and the Hypercomputing Center at Michigan State University, the Deep Sequencing Core Facility at the University of Massachusetts Medical School, and the Genomics Resource lab at the University of Massachusetts-Amherst. I would also like to thank Dr. Alicia Withrow and Dr. Abigail Vanderberg at the Center for Advanced Microscopy at Michigan State for help with transmission and scanning electron microscopy, respectively. Dr. Sanela Lampa-Pastirk and Krista Cosert, from the Reguera lab, are also acknowledged for their assistance with the Atomic Force Microscopy work. I also thank Kelly Nevin for advice to make the entrapped Fe(III) oxides. My two undergraduate mentees, Michael Paxhia and Lucas Demey, are also acknowledged for their assistance with my work and for being the (often) willing subjects of my unconventional and experimental mentoring techniques. Finally, I would like to acknowledge Dr. Melissa McDaniels and the entire ‘Inside Teaching’ network for ensuring that I matured as both a researcher and as an instructor while at MSU. Teaching is my future, and I owe that to you.

This work was supported with funds from a Strategic Partnership Grant from the MSU Foundation, a continuation fellowship from the College of Natural Sciences, a GAANN fellowship by the Department of Education, a DuVall Award, and an award from the Rudolph Hugh

fellowship. The Microbiology and Molecular Genetics department and the College of Natural Science has taken great care of me since my admission, and I hope I can make you all proud.

In addition, scientific and personal support from my friends and (past and present) lab-mates (particularly Rebecca Steidl) is acknowledged. While the support you all have given me with my science helped me get my work done, the social support you all provided helped to ensure I stayed happy and saw this through to the end. Lastly, I would like to thank Megan Goodall for providing that last “kick in the pants” to make sure I, eventually, finished.

I wouldn’t have been able to do this without you all. Thank you.

TABLE OF CONTENTS

LIST OF TABLES

LIST OF FIGURES

KEY TO ABBREVIATIONS

APS	adenosine 5’-phosphosulfate
23G	23 gauge
AFM	atomic force microscopy
AQDS	anthraquinone-2,6-disulfonate
ATCC	American Type Culture Collection
BLAST	basic local alignment search tool
CDS	coding sequence
COG	clusters of orthologous group
CP-AFM	conductive probe - atomic force microscopy
DHAP	dihydroxyacetone phosphate
DNA	deoxyribonucleic acid
DSMZ	Deutsche Sammlung von Mikroorganismen und Zellkulturen
EB	elution buffer
EC	enzyme commission
EDTA	ethylenediaminetetraacetic acid
EET	extracellular electron transfer
EPS	extracellular polysaccharide
Fe-S	iron-sulfur
GAPOR	glyceraldehyde-3-phosphate:ferredoxin oxidoreductase
GDH	glutamate dehydrogenase
gDNA	genomic deoxyribonucleic acid
GS-GOGAT	glutamine synthetase-glutamate synthase
Gya	gigayears ago

Gyr	gigayears
HOPG	highly ordered pyrolytic graphite
HPLC	high performance liquid chromatography
ICP-AES	inductively coupled plasma atomic emission spectroscopy
IEB	iron extraction buffer
IGS	Institute for Genome Sciences
IMG-ER	Integrated Microbial Genomes – Expert Review
KEGG	Kyoto Encyclopedia of Genes and Genomes
LSU	large subunit ribosomal RNA
MEC	microbial electrochemical cell
MM	marine medium
MMWB	modified marine wash buffer
Mya	million years ago
Myr	megayears
N_{50}	50% of the assembly is contained in contigs or scaffolds equal to or larger than this value
NR	non-redundant
NTA	nitrilotriacetic acid
ORB	origin recognition box
PacBio	Pacific Biosciences
PAPS	3'-phosphoadenylyl sulfate
PCR	polymerase chain reaction
PRPP	5-phosphoribosyl diphosphate
RAST	Rapid Annotations using Subsystem Technology
RNA	ribonucleic acid
rRNA	ribosomal ribonucleic acid

ROK	repressor protein, open reading frame, sugar kinase
RT	room temperature
RuMP	ribulose monophosphate
SDS	sodium dodecyl sulfate
SDS-PAGE	sodium dodecyl sulfate polyacrylamide gel electrophoresis
SSU	small subunit (16S) ribosomal ribonucleic acid
TCA	tricarboxylic acid
TE	Tris- ethylenediaminetetraacetic acid
ThT	thioflavin T
T_m	melting temperature
TMBZ	3,3',5,5'-tetramethylbenzidine
T_{opt}	optimum temperature

CHAPTER 1. HYDROTHERMAL VENTS AND MICROBIOLOGICAL ISOLATES AS MODEL SYSTEMS TO STUDY THE ORIGINS OF IRON RESPIRATION AND LIFE ON EARTH

1.1 *Life on early Earth*

The formation of planet Earth some 4.55 gigayears ago (Gya) marks the beginning of the Precambrian Supereon (4.55 – 0.54 Gya) (Figure 1.1). The early periods of Earth's geologic history can be further divided chronologically into the Hadean Eon (4.55 – 3.9 Gya), where the Earth was cooling and recovering from the formative process, the early (3.9 – 2.9 Gya) and late (2.9 – 2.5 Gya) Archaean Eon, and the Proterozoic Eon (2.5 – 0.54 Gya). Geological evidence (discussed later, and reviewed in (1)) supports the notion that life was already present on our planet 3.5 Gya, and likely emerged 3.8 Gya or earlier. Thus, even with the most restrictive estimates, life existed on our planet only 950 megayears (Myr) after its formation, and only 1,050 Myr after the formation of our solar system (2).

The study of life, and of its origins, on early Earth is challenging because organisms present at the time, including the ancestors of all extant organisms, seldom, if ever, left a fossil record (3–5). This contrasts with the relative abundance of micro- and macro-fossils identified that date back to the Proterozoic Eon (3). The lack of a fossil record in earlier periods can be attributed in part to the metamorphosis or tectonic submission of strata from that age, effectively erasing the majority of the fossil record (4, 6, 7). Based on evidence discussed later, researchers theorize that life originated during the early Archaean, although it would not emerge until after the development of the theorized pre-cellular systems (8, 9).

Some microscopic structures from the early Archaean do exist in the fossil record, mainly contained within macroscopic 'stromatolites' (4). 'Stromatolites' are fine-grained, thinly layered, mounded sedimentary structures which are presumed to have been created primarily by mat-building microbial communities of mucilage-secreting photoautotrophs (3, 4, 7). Some of the most

ancient fossil records in existence, including those within the 3.5 Gya Warrawoona Group (Western Australia) (10, 11) and the 3.5 – 3.3 Gya Swaziland Sequence (South Africa) (12) remain intact and some have undergone morphotypes or species identification (4). These morphotypes were compiled in 2006, by J. William Schopf, who tallied 40 microorganism-like morphotypes residing within 6 distinctive classes – all identified in Archaean-age deposits (reference (4) Table 2).

Yet, physical fossils are not the sole evidence of when life began on Earth. Living systems tend to utilize, and therefore enrich for, lighter isotopes of carbon. Thus, examination of the $^{12}C/^{13}C$ ratio in Archaean age (and more ancient) rocks compared to abiogenic carbon can lend further evidence to the origin of life in this age (7, 13). Archaean-age carbonate, for example, is isotopically similar to carbonates produced in modern systems, where light carbon isotopes are sequestered by living systems and heavier isotopes are left to precipitate out as carbonate (14).

While researchers may have a reasonably accurate guess regarding the time period at which life originated, a variety of theories exist for the origin of life on Earth and where it began. One theory that has received the most attention is nicknamed the “hyperthermophile Eden” hypothesis (14) in which life originated in a warm, if not hot, marine environment. The hypothesis that life originated in a warm or hot environment was first proposed by Darwin in 1871 in a letter to J. D. Hooker, and was again proposed in 1924 by R. B. Harvey (15) and speculation has continued to this day. Initial speculations were based on high temperature substitution of enzymatic hydrolysis (15), while current proponents of the hypothesis point to the environmental conditions at the time and the conditions required for the pre-biotic synthesis and use of RNA as a biomolecule.

The foremost theory of how ‘life’ could have started on early Earth is with abiotically produced nucleotide precursors self-assembling into ribonucleic acid (RNA) (9). While RNA and deoxyribonucleic acid (DNA) are both able to store genetic information, only RNA is able to catalyze chemical reactions, including the synthesis of additional RNA, the basis of self-replication

(8, 14). Thus, the utilization of a single molecule able to serve both a hereditary and a functional role is believed to have opened the proverbial flood-gates for life on Earth (9). Some critics argue that this “RNA world” could not have emerged and evolved in a hot environment because the stability of the nucleotide precursors and RNA itself is minimal at high temperatures (6). Yet pre-biotically synthesized oligonucleotides have been known to form under Archaean-age atmospheres, hydrothermal vent systems, and meteorites (6, 16). Furthermore, the early biomolecules were likely functional only immediately following their synthesis (6) or were contained within a low water activity environment to maintain functionality (7). Additionally, it is well known that reaction rates increase as temperatures increases (17). Thus, these RNA enzymes, or the proteinaceous enzymes contained within early microorganisms, could have been relatively inefficient when compared to modern enzymes while still maintaining reaction rates suitable to sustain life (6, 15).

Evidence in the form of the molecular record also supports the notion that the cellular ancestor of all extant organisms was thermophilic. Alignments and phylogenetic trees derived from the commonly used phylogenetic timepiece, the small subunit (16S) ribosomal RNA (18, 19), place thermophiles at the base of the tree of life (20). However, the position of these same thermophilic organisms at the base is challenged when other molecular markers, such as DNA-dependent RNA polymerases (21, 22) and DNA topoisomerases (22), are used instead. The widespread presence of heat-shock proteins in nearly all modern organisms has also led to the proposal that a (hyper)thermophile was the cellular ancestor of all extant microorganisms (6). Modern heat-shock proteins play critical roles in stress responses in the cell (6, 23) and, along with other housekeeping proteins, could have evolved from a (hyper)thermophilic ancestor (14). Alternatively, (hyper)thermophiles could have outcompeted earlier mesophilic organisms due to their increased ability to deal with a range of stressors (6). Furthermore, the bombardment of early Earth by extra-planetary bodies could have super-heated the shallow oceans present at the time to over 100 °C, thereby creating a hot-ocean bottleneck (14) and the extinction of any early

mesophiles (6, 14). Whether (hyper)thermophiles were the earliest cellular forms or emerged later, scientists do agree on the fact that these organisms played a critical role in the evolution of early life. Thus, critical insights about the ancestral microorganisms can be gained by studying extant (hyper)thermophiles and extrapolating backwards.

1.2 *Hydrothermal vents as analogous sites for life on Early Earth*

Evidence to date indicates that the ecology of the Archaean eon was solely microbial and was likely less productive than the systems in place today (24). Despite their reduced productivity, early microorganisms are believed to have carried out the same biogeochemical processes as on modern Earth (14, 24). Life on early Earth relied on the availability of electron donors and acceptors, as well as carbon sources generated independently of photosynthetic primary producers. Dark sites were especially important on early Earth as the lack of an ozone layer permitted extreme amounts (1000x current values) of ultraviolet radiation to reach the ocean surface and permeate into the shallow seas (25, 26). Similar dark environments, though rare on modern Earth, do exist in deep-sea hydrothermal vent systems (5, 14, 24, 27). Whereas photosynthetic primary producers drive life on the surface of our planet, elemental gradients drive life in and around hydrothermal vents, be they diffuse-flow sites where superheated water flows gently from the subsurface or in chimney- sites where the flow is concentrated and flows from, often, a single chimney-like outflow (5, 14, 24, 27).

The geochemistry of hydrothermal vent fluids can be affected by magmatic intrusions, tidal processes, and seismic activity (28). For this reason, the chemistry of individual vents from the same hydrothermal system is often distinct, though relatively constant over time (28). Seawater seeps down through faults in the seafloor, becoming superheated as it gets closer to the sub-seafloor magma chambers. The heat strips chemicals such as sulfate (SO_4^{2-}) and manganese (Mn) from the seawater (5). However, once discharged from the vents, the fluids become enriched in compounds leeched from the oceanic crust such as CH_4, CO_2, CO, H_2, H_2S, and various metals

including Ca, Fe, Cu, Zn, Ba, and Mn, which precipitate out of solution as soon as they interact with the cold (*ca.* 2-4 °C (29)), oxygenated (*ca.* 150 µmol kg^{-1} (30)) seawater (5). In addition, the primary nitrogen source in modern vent systems studied to date is, as in Archaean systems, abiotically-produced NH_3 (5). Hence, hydrothermal vents and plumes provide vent- and plume-associated communities with a constant flow of electron donors, acceptors, carbon-, and nitrogen sources that closely mimic the geochemistry and physical conditions of Archaean environments inhabited by the ancestral (hyper)thermophiles.

While modern hydrothermal vent systems are both geochemically and geothermally similar to those on early Earth, the characteristics of the surrounding seawater are expected to be different. The Archaean atmosphere, unlike that of modern Earth, was reducing and composed primarily of methane, nitrogen gas and/or carbon dioxide, and molecular hydrogen (5, 6). This reducing environment, which would persist into the shallow seas, is essential for the abiotic synthesis of amino acids (purines, pyrimidines) and sugars (16). Furthermore, it maintained elements, gases, and other vent exudates in a reduced state that would keep them in solution (5). Such a chemically-reduced environment may have been relatively stable for some time. However, decreases in hydrothermal vent activity as the Earth cooled and increases in oxygen production from abiotic and microbial oxidative processes during the Archaean eon eventually altered the reduced atmosphere and changed conditions in the seas (5). Although differences in the surrounding seawater can affect the thermal and chemical gradients present at the site, hydrothermal vent systems are valuable Archaean mimics based on their geological, geothermal, and geochemical similarities (5). For this reason, it has been suggested that microbial isolates and communities present in and around hydrothermal vent systems may be physiologically and morphologically similar to those present during the Archaean (5, 14, 31).

1.3 *Hydrothermal vent community physiology, metabolism, and ecology*

Free-living organisms from deep-sea hydrothermal vent systems are often thought of as evolutionarily primitive, due to their position on the tree of life (32). While “primitive” in the evolutionary sense, these microorganisms are in fact physiologically, metabolically, and ecologically diverse. Complex communities have been identified in a range of hydrothermal habitats including vent chimneys (33–36), vent fluids (35, 37, 38), and in the microbial mats surrounding both chimneys and diffuse-flow sites (39, 40). Furthermore, there is great physiological diversity in the hydrothermal vent communities (34, 41–43). Yet, all are adapted to growing at elevated temperatures, utilize geothermally-provided electron acceptors such as sulfur, molecular hydrogen, and iron for respiration; fix CO_2 to assimilate carbon; and have anaerobic metabolisms. Thus, all of these organisms must rely on chemo- rather than photo-synthetic processes for survival. Chemotrophy dominates: methane producers (methanogens) and utilizers (methane oxidizers) as well as hydrogen producers and consumers (H_2 oxidizers) thrive in these environment. Furthermore, CO_2 is often the most abundant carbon source and can be assimilated using a variety of carbon-fixation mechanisms (41). A number of sulfur/metal oxidizers are present in addition to sulfate- and iron-respiring bacteria and archaea (41). Thus, these systems, though unique in their chemistry, follow the same principle of life as on the surface of the planet: what is available for consumption is undoubtedly consumed.

The remote location of hydrothermal vents in the deep sea makes sampling challenging and costly. The majority of subsurface studies have been obtained from sediment cores obtained from deep-sea drilling operations (44–46) or from fluids obtained exiting chimneys, diffuse-flow sites, or even at sites of recent volcanic activity (47–50). Additional studies ((51–53) for example) have relied on submersibles launched from scientific research vessels, a costly and limiting step. Even the enumeration of these deep-sea microorganisms is difficult, as these microbial communities rest on a knife’s edge in terms of thermal and chemical gradients. Geological,

geochemical, and geothermal analyses of vent chimney sections show that within the vent chimney walls thermal and chemical gradients exist (54, 29). The vent's chimney walls, which can have centimeter to meter scales, often have steep gradients of temperature ranging from more than 200 °C in the inner layers to 5 °C on the external surface, and drastically different mineral compositions throughout. This, along with the permeation of vent- and ocean-derived compounds from both the interior and the exterior, leads to drastically different zones within centimeters or millimeters of each other (54, 29). Therefore, microorganisms or microbial communities must maintain their position within the vent chimney or hydrothermal vent system or risk freezing, boiling, or starving because of a millimeter change in locale (29). Despite this, large and active communities exist within these subsurface systems (55–59). Microorganisms are even abundant in the vent water: bacterial cell counts range, for example, from 10^5 to over 10^9 cells/mL. Furthermore, microbial productivity (measured by cell counts, GTP:ATP ratios, and uptake of $^{14}CO_2$) is even greater than in the surrounding seawater (100 – 1000 x) and overlying surface waters (3 – 4 x) (5, 60).

The extreme conditions of these environments also make culture enrichments and isolations of native microorganisms complex, thus limiting the opportunities for standard culture-based screens (61). In spite of this, several culture-based methods have been used to examine the biodiversity at hydrothermal vent sites (62, 63). Culture-dependent studies indicate that the majority of these isolates are chemolithoautotrophs which can utilize the abundant, albeit atypical, nutrients produced by hydrothermal vents to sustain life and build biomass (64). They are predominantly anaerobic and isolates typically utilize sulfur- or iron-containing compounds in oxidative or reductive reactions. Methane oxidation also predominates in vent systems as methane is produced both by the vents themselves and via methanogenesis from CO_2 by archaeal methanogens (64). Techniques have been developed, such as the use of insoluble Fe(III) oxides as the sole electron acceptor during sample enrichment, to select for these

microorganisms (65). These studies have led to the isolation of novel bacterial and archaeal clades (52, 65, 66).

Because of the challenges associated with culturing these organisms, culture-independent phylogenic approaches such as those based on 16S rRNA analysis have also been used to examine the phylogenetic diversity of the hydrothermal vent communities (see (35, 42, 57, 59, 67, 68) for examples). These approaches can be performed on whole-community samples and effectively 'bin' specific microbial sequences into genus- and species-level groups, therefore providing a near complete picture of the community, pending bias of the conditions used to amplify and sequence the available DNA (69). As phylogeny provides little to no information about the microorganism's physiology, phylogenetic studies are often coupled to genomic studies, which identify genomic indicators of microbial physiology or metabolic capabilities. These studies, termed metagenomics, can often shed additional light on poorly-studied systems.

1.4 *From phylogenetics and physiology to metagenomics*

Metagenomics extends the phylogenetic and physiologic information derived from culture-independent and culture-based techniques, respectively, to provide a community-wide view of microbial proteins and pathways which could drive the functioning of an ecosystem. This is particularly important in hydrothermal vents and hydrothermal vent chimneys, where the microenvironment can change drastically over the scale of millimeters (54, 29) and many highly diverse microbial communities may live within the short distances across the hydrothermal vent chimney walls (29, 68). The metabolic potential of these difficult to study and spatially-distinct communities can be assessed using metagenomics by examining the presence or absence of genes encoding known enzymes within well-characterized metabolic pathways. Xie *et. al.* (41) used metagenomics to examine, for example, microbial communities from a range of hydrothermal vent sites and identified several pathways for CO_2 fixation, sulfur oxidation, and nitrogen metabolism. The presence and absence of several of these pathways was found to

change based on the microenvironments present within a site. Thus, the technique not only identifies the metabolic pathways present in defined communities, but can provide valuable insights into the specific conditions and microhabitats that exist within the larger environment under examination (41).

Yet limitations in metagenomic studies exist in that community physiologies often do not match the capabilities predicted by metagenomic methods. Physiological studies performed within the Juan de Fuca Ridge hydrothermal vent system showed, for example, that chemoautotrophs present in the plumes of hydrothermal vent chimneys at the site were able to rapidly consume ammonium (70), but metagenomic analysis did not detect the presence of a key enzyme, ammonia monooxygenase, required for ammonia oxidation (41). Thus, even for well-characterized systems, metagenomics fails when novel pathways or confounding evidence is present.

1.5 *"To really know them, you have to grow them"*

The limitation of culture-independent approaches to understand the metabolic potential and phylogenetic diversity of microorganisms from hydrothermal vent systems is clearly seen when studying dissimilatory iron reduction. In contrast to other respiratory metabolisms that rely on soluble electron acceptors (such as the sulfate respiration prevalent within hydrothermal vent systems and on early Earth (14)), dissimilatory iron reducers respire iron (Fe(III)) oxides, an insoluble electron acceptor (71). In contrast to soluble electron acceptors, which are typically reduced by terminal reductases in the periplasm or cytoplasm (72), iron oxides must be reduced extracellularly. To accomplish this, a number of bacterial and archaeal clades have members that have evolved mechanisms to transfer respiratory electrons to the insoluble oxides outside the cell. The best studied dissimilatory iron reducers are those within the bacterial family *Geobacteraceae* (73).

The *Geobacteraceae*, which are members of the *Desulfuromonadales* within the *Deltaproteobacteria*, are obligate anaerobes and iron reducers but otherwise physiologically diverse (73). The most commonly studied members of the family are *Geobacter sulfurreducens* (74) and *Geobacter metallireducens* (75). Both are mesophilic, with an optimal growth temperature of *ca.* 30 °C, and can couple the reduction of both soluble and insoluble forms of Fe(III) in addition to the oxidation of a range of electron acceptors (74, 75). Many members in the family have sequenced genomes (76–80) and genetic systems are available for both *G. sulfurreducens* (81) and *G. metallireducens* (82). Genomic studies have provided very valuable insights into the respiratory strategies of these organisms (83) but mechanistic information on iron oxide reduction is not easily deduced from genome data and often requires coupled physiological and genetic studies. These studies have identified several strategies to transport electrons to the extracellular iron oxides, which can be grouped in two: those requiring direct contact between the cell and the oxides and indirect strategies using electron shuttles or metal chelators (84).

1.6 *Mechanisms for iron oxide respiration in mesophilic environments*

An efficient strategy to reduce iron oxides is one in which the cell establishes direct contact with the insoluble electron acceptors. To do so, the cell must express a terminal iron reductase on its outer surface and be able to access and attach to the mineral surface in order to transfer the respiratory electrons. The most common iron reductases in mesophilic dissimilatory metal-respiring bacteria and archaea are *c*-type cytochromes (84). They are so named due to the presence of a heme motif related to Cytochrome C (85), are found in numerous organisms (84), and are especially abundant within microorganisms able to respire insoluble metal oxides (86). These cytochromes carry a conserved heme binding motif (CXXCH) and can also carry a signal peptide that is recognized and processed prior to exporting the protein to the periplasm of gram-negative bacteria or the periplasm-like space of archaea (72, 87–89). Cells can further extend

their electroactive surface anchoring *c*-cytochromes in an exopolysaccharide (EPS) matrix, a strategy that also allows them to build electroactive biofilms (90).

In addition to *c*-cytochromes, dissimilatory iron reducers in the family *Geobacteraceae* produce conductive type IV pili, termed “microbial nanowires”, as electronic conduits between the cell and the Fe(III) oxides (91). The expression of protein nanowires increases the redox-active surface of the cell beyond the confines of the cell envelope, thus facilitating access to the Fe(III) oxide particles, which are often dispersed in soils and sediments (91). The pilus nanowires produced by the *Geobacteraceae* also function as electronic conduits between the cell and soluble metals, such as the uranyl cation, a respiratory strategy that also serves as a protective mechanism because the extracellular reduction of the toxic metals also prevents their permeation and reduction inside the cell (92). Nanowire-like appendages have been reported in other bacteria, including *Acidithiobacillus ferrooxidans* (93) and the mesophilic iron-reducing bacterium *Shewanella oneidensis* (94). However, the ‘nanowires’ of *S. oneidensis* have recently been shown to be extensions of the cell’s periplasm and outer membrane (95) and the nanowires of *A. ferrooxidans* function to transfer electrons from extracellular electron donors. Hence, to date, protein nanowires have only been identified in mesophiles, and those enabling growth on insoluble electron acceptors have only been identified in the *Geobacteraceae*.

In contrast to direct-contact mechanisms, some microorganisms rely on indirect strategies to reduce the insoluble electron acceptors at a distance. One such strategy is employing metal-chelating compounds, which can be produced by the same or other microorganisms or in abiotic reactions (96). The chelators can therefore be exogenous compounds, such as nitrilotriacetic acid (NTA), which is often used in laboratory studies to stimulate the growth of iron reducers (96), or can be produced by the iron-reducing microorganism itself, as reported for the mesophilic bacterium *Geothrix fermentans* (97). Whether exogenous or endogenous, chelators solubilize the Fe(III) from the oxides and provide a soluble, chelated form of iron as an electron acceptor for respiration. This alleviates the need for the cell to establish electronic contact with the insoluble

electron acceptors (91, 98). Not only can the chelators diffuse in and out from the cell, they can also diffuse through biofilms, thus passively chelating the mineral and increasing its bioavailability (96, 99). Alternatively, some microorganisms use contact-independent mechanisms based on soluble molecules called electron shuttles, which function like electroactive “ping-pong balls” that bounce between the cell and the mineral surface to deliver respiratory electrons (100). Electron shuttles are abundant in many environments where iron reduction is a significant process, primarily as humic substances produced during the degradation of plant matter (99), but can also be synthesized and secreted by microbial cells (97, 100, 101). By shuttling electrons between the cell and the extracellular minerals they stimulate extracellular electron transfer in dissimilatory iron reducers and also confer on other microorganisms the ability to respire insoluble electron acceptors (99).

As discussed previously, genome data do not always provide sufficient information to predict whether an organism participates in dissimilatory iron reduction and genetic and physiological studies are still needed to identify genetic markers for this metabolic capability. In the model representative of the family *Geobacteraceae*, *G. sulfurreducens*, for example, genetic markers include the presence of a great number (more than 100) of genes encoding *c*-cytochromes, including some predicted to be exported to the outer membrane (76) and a *pilA* gene encoding the divergent type IV pilin of the *Geobacteraceae* (91). *Geobacteraceae* also produce the Xap EPS to anchor extracellular *c*-cytochromes and reduce Fe(III) oxides (90). Furthermore, flagellar motility, chemotaxis to Fe(II), which is the soluble product of Fe(III) oxide respiration, and type IV pili allows bacteria in the *Geobacteraceae* to locate and access the insoluble oxides (102). Yet, conservation in some of the genes, most notably in those encoding *c*-cytochromes, is low and it is challenging to predict the respiratory path for iron reduction from genomic data (reviewed in (103)). This is due to the fact that the specific roles of pili, cytochromes, and EPS in Fe(III) reduction are not yet fully understood (reviewed in (103)). *Geobacteraceae* type IV pili, for example, are essential for Fe(III) oxide reduction (91), yet may also anchor *c*-

cytochromes (104). Furthermore, adaptive evolution of a pilin-deficient mutant of *G. sulfurreducens* in Fe(III) oxides cultures restored its ability to reduce the insoluble electron acceptor, presumably because the *c*-type cytochrome PgcA was overexpressed and able to shuttle electrons between the cell and the mineral (105). Hence, several pathways may operate, each with different components.

Thus, although metagenomic, genomic, and phylogenetic studies have been successful in identifying components used in well-characterized pathways such as sulfurous and nitrogenous compound reduction, its use in the field of dissimilatory iron reduction is inherently challenging. Furthermore, mechanistic information about dissimilatory iron reduction in thermophilic and hyperthermophilic bacteria and archaea is even scarcer. The decreasing costs of genomic sequencing has increased the availability of sequenced genomes from (hyper)thermophiles (68) but there is a need to identify model organisms for mechanistic studies of metal respiration at high temperatures.

1.7 *Identification of model iron-reducing organisms from hydrothermal vents*

Hydrothermal vent systems can be grouped into mid-ocean zones and those located in close proximity to landmasses. The location of mid-ocean zones far away from continental land minimizes the amount of organic material that can accumulate in the hydrothermal vent sediments and creates conditions for microbial growth that are primarily influenced by hydrothermal activity. By contrast, hydrothermal vent systems geographically close to continental land, are exposed to the coastal runoff and, therefore influenced by both the hydrothermal vent and coastal discharges. Hence, iron reducers from mid-ocean versus off-shore hydrothermal vent systems are expected to have evolved unique metabolic adaptations to the specific conditions of their environment. For this reason, two hydrothermal vent systems were selected for further studies that represented the two types of hydrothermal vent environments.

1.7.1 Geothermobacter ehrlichii *as a model organism for the thermophilic bacteria isolated from a diffuse-flow mid-ocean vent system*

The Axial Seamount system, located off the coast of Washington (USA) within the Juan de Fuca Ridge, is a spreading site that has been well studied due to its shallow depth (*ca.* 1500 m) and proximity (250 nautical miles off the coast) to several oceanography centers (Figure 1.2) (106). The seamount itself forms a large (3 x 8 km) caldera and has repeatedly been active in the past century (28). The caldera itself contains a number of different hydrothermal vents (28), including the Bag City vent site in the southern region, which receives its name from the numerous gelatinous polysaccharide coagulants or "bags" that coat its sediments (66). The Bag City resides within the pre-1987 lava flow zone and just outside of the 1998 lava flow (28). It is a stable diffuse-flow vent system with an examined temperature range of 12.9 - 31.3 °C (28). The vent site has relatively low concentrations (nM/J of heat) of H_2, CH_4, H_2S, and Fe when compared to other vents on the Axial seamount included in the analysis (28). This may be due to the difficulty in assessing vent flow from diffuse sites when compared to chimney systems. Despite the relative scarcity of these chemical compounds at the time of sampling (28), the Bag City site and the Axial Seamount support the growth of an active vent community and, for this reason, continue to be a prime model site to examine life in off-shore spreading systems.

As stated above, the name Bag City originated from the discovery of numerous gelatinous polysaccharide coagulants or "bags, at the site, which were believed to be secreted by native microorganisms (66). *Geothermobacter ehrlichii* was isolated from anoxic diffuse-flow vent fluid samples collected from the Bag City hydrothermal vent by the research submersible 'Jason' using Fe(III) oxide enrichments and produces copious amounts of exopolysaccharide when grown under conditions of stress (66), thus serving as a good model representative iron reducer from the Bag City environment. Phylogenetic analysis placed *G. ehrlichii* within the *Geobacteraceae* family (66), which includes the best known mesophilic iron reducers, as discussed previously. However, recent studies suggest a placement within the related *Desulfuromonadaceae* family,

also within the delta subclass of *Proteobacteria* (66, 107, 108). Unlike other cultured members of the *Geobacteraceae* (73) or *Desulfuromonadaceae* (107), which are mesophiles or psychrophiles, *G. ehrlichii* is a thermophile, growing at temperatures ranging from 35 to 65 °C and optimally at 55 °C (66). The low temperature range that supports the growth of *G. ehrlichii* matches well the temperature maxima (31.3 °C) recorded at the Bag City site (28). This observation is also consistent with isolates from other hydrothermal vent sites, which often have a minimum growth temperature that is higher than the site of isolation (48, 55). *G. ehrlichii* used only Fe(III) and nitrate (which was reduced to ammonia) as terminal electron acceptors for respiration using organic acids as electron donors (66). But unlike most other *Geobacteraceae*, it was also able to couple the oxidization of sugars, starch, and amino acids to the reduction of Fe(III) (66). The phylogenetic proximity of this isolate to the intensely-studied mesophilic representatives *G. sulfurreducens* (74) and *G. metallireducens* (75), combined with its thermophilic growth range and isolation site (66) make it a prime model organism for bacterial dissimilatory iron reduction at thermophilic temperatures.

1.7.2 Geoglobus ahangari *as a model organism for the hyperthermophilic archaea isolated from a coastal hydrothermal vent chimney*

Unlike the Axial Seamount system, the Guaymas Basin hydrothermal vent system is located close to shore (Figure 1.3). In fact, this hydrothermal field is located between the Baja Peninsula and the coast of Mexico within the Gulf of California (109). This placement has led to the accumulation of deep sediments throughout the site (51, 109). Hydrothermal fluids must proceed through nearly 500 meters of organic-rich sediments before they arrive at the seafloor (51, 110). Thus, unlike the previously mentioned Juan de Fuca ridge system, the diversity of carbon sources and electron donors is greatly increased within the Guaymas Basin (51, 110). This abundance of compounds supports the development of thick microbial mats within and on top of the sediments in the basin and these systems need not rely solely on hydrothermally-produced compounds for growth (51). The Guaymas Basin can then serve as a model system to

examine a relatively nutrient-rich oasis when compared to the desert-like mid-ocean systems, such as the Axial Seamount discussed earlier.

Geoglobus ahangari 234^T was enriched and isolated from a Guaymas Basin vent sample using Fe(III) oxides (52). Phylogenetic analysis placed the strain as a new genus within the family *Archaeoglobales*; thus, *G. ahangari* is the type strain of the *Geoglobus* genus (52). All members of the *Archaeoglobales* are hyperthermophiles with optimal growth temperatures ranging between 70 and 88 °C, with *G. ahangari* thriving at the upper limit (52). They are closely related to the archaeal methanogens, with whom they share many metabolic similarities (111). Unlike the thermophilic *G. ehrlichii* which can respire nitrate in addition to Fe(III) (66), *G. ahangari* is an obligate iron reducer (*i.e.,* it can only use soluble or insoluble Fe(III) electron acceptors) (52). Consistent with the abundance of organic compounds in the site of isolation, *G. ahangari* can oxidize a large number of electron donors during Fe(III) respiration including short- and long-chain fatty acids, TCA cycle intermediates, and amino acids such as isoleucine, arginine, and serine (52). Furthermore, it was the first hyperthermophile reported to use acetate, an electron donor previously thought to only support mesophilic respiratory processes (52, 112). *G. ahangari* was also the first dissimilatory Fe(III)-reducing microorganism capable of autotrophic growth with molecular hydrogen, an unsuspected metabolic capability of these organisms (52). Thus, *G. ahangari* represents a model organism to represent a hyperthermophilic iron-reducing archaeon isolated from a nutrient-rich hydrothermal vent system.

1.8 Mechanistic studies of (hyper)thermophilic iron reduction and the need for additional model systems

Models, by definition, are meant to represent a system full of uncertainties. Thus, while arguments persist regarding the origins of life and the settings in which it formed, the use of extant organisms as model systems to study early life warrants special attention. The identification of conserved mechanisms for iron respiration in (hyper)thermophilic bacteria and archaea could

provide valuable insights into the ancestral mechanisms that supported early forms of Fe(III) respiration. Furthermore, when compared to mesophilic mechanisms, the evolution of Fe(III) respiration and adaptations to the environment can be better understood.

The availability of *G. ehrlichii* and *G. ahangari* in pure culture and the unique physiological characteristics of these iron reducers make them particularly suitable as model systems for Fe(III) respiration in mid-ocean and off-shore hydrothermal vents. They are also phylogenetically distinct, one being a bacterium (*G. ehrlichii*) and the other, an archaeon (*G. ahangari*). Furthermore, the temperature growth range is also distinct (thermophilic and hyperthermophilic). Thus, genomic data coupled with physiological studies in these organisms can provide valuable insights into iron respiration at high temperatures. Furthermore, when compared to the respiratory strategies of other thermophiles and hyperthermophiles (113, 114), insights into the evolution of microbial respiration on Earth can be gained.

1.9 *Dissertation Outline*

1.9.1 *The high-quality draft genome sequence of the thermophilic Fe(III)-reducing bacterium* Geothermobacter ehrlichii *strain SS015*

Chapter 2 describes the sequencing, assembly, and annotation of the genome of the iron-reducing bacterium *Geothermobacter ehrlichii* strain SS015. Annotated genes and pathways are compared to other members of the order *Desulfuromonales* and predictions about the mechanism for iron respiration at thermophilic temperatures are discussed. This work was performed in collaboration with Dr. Spurbeck and Dr. Sandhu from Swift Biosciences (Ann Arbor, MI, USA), who assisted with the genome sequencing and assembly, and an undergraduate mentee from MSU, Lucas Demey, who assisted in the genome annotation.

1.9.2 *The complete genome sequence and emendation of the hyperthermophilic, obligate iron-reducing archaeon "*Geoglobus ahangari*" strain 234^T*

Chapter 3 describes the sequencing, assembly, and annotation of the genome of *Geoglobus ahangari* strain 234^T. Annotated genes and pathways are compared to other members of the family *Archaeoglobaceae* and predictions about the metabolic potential of the isolate and mechanism of iron respiration at hyperthermophilic temperatures are discussed. This work was performed in collaboration with Dr. Dawn Holmes' group at Western New England University (Massachusetts, USA) who assisted with the genome sequencing, assembly, analysis of metabolic pathways, and drafting of the manuscript.

1.9.3 *Extracellular electron transfer to Fe(III) oxides by the hyperthermophilic archaeon* Geoglobus ahangari *via a direct contact mechanism*

Chapter 4 describes physiological studies aimed at elucidating the mechanism employed by *Geoglobus ahangari* strain 234^T to reduce insoluble Fe(III) oxides. Assays were performed to determine if exogenous compounds such as electron shuttles and chelators could promote the growth of this strain on insoluble iron oxides and to determine if these compounds were produced endogenously. Putative *c*-type cytochromes were identified among proteins separated in SDS-PAGE gels and stained for heme. Furthermore, the localization of putative *c*-cytochromes on the outer membrane of the cells was assessed by performing similar studies with proteins mechanically sheared from the cell's outer membrane and their essential role during the reduction of insoluble, but not soluble, Fe(III) was demonstrated. A model for iron reduction by *G. ahangari* based on a direct-contact mechanism is presented.

1.9.4 *Microbial Nanowires: A conserved mechanism for extracellular electron transfer*

Chapter 5 describes the biochemical characterization and conductive properties of protein filaments produced by the thermophilic bacterium *G. ehrlichii* strain SS015 and the hyperthermophilic archaeon *G. ahangari* strain 234^T for the reduction of Fe(III) oxides. Mechanical sheared samples, which contain the protein filaments as well as flagella, and protein filaments

purified from both organisms were probed with a Conductive Probe – Atomic Force Microscope (CP-AFM) to demonstrate their conductivity. The thermal and chemical stability of the protein filaments was also investigated using the mesophile *G. metallireducens* as a reference. The CP-AFM work was performed in collaboration with graduate student Krista Cosert and Dr. Sanela Lampa-Pastirk from the laboratory of Dr. Gemma Reguera.

CHAPTER 2. THE HIGH-QUALITY DRAFT GENOME SEQUENCE OF THE THERMOPHILIC FE(III)-REDUCING BACTERIUM *GEOBACTER EHRLICHII* STRAIN SS015

2.1 *Abstract*

Geothermobacter ehrlichii strain SS015 is the only thermophilic member of the family *Desulfuromonadaceae* available in pure culture. It was isolated from vent fluid samples of the Bag City hydrothermal vent system, within the Juan de Fuca Ridge, and produces copious amounts of exopolysaccharide (EPS) such as those reported to make the “bags” that decorate the Bag City landscape. The bacterium couples the reduction of soluble and insoluble Fe(III) oxides and of nitrate to the oxidation of a wide range of electron donors. It is the only thermophilic member of the *Desulfuromonadales*, a bacterial order containing the *Pelobacteraceae*, *Desulfuromonadaceae* and the *Geobacteraceae* families, a predominant clade in nearly all metal-reducing mesophilic subsurface communities. Hence, it is a good model system to also understand the thermophilic adaptation of Fe(III) reduction. Here I describe the sequencing and annotation of the genome of *G. ehrlichii* strain SS015 and discuss the metabolic capabilities predicted from genome data that are shared with other members of the *Desulfuromonadales* or unique to its thermophilic member, *G. ehrlichii*. I also discuss what physiological properties may have allowed this bacterium to grow at thermophilic temperatures, which are otherwise lethal to all other members of the *Desulfuromonadales*. The high-quality draft genome presented here contains 3,276,179 base pairs (bp) in 84 contigs containing 3,059 protein-coding genes, 53 RNA genes, and a predicted 60 missing genes.

2.2 *Keywords*

Desulfuromonadales; *Geobacteraceae*; *Geobacter*; hydrothermal vent; Bag City; Fe(III) respiration; extracellular electron transfer.

2.3 *Introduction*

The recovery of the thermophilic iron-reducing bacterium *Geothermobacter ehrlichii* in pure culture and its initial placement within the family *Geobacteraceae* added thermophily to the physiological properties of this otherwise mesophilic group of iron reducers in the *Deltaproteobacteria* (66). The family includes some of the best studied dissimilatory metal-reducing bacteria (73), with *Geobacter sulfurreducens* and *Geobacter metallireducens* serving as model representatives (reviewed in (71, 99, 103)). Recent phylogenetic analyses now place the *Geobacteraceae* as a clade within the family *Desulfuromonadales*, and *G. ehrlichii* outside the *Geobacteraceae* but within the *Desulfuromonadaceae* (107, 108). Hence, *G. ehrlichii* strain SS015 is the type strain of the *Geothermobacter* genus and the only isolated thermophilic member of the *Desulfuromonadales* (66, 108), which also includes two psychrophilic isolates, *Geobacter psychrophilus* (115) and *Geopsychrobacter electrodiphilus* (116).

G. ehrlichii strain SS015 has a reported growth range of 35 to 65 °C and an optimum growth temperature of 55 °C (66). Originally isolated from the Bag City site within the Axial Seamount system, *G. ehrlichii* produces an abundance of acidic extracellular polymeric substances which may explain the namesake polysaccharide “bags” seen at the site (66). The EPS is produced in response to sub-optimal temperatures and the presence of antibiotics, suggesting it plays a protective role (66). *G. ehrlichii* strain SS015 shares many characteristics with members of the *Geobacteraceae* (73) and the *Desulfuromonadaceae* (108) in that it is able to couple the oxidation of a broad range of organic acids to the reduction of soluble and insoluble Fe(III) as well as nitrate (66). Yet, unlike the *Geobacteraceae*, it can use amino acids, starch, and sugars as electron donors with Fe(III) serving as sole electron acceptor (66). Genomic evidence suggests that certain *Geobacteraceae* species may have the capability to utilize these donors yet this ability has not been demonstrated in the laboratory (74, 117).

The mechanisms for Fe(III) respiration have been extensively studied in the mesophilic members of the family ((103) and references within), but less is known about Fe(III) reduction at

thermophilic temperatures. Cells of *G. ehrlichii* strain SS015 are motile via a single flagellum, which could allow the cell to access the Fe(III) oxides, provided chemotaxis to Fe(II) is present as in the *Geobacteraceae* (102). Pilus-like filaments are also apparent in electron micrographs of *G. ehrlichii* cells (66), which could be conductive and function as nanowires between the cell and the minerals as in mesophilic *Geobacter* species (91). The nanowire pilins form an independent line of descent among bacterial pilins and pseudopilins (91) and are divergent in structure and amino acid composition to provide a protein environment optimized for electron transfer (118). For example, unlike other bacterial type IV pilins, they lack the conserved C-terminal globular domain of other bacterial type IV pilins and are predominantly an α-helical peptide, a structure that promotes electronic coupling and electron transfer (118). Hence, pilin-encoding genes can provide valuable information about the putative role of the pili in electron transfer. Another conserved feature of the *Geobacteraceae* that is linked to their ability to reduce Fe(III) oxides is the presence of a great number of genes encoding *c*-type cytochromes (83). Here, I report on the draft genome sequence of *G. ehrlichii* strain SS015 and summarize the physiological features that are conserved and divergent between this thermophile and other members of the *Desulfuromonadales*, with a focus on the features that could be involved in Fe(III) reduction.

2.4 *Organism information*

2.4.1 *Classification and features*

Isolated from the Bag City hydrothermal vent chimney, within the Axial Seamount system (46 °N, 130 °W), at a depth of 1,400 m, *Geothermobacter ehrlichii* strain SS015 was originally described as the only thermophilic member of the *Geobacteraceae* available in pure culture (66). The sequence of the previously published (66) partial sequence for the 16S rRNA gene (NR_042754.1) matches (92 %) to the 16S rRNA gene (rna.42) found within the genome. This rRNA gene was used to construct a new phylogenetic tree in reference to the 16S rRNA gene sequences from other members of the *Desulfuromonadales*, using *Escherichia coli* as the

outgroup, and allowed the revision of the phylogenic position of *G. ehrlichii* in relation to the *Geobacteraceae* and the *Desulfuromonadaceae* (Figure 2.1). In this new tree, *G. ehrlichii* is most closely related phylogenetically to sequences of other *Geothermobacter* species not yet available in pure culture and, based on the 16S Ribosomal RNA Reference Sequence Similarity Search (RefSeq – NCBI), to several *Desulfuromonas* species including *D. palmitatis* (93.2 %) and *D. thiophila* (93.0 %). However, alignment of the 16S genes using SILVA (119) places *D. palmitatiis* at a distance from *G. ehrlichii*. The low confidence level within the *Geothermobacter* branch of the phylogenetic tree indicates that there is a vast diversity of *Geothermobacter* species remaining to be discovered.

Cells of *G. ehrlichii* strain SS015 are rod-shaped, 1.2 to 1.5 µm in length, can appear as single cells or in chains (Figure 2.2), and spores were not observed (66). Cells were motile, which was predicted to be enabled by the single polar flagellum produced by the cell (66). In addition, numerous pilus structures could be seen on the surface of the cell (Figure 2.2) (66). Gram stain and thin section microscopy revealed *G. ehrlichii* to be Gram-negative (66). When stressed, by sub-optimal temperatures or antibiotics, cells were seen to produce an abundance of extracellular polymeric substances, as visualized by ruthenium red (66). Growth was supported from 35 to 65 °C with an optimal growth temperature of 55 °C (66). The pH range for growth was 5.0 to 8.0, with an optimum at 6.0, while the salinity range was from 5.0 to 50 g/L, with an optimum at 19 g/L (66). In addition, cell pellets of *G. ehrlichii* appear as red/pink and exhibit an absorption characteristic of *c*-type cytochromes (66).

G. ehrlichii strain SS015 was able to couple the oxidation of a range of electron donors, such as DL-malate, pyruvate, acetate, glutamate, propionate, butyrate, ethanol, and methanol, to the reduction of both Fe(III) and nitrate (66). While the strain was isolated and characterized to solely use insoluble Fe(III) oxides (66), it rapidly adapted to utilize the soluble form of Fe(III), ferric citrate, when supplied (presented within this work). The main physiological features of the organism are listed in Table 2.1 (18, 120–124).

2.5 *Genome sequencing and annotation*

2.5.1 *Genome project history*

Based on a) its unique position as the only thermophilic member of the *Desulfuromonadaceae* available in pure culture; b) its ability to use acetate as an electron donor for Fe(III) reduction; and c) its ability to use sugars, starch, and several amino acids as electron donors; *G. ehrlichii* strain SS015 was selected for genome sequencing and annotation. This annotation thus provides information regarding the wider metabolic niche occupied by *G. ehrlichii* strain SS015 and the changes within the genome, when compared to the mesophilic members of the order, which likely permit growth at thermophilic temperatures. A summary of the project information is presented in Table 2.2.

2.5.2 *Growth conditions and DNA isolation*

G. ehrlichii strain SS015 was obtained from the Kashefi lab culture collection while it can also be obtained from the American Type Culture Collection (ATCC BAA-635) and the Deutsche Sammlung von Mikroorganismen und Zellkulturen (DSM 15274). Media, as previously described (66), contained 10 mM *DL*-malate as the electron acceptor and 50 mM soluble Fe(III) citrate as the electron acceptor. Growth on soluble Fe(III) citrate was obtained only after successive transfers in a mixture of soluble and insoluble Fe(III) oxides. Cultures were incubated at 55 °C under a N_2:CO_2 (80:20) atmosphere in the dark. Strict anaerobic techniques were utilized throughout (125).

Genomic DNA (gDNA) was extracted as previously described for *Geoglobus ahangari* (126). In brief, *G. ehrlichii* cultures grown to mid-exponential phase were harvested by centrifugation, washed with an oxalate solution, an iron extraction buffer, and finally a marine wash buffer to remove any remaining chelating compounds. Cell pellets were frozen at -20 °C before being treated with a lytic buffer. gDNA was subsequently purified with the MasterPure DNA Purification Kit (Epicentre Biotechnologies) according to manufacturer suggested guidelines.

2.5.3 *Genome sequencing and assembly*

Two high-quality draft genomes of *G. ehrlichii* strain SS015 were generated from Illumina (127) draft sequences obtained from Swift Biosciences (Ann Arbor, MI). Genomic DNA was fragmented to an average size of 200 bp using a Covaris M220 ultrasonicator (Covaris, Woburn, MA). Two whole-genome libraries were made: one using the Accel-NGS 2S DNA Library kit and the other using Accel-NGS 1S DNA Library Kit (Swift Biosciences, Ann Arbor, MI). These libraries were sequenced on an Illumina MiSeq (Illumina, San Diego, CA) using MiSeq Reagent kit v2. Approximately 3-4 million reads were used for *de novo* genome assembly from each library using the assembler MIRA 4 (128). In addition, one library was prepared, using BluePippin (Sage Science) size selected gDNA fragments, for PacBio sequencing on a single SMRT cell. 428,481 reads containing 2,052,390,107 bp after filtering were generated at the Weill Cornell Medical College of Cornell University and an HGAP 2.0 (129) assembly was generated by the sequencing facility for use. Table 2.2 presents the project information.

Assembly reconciliation software (130) combined with the alignment of short reads to the scaffolds before polymerase chain reactions (PCRs) were used to further close the genome. Minimus2 (130) was used as an assembly reconciliation program to verify, sew, and create a consensus genome from the three different assemblies. Pairwise comparisons were performed with the 1S and 2S genomes, 1S and PacBio, 2S and PacBio. Finally, these initial pairwise assemblies were again reconciled with the third, unused, assembly. The results of the assembly reconciliation are presented in Table 2.3. The assembly reconciled from the 2S Illumina library combined with the PacBio was determined, based on alignment of short reads to the genome, to be the optimal assembly. Attempts were then made to close any gaps and low coverage regions using primers designed to span the gaps (Table 2.4). GoTaq Green PCR Master Mix (Promega) was used with purified gDNA from *G. ehrlichii* strain SS015. All possible primer combinations were tested by pairing each ‘start’ primer (S-primer) with each ‘end’ primer (E-primer). Products obtained from the closure reactions were run on an agarose gel before excision, purification with

the Zymoclean™ Gel DNA Recovery Kit (Zymo Research), and submission to the Research Support and Training Facility at Michigan State University for Sanger sequencing. These reactions have yet to provide a closure based on the PCR products obtained. As such, this work is ongoing.

2.5.4 *Genome annotation*

Genome annotation and ORF analyses were performed using free and publically-available software. The RAST platform (131) was used to obtain the genome annotation, pseudogene detection was performed using the GenePRIMP pipeline (132), pfam domains were detected using Pfam-A from EMBL_EBI (133), signal peptides were detected using SignalP v.4.1 (134) set to Gram negative, and transmembrane domains were detected using TMHMM (135). Finally, CRISPR repeats and spacer regions were identified using CRISPRFinder (136).

For the 1S assembly, a total of 3,275,488 bp were assembled into 81 contigs with the largest contig containing 328,564 bp, an N_{50} of 112,152 bp, 3,045 coding sequences, and 67 RNA genes. For the 2S assembly, a total of 3,279,720 bp were assembled into 84 contigs with the largest contig containing 382,770 bp, an N_{50} of 110,457 bp, 3,058 coding sequences, and 53 RNA genes. For the PacBio HGAP assembly, a total of 2,450,313 bp were assembled into 151 contigs with the largest contig containing 84,277 bp, an N_{50} of 22,144 bp, 2,377 coding sequences, and 40 RNA genes. Assembly 2S was chosen to proceed with genome annotation and analysis, during the genome-closure work described previously, due to the increased genome size and number of coding sequences.

C-type cytochromes present within the genome, which could enable extracellular electron transfer to insoluble Fe(III) oxides, were identified as previously described for the hyperthermophilic iron-respiring archaeon *G. ahangari* (126). In brief, proteins containing one or more *c*-type heme binding motifs (CXXCH) were selected from the genome annotation and screened for the presence of a signal peptide or an N-terminal membrane helix anchor (134). Proteins meeting this requirement were then subjected to DELTA-BLAST analysis against the NR

protein database to determine homology to known *c*-type cytochromes. Molecular weight estimations (137) were performed as previously described (126) on these putative cytochromes to compare them to putative *c*-type cytochromes identified by SDS-PAGE analysis followed by TMBZ staining (138).

Samples for the SDS-PAGE analysis were obtained as follows. Outer-surface proteins were removed by mechanical shearing (5x in and 5x out) with a 23G needle. Prior to shearing, an aliquot was removed to represent pre-sheared cultures. Cells and cell debris were then harvested by repeated centrifugation, 2x (3,220 x *g*, 60 min, 25 °C) and 1x (16,873 x *g*, 5 min, 25 °C), and collected to represent the cell fraction removed of their outer-membrane associated proteins. Finally, the remaining supernatant was passed through a Pall 10 kDa centrifugal filter (1,811 x *g*, 25 °C) to collect sheared proteins remaining in solution. Cell pellets were washed 1x with an oxalate solution (52), incubated 30 min in IEB (139) to remove residual metals, and finally rinsed once with MMWB (139). Proteins collected on the filter were washed with the same solutions and resuspended in MMWB. Samples were then run on a Tris-Tricine 4-20% acrylamide gel (Bio-Rad Laboratories, Inc.) at 100V for 40 minutes and stained using the TMBZ protocol (138) to visualize heme containing bands.

2.6 *Genome properties*

The genome of *G. ehrlichii* strain SS015 presented within this work contains 3,279,720 bp and no plasmids. The genome size is the smallest reported within the *Geobacteraceae* (73) or the *Desulfuromonadaceae* (107), indicating genome shrinkage; however, this may be the result of the unfinished genome. The mol percent G+C is 61.7, which closely matches the percentage (62.6 mol %) estimated by the Identification Service of the DSMZ and within the range of both the *Geobacteraceae* (50.2 – 63.8 mol %) (73) and the *Desulfuromonadaceae* (46 – 62.3 mol %) (107). Out of the 3,112 genes annotated within the genome, 3059 were identified as protein coding genes (98.2 %) and the remaining 53 as RNA genes (2.5 %). 1,580 of the predicted protein coding

genes (51.7 %) are represented by KEGG functional categories. In addition, the RAST annotation server approximates that 60 genes may be missing from the assembled genome. The GenePrimp pipeline predicted 3,059 CDSs, 39 long genes, 49 short genes, 19 broken genes, 8 interrupted genes, and 163 intergenic regions with BLAST hits; totaling 278 total anomalies. Thus, the 60 missing genes within the RAST annotation may exist in these intergenic regions. The genome characteristics and percentage representation of these genes is listed in Table 2.5 and Table 2.6, respectively.

In addition, the following genome characteristics have been calculated. The preferred start codon is ATG (81.4 %), then GTG (11.6 %), and finally TTG (7.0 %). There is a single rRNA gene cluster comprised of the SSU RNA (rna.42), two tRNAs (rna.43-44), the LSU RNA (rna.44), and finally the 5S RNA (rna.46). The origin of replication could not be identified by Ori-Finder analysis (140) due to the draft nature of the genome. However, a gene cluster of proteins involved in chromosomal partitioning and cell division was annotated from peg.1414-1420, which likely indicates that this region is important for cell division and genome replication.

2.7 *Insights from the genome*

2.7.1 *Thermophilic adaptations*

As the only thermophilic member of the *Desulfuromonadales* (66) it was important to identify critical components for its ability to survive and replicate at temperatures which would be lethal to the majority of the order (73, 107). Present in the genome are various heat shock and chaperone proteins; however, homologous proteins contained in similar gene clusters are present in a number of mesophilic *Geobacter* species (76, 77, 80, 141). As such, pending increased expression within *G. ehrlichii,* these gene clusters are likely not the causative agent of the increased growth temperature of *G. ehrlichii* strain SS015.

Outside of the aforementioned stabilizing proteins is the likelihood that *G. ehrlichii* proteins themselves have an increased thermostability over homologues in mesophilic *Geobacter* species.

A number of factors have been linked to increased thermal stability of proteins including the use of decreased utilization of heat-labile amino acids, changes in protein packing, and the inclusion of charged amino acids (17, 142, 143). These studies, however, have focused primarily on protein engineering (144–146) and thus lack a pan-proteome approach. This causes conflicting results as amino acid substitutions that stabilize one protein may destabilize another (142). Thus, meta-analysis of stability data has provided insights into the subject (142). Based on the literature it was evident that several heat-labile amino acids including cysteine, serine, methionine, asparagine, and glutamine have been implicated in reducing protein thermostability while others, including arginine and threonine, were implicated in increasing thermostability (17, 143). Yet, other resources suggest that, of these residues, only cysteine is statistically significant (142). In addition, the amino acids glutamic acid, lysine, tyrosine, and isoleucine are used with a statistically increased rate in thermophilic and hyperthermophilic organisms (142). To this end, the entire proteomes of all sequenced member of the *Geobacteraceae* (NC_010814.1, NC_007517.1, NZ_CP009788.1, NZ_JXBL00000000.1, NC_002939.5, NC_009483.1, and NC_007498.2), with the exception of *Geoalkalibacter ferrihydriticus* due to the additional variable of life in an alkaline environment (with a pH optimum of 8.6) (147), was used to create an amino acid bank.

Comparisons of amino acid usage across these organisms (Figure 2.3) enabled me to determine if any of these amino acids had an increased abundance over those in mesophilic species. Also included is the only psychrophilic member of the *Desulfuromonadales* with a sequenced genome, *Geopsychrobacter electrodiphilus* (NZ_ARWE00000000.1) (116). Several heat-labile amino acids, methionine and asparagine, showed a decreased abundance in *G. ehrlichii* while glutamine and the statistically-significant residue cysteine did not show a decreased abundance when compared to the mesophilic and psychrophilic strains. Tyrosine was also not significantly increased in *G. ehrlichii*, indicating that this amino acid may not stabilize proteins within the *Desulfuromonadales*. Serine, which has been linked to decreased thermostability, and arginine, which has been linked to increased thermostability, are utilized as expected in *G.*

ehrlichii and likely function to increase protein thermostability. Similarly, threonine and glutamic acid residues show the expected increase in abundance, suggesting their contribution to increases in thermostability. As predicted, *G. electrodiphilus* shows the opposite trend as *G. ehrlichii* for serine, glutamic acid, valine, asparagine, glutamine, and threonine – suggesting an optimization for increased protein flexibility and function within *G. electrodiphilus* at low (4–30 °C with a T_{opt} of 22 °C) temperatures (116).

A more telling metric for predicting the thermal stability of an organism's proteome was established after the publication of these initial studies (148, 149). These works state that the single most reproducible and characteristic metric by which to assess the thermal stability of a proteome is to examine the ratio of charged to polar (non-charged) amino acids. The increased abundance of charged residues is expected to present itself on the protein surface and stabilize the protein through ion bonds. Thus, using the same proteomes discussed above, the ratio of charged (aspartic acid, glutamic acid, lysine, and arginine) to polar (asparagine, glutamine, serine, and threonine) amino acids was calculated (148, 149). As above, values were calculated as a percentage of the proteome, and as such it is possible to determine the normalized ratio. As expected, the charged/polar ratio was correlated with growth temperature of the organisms under investigation (Figure 2.4). The psychrophile, *G. electridophilus*, had the lowest ratio (1.17), followed by the mesophilic strains (1.32 +/- 0.07), and the highest value was from *G. ehrlichii* (1.53). Thus, as predicted, the charged to polar ratio increased with increased optimal growth temperature of the organisms examined. This analysis thus presents a simplified and definitive reiteration of the amino acid usage presented above and confirms that the proteome has been optimized in *G. ehrlichii* to grow at elevated temperatures.

2.7.2 *Central metabolism*

G. ehrlichii strain SS015 contains a near complete glycolytic pathway (Figure 2.5) for the utilization of hexose sugars, even though no transporter could be found to permit glucose to enter the cell. In glycolysis, glucose is first phosphorylated to glucose 6-phosphate by a hexokinase

protein. Chains A and B of the *Thermus thermophilus* ROK hexokinase (3VOV), of which a crystal structure is available (150), resulted in weak hits (7e-11) to peg.1432 which is annotated as a polyphosphate glucokinase. DELTA-BLAST analysis of this protein shows that it is a member of the ROK family of proteins and produces strong hits to polyphosphate glucokinase proteins, which indeed take glucose to glucose-6-phosphate. Thus, it is likely that peg.1432 is a ROK hexokinase that could catalyze this first step in glycolysis. Glucose 6-phosphate is next isomerized to fructose 6-phophate, by a glucose-6-phosphate isomerase (peg.1967). Next, a 6-phosphofructokinase protein (peg.1207 and peg.2741) phosphorylates the fructose 6-phosphate to fructose 1,6-bisphosphate in a unidirectional reaction. Therefore, during gluconeogenesis, fructose 1,6-bisphosphate is hydrolyzed to fructose-6-phosphate by fructose 1,6-bisphosphatase proteins (peg.2234 and peg.2805). Fructose 1,6-bisphosphate is next split into DHAP and glyceraldehyde 3-phosphate by a class II fructose-bisphosphate aldolase (peg.2104). DHAP can next be isomerized into glyceraldehyde 3-phosphate by a triosephosphate isomerase (peg.1641). Glyceraldehyde 3-phosphate is next dehydrogenated and, with the addition of inorganic phosphate, produces 1,3-bisphosphoglycerate by a glyceraldehyde-3-phosphate dehydrogenase. Two glyceraldehyde-3-phosphate dehydrogenase proteins were identified in the genome; peg.1643 is annotated as being NAD-dependent while peg.2105 is instead annotated as being NADH-dependent. Next, 1,3-bisphosphoglycerate is phosphorylated into 3-phosphoglycerate by a phosphoglycerate kinase (peg.1642). 3-phosphoglycerate is next converted into 2-phosphoglycerate by a phosphoglycerate mutase (peg.1614). Also, a 2-3-bisphosphoglycerate-independent phosphoglycerate mutase can be found at peg.724 which may also catalyze this reaction. 2-phosphoglycerate is next converted to phosphoenolpyruvate by an enolase protein (peg.2933). Finally, phosphoenolpyruvate is phosphorylated to pyruvate via a pyruvate kinase (peg.253). To proceed in the reverse direction during gluconeogenesis, a pyruvate carboxylase (peg.2794) and a phosphoenolpyruvate carboxykinase (peg.483) were identified within the genome. Therefore, with the exception of the weak hit to the hexokinase

responsible for the initial step in the pathway, *G. ehrlichii* strain SS015 contains a complete glycolytic pathway for the processing of extracellular glucose to pyruvate to then enter the TCA cycle. Thus, *G. ehrlichii* strain SS015 matches members of the *Geobacteraceae* in that it too contains a complete or nearly complete glycolysis pathway which likely functions primarily during gluconeogenesis (117).

Yet, the ability of *G. ehrlichii* to grow on starch, a trait uncommon in the *Desulfuromonadales* (66), could permit the released sugars to feed into the start of glycolysis (151). Starch is uncommon in hydrothermal vent environments while glycogen, a branched polysaccharide of glucose, can serve as a storage molecule for thermophilic archaea (reviewed in (151, 152)). A gene cluster encoding a glycogen synthase, alpha-amylase,galactose-1-phosphate-uridylyltransferase, amylopullanase (type II), and a phosphomannomutase was found in the genome (peg.2499-2503, respectively) in addition to a glucoamylase (peg.1002). The type II pullanase would be sufficient to degrade both the alpha-1,6 and alpha-1,4 glucosidic bonds present within starch and glycogen (151). In combination, these enzymes could serve to hydrolyze glycogen to glucose. Available glycogen could thus provide a source of glucose in the Bag City, and could be degraded to support the production of the EPS bags (66) found at the site.

G. ehrlichii was also isolated as the first member of the *Geobacteraceae* able to catabolize amino acids to support growth (66). Free amino acids are commonly present in hydrothermal vent sites and provide a source of carbon, nitrogen, and energy if they are able to be degraded (59, 153, 154). Anaerobic bacteria have been studied for decades for their ability to degrade amino acids (155). This provides a sufficient pool of knowledge to investigate the ability of *G. ehrlichii* to utilize amino acids. Within the genome of *G. ehrlichii* are four gene clusters encoding ABC transporters for branched-chain amino acids (peg.1013-1018, peg.1724-1729, peg.2177-2181, and peg.2535-2539). Two copies of a branched-chain amino acid aminotransferase (peg.1029 and peg.2465) and one gene cluster containing a branched-chain keto acid dehydrogenase (peg.2084-2086) were also identified within the genome. In addition to these enzymes, a D-amino

acid dehydrogenase is required for the primary pathway for branched-chain amino acid hydrolysis. However, a D-amino acid dehydrogenase was not found in the genome. Yet, additional proteins are encoded within the genome to enable the degradation of leucine, isoleucine, and valine. Additionally, genes for glycine and serine utilization were identified by the annotation server. The combined effort of these proteins likely contribute to the ability of *G. ehrlichii* to couple the oxidation of these amino acids to the reduction of Fe(III) oxides.

The predominance of *Geobacteraceae* species in anaerobic environments is partially attributed to their ability to fully oxidize acetate to CO_2 and couple this to the reduction of metals (156). This complete oxidation, which is conserved in the *Geobacteraceae* yet absent in a number of closely related bacteria, is enabled by the complete TCA cycle in these organisms and the acquisition of a eukaryotic citrate synthase (156). The genome annotation suggests that *G. ehrlichii* strain SS015 contains a complete TCA cycle (Figure 2.5). Pyruvate can be decarboxylated to acetyl-CoA by a pyruvate dehydrogenase protein (peg.740-741). Next, acetyl-CoA and oxaloacetate are condensed into citrate by a citrate synthase (peg.1329) which, in *G. ehrlichii* strain SS015, is annotated as a Citrate Synthase (SI) and matches closely to the eukaryotic citrate synthase proteins present within *Geobacteraceae* genomes (156). Several aconitate hydratase proteins, for the isomerization of citrate to D-isocitrate, were identified (peg.1005, peg.2651, and peg.2824). Blasting the acontitate hydratase 1 and 2 (YP_006889862.1 and ADI84496.1, respectively) from *G. sulfurreducens* provided top hits to peg.2651 and peg.2824 respectively, and thus the functionality of the other putative aconitate hydratase (peg.1005) is unclear. Following the production of D-isocitrate, an isocitrate dehydrogenase (peg.2812) is expected to produce alpha-ketoglutarate. Alpha-ketoglutarate is then decarboxylated to succinyl-CoA by an alpha-ketoglutarate dehydrogenase (peg.116-117). Succinyl-CoA is next converted into succinate by a succinyl-CoA synthetase (peg.374-375) and next dehydrogenated to fumarate by a succinate dehydrogenase (peg.2927-2929). Malate is then produced by a fumarate hydratase (peg.1890) and, subsequently, oxaloacetate by a malate

dehydrogenase (peg.2810). Additionally, a NADP-dependent malic enzyme (peg.1602), a pyruvate decarboxylase (peg.2794), and a phosphoenolpyruvate carboxykinase (peg.483) were annotated in the genome. Thus, *G. ehrlichii* strain SS015 encodes a complete TCA cycle in addition to the eukaryotic citrate synthase, a trademark of the *Geobacteraceae*.

An incomplete pentose phosphate pathway is present in the genome of *G. ehrlichii* strain SS015. Lacking, by annotation and homology searches from related organisms, are all genes which would be used in the oxidative phase of the pathway including a glucose-6-phosphate dehydrogenase, a glucolactonase, and a 6-phosphogluconate dehydrogenase. This lack of the oxidative phase is conserved in a majority of the *Geobacteraceae* (77), indicating that the absence of these genes is not an artifact of the assembly. Yet, a near complete non-oxidative phase is encoded within the genome. A ribulose-5-phosphate isomerase (peg.1302), ribulose-phosphate 3-epimerase (peg.387), transketolase (peg.913), and a transaldolase (peg.373) were annotated. Thus, it appears as though the non-oxidative phase of the pentose phosphate pathway is likely functional and would permit the biosynthesis of necessary amino acids.

2.7.3 *Utilization of sulfur-containing compounds*

Unlike the majority of the *Geobacteraceae* (73), but common within the *Desulfuromonadales* (141), is the inability of *G. ehrlichii* strain SS015 to use sulfate as a terminal electron acceptor (66). Thus, an examination of both the assimilatory and dissimilatory pathways was performed to determine why *G. ehrlichii* strain SS015 is unable to use sulfate. Sulfate is initially brought into the cell by two putative sulfate permease proteins (peg.3037-38) and subsequently activated to APS by a sulfate adenylyltransferase protein. Two copies of an annotated sulfate adenylyltransferase subunit 1/adenylylsulfate kinase were identified within the genome (peg.2438 and peg.564) and two copies of the second subunit of the adenylyltransferase were also identified (peg.736 and peg.3064). APS can then proceed to sulfite and AMP or to PAPS. APS can presumably be phosphorylated to PAPS via the previously mentioned hybrid proteins containing adenylylsulfate kinase activity (peg.564 and peg.2438). Interestingly, the

generation of sulfite during either pathway is likely catalyzed by a bifunctional gene at peg.2029. This gene is annotated as a phosphoadenylyl-sulfate reductase [thioredoxin] / adenylyl-sulfate reductase [thioredoxin] and thus likely serves to take both APS and PAPS to sulfite, an enzymatic process that has been characterized in other organisms (157). Sulfite is next reduced to sulfide by a sulfite reductase. Peg.2567 is annotated as both the alpha and beta subunits of a dissimilatory sulfite reductase while an additional, assimilatory, ferredoxin--sulfite reductase can be found at peg.565. No strong hits could be found to the cytochrome c nitrite and sulfite reductase of *G. sulfurreducens* KN400 (ADI85905.1), yet a decaheme cytochrome (peg.568) is found near the previously mentioned ferredoxin--sulfite reductase and peg.569 is a lipoprotein which may similarly be involved in the reduction of sulfite. Completing the assimilatory pathway are several cysteine synthase genes (peg.566 and peg.2657), a cystathionine gamma-synthase (peg.567), and a serine acetyltransferase (peg.1893). Yet, it appears as though the genome of *G. ehrlichii* encodes most, if not all, enzymes required for dissimilatory sulfate reduction, even though this physiology has not been observed (66).

2.7.4 *Nitrogen compounds as electron acceptors*

Nitrate metabolism is known to take place in only a few *Desulfuromonadale* species including *G. metallireducens, G. lovleyi, G. argilaceus*, and *G. ehrlichii* (73, 107). *G. ehrlichii* has two nitrate/nitrite transporter genes (peg.657-58) for the uptake of nitrogenous compounds into the cell. Once in the cell, nitrate can proceed through an assimilatory or dissimilatory pathway. The assimilatory pathway results in the incorporation of nitrogen into the cell in the form of ammonium while the dissimilatory pathway is a catabolic pathway (158) where the reduction of nitrate and nitrite produce ATP (159). Dissimilatory nitrate metabolism can be split further into two pathways: denitrification and nitrate ammonification (158). Denitrification reduces nitrate in a stepwise fashion to nitrous oxide or dinitrogen while nitrate ammonification is a two-step process which reduces nitrate to nitrite, and then nitrite is subsequently reduced to ammonium (159).

Regardless of the pathway used, once nitrate has entered the cell it must first be reduced to nitrite. Nitrate reduction can be catalyzed by either NapAB or NarGHI nitrate reductase, which both require molybdenum cofactors to function (160). Based on the genome annotation, *G. ehrlichii* encodes a NarGHI gene cluster (peg. 653-656) and no NapAB genes. Nitrite then proceeds down the ammonification pathway, via NrfA, or the denitrification pathway, via NirK or NirS. Interestingly, no NrfA, NirK, or NirS genes could be found within the genome to complete the ammonification or denitrification pathway. However, two cytochrome proteins (peg.65 and peg.68) were identified near a nitrate reductase beta chain (peg. 64). Peg.65 is a member of the c3-cytochrome superfamily, the same superfamily as NrfA, and may serve a similar function.

Since nitrite is an intermediate in the production of ammonium, most dissimilatory nitrate reducing bacteria demonstrate biphasic growth when grown with nitrate as the sole electron acceptor (161). *G. ehrlichii* lacks biphasic growth when nitrate is provided as the sole electron acceptor and ammonium is accumulated in the culture vial (66). Similar behavior has been shown in another member of the *Desulfuromonadales*, *G. metallireducens* (161). It too possesses a NarGHI gene cluster, but also possesses NrfA. The lack of biphasic growth in *G. metallireducens* is thought to occur because nitrite is reduced immediately after production to avoid reaching toxic levels (161). Thus, the shared physiology and genomic data suggest a similar reasoning may function in *G. ehrlichii*. Interestingly, the nitrate reductase of *G. metallireducens* is resistant to tungstate, indicating that it lacks the conserved molybdenum cofactor (161). To provide further evidence that *G. ehrlichii* and *G. metallireducens* follow the same pathway, nitrate reduction to ammonia in the presence of tungstate must be observed in *G. ehrlichii* strain SS015.

2.7.5 *Motility and chemotaxis*

Motility has been observed in *G. ehrlichii* strain SS015 and this motility is presumed to be due to the presence of a bacterial flagellum (66). Flagellated members of the *Geobacteraceae* have been known to be chemotactic towards iron (102). Thus, I thought it important to identify genes encoding proteins involved in both flagellar assembly, motility, and finally chemotaxis within

the genome of *G. ehrlichii* strain SS015. A single, large, and nearly uninterrupted gene cluster was identified within the genome which contains an extensive number of genes involved in flagellar biosynthesis and function. This gene cluster stretches from peg.1217 to peg.1267 with a minimal number of genes not annotated as belonging to this family of proteins. A similar organization can be seen in a number of *Geobacter* species (76, 77, 80, 141).

Several gene clusters involved in chemotaxis were identified within the genome. Within these gene clusters were proteins annotated as CheA, CheB, CheC, CheD, CheR, CheW, CheX, CheY, Tsr, and several Fli genes including FliG, FliM, and FliN. The presence of multiple chemotaxis gene clusters is conserved in a number of sequenced *Geobacteraceae* species (162). Interestingly, a large chemotaxis gene cluster is found almost immediately adjacent to the flagellar cluster (peg.1269-77), a gene organization which has not been reported in the *Geobacteraceae* (162), but is present in *Pelobacter carbonolicus* (141) a member of the *Desulfuromonadales.* The conserved alpha group of chemotaxis proteins, found only within the *Geobacteraceae* (162), was not found in *G. ehrlichii*. Proteins within the alpha chemotaxis cluster from *G. sulfurreducens* (gsu0297-0293) did, however, match closely to proteins within one *G. ehrlichii* chemotaxis gene cluster (peg.1075-1086). Thus, the shared organization of these gene clusters, combined with the previously mentioned chemotaxis towards iron in flagellated mesophilic *Geobacter* species (102) may lend credence to similar strategies functioning in thermophilic environments.

2.7.6 *Fe(III) as electron acceptor*

The Bag City hydrothermal chimney is a stable diffuse vent in the southern portion of the Axial Seamount caldera and just outside of the well-studied 1998 eruption zone (28). A substantial southward flow around the Axial Seamount (106, 163) combined with hydrothermal effluent exiting the caldera via a break in the southern wall (163) likely leads to the deposition of metals at the Bag City site. Phase separation at the site, due to the Axial Seamount being a shallow system, alters the redox state, temperature, chlorinity, and pH of the efflux water and minerals within (28). Thus, the lowered pH and increase in H_2S lead to changes in mineral solubility and transport

when compared to traditional vent systems (28). Only after mixing with the surrounding seawater in the caldera will dissolved minerals, of which Fe(III) is a primary component, fall out and form metal-rich deposits (28). These environmental conditions likely enrich for microorganisms, such as *G. ehrlichii,* which are able to respire these insoluble metal oxides.

A direct-contact mechanism for Fe(III) respiration has been established in the *Geobacteraceae* and relies on the presence of a unique type IV pilus and *c*-type cytochromes (91, 164–166). Two distinct gene clusters encoding the type IV pilus and associated assembly proteins of *G. ehrlichii* strain SS015 can be found within the genome. These gene clusters are separated by a cluster of genes related to the Xap operon (discussed within 2.7.7) found in *G. sulfurreducens* (90). The first of these gene clusters is comprised of PilSe (peg.2833), PilR (peg.2834), PilY1 (peg.2838), and then PilB, PilT, PilC, PilSe, PilR, PilA, and a hypothetical protein related to the PilA-C protein found in *G. sulfurreducens* (peg.2843-49; respectively). The PilA pilin protein aligns well to homologous pilin proteins present within the *Geobacteraceae* (Figure 2.6A and 5B) and, based on a phylogenetic tree constructed using the aligned pilin sequences (Figure 2.6C), is most similar to the pilin of *G. metallireducens* (Figure 2.6 contains the references (167–169)). Following the previously mentioned extracellular polysaccharide gene cluster is another gene cluster of pilin genes comprised of PilD, a transcriptional regulator, PilM, PilN, PilO, PilP, and PilQ (peg.2860-66; respectively). Also found within the genome is an additional copy of PilB (peg.1883) and three additional copies of PilT (peg.951, peg.1637, and peg.1687). This organization, again, is similar to other sequenced members of the *Geobacteraceae* in which multiple PilT copies have been identified (76, 91).

A trademark of the *Geobacteraceae* is the extreme number of *c*-type cytochromes present within the genome of all sequenced members of the family (73). Several of these cytochromes, including PpcA, OmcS, and OmcZ have been implicated in *G. sulfurreducens* in metal respiration or in the transfer of electrons to the anode of a microbial electrochemical cell (104, 170–173). Yet, the majority of the annotated cytochromes have not been implicated in essential processes. Some

suggest that the majority of these cytochromes provide a capacitor-like ability for *Geobacteraceae* isolates to store electrons when available electron acceptors are limiting (174). Other possibilities exist such as customized cytochromes for differing electron acceptors or cytochromes poised to reduce at different voltages (175). Regardless of which reasoning is correct, the prevalence of *c*-type cytochromes within the *Geobacteraceae* is a trademark of the family (73).

G. ehrlichii strain SS015, similarly to the remainder of the *Geobacteraceae*, does contain a number of *c*-type cytochromes. 34 putative *c*-type cytochromes were identified within the genome (Table 2.7). This, while well above the number of cytochromes present in most microorganisms sequenced to date, pales in comparison to many sequenced members of the *Geobacteraceae* (73). The majority of the 34 cytochromes contain fewer than 10 heme-binding motifs while several (peg.622, peg.623, peg.810, peg.1443, peg.2155, and peg.2156) contain higher numbers (13, 10, 23, 11, 19, and 57, respectively) of heme binding motifs. Peg.2156 containing 57 heme-binding motifs, is impressive for a *c*-type cytochrome yet unremarkable within the *Geobacteraceae* where *ca.* 85 % of cytochromes are multi-heme (83). These may be too energetically taxing for *G. ehrlichii* to produce, as life at the Axial Seamount is likely nutrient-limited due to its location (106), yet their existence within the genome indicates that these heme-rich proteins are widespread within the family. *G. ehrlichii* has an average heme/cytochrome value of 7.2. This value is similar to the values reported for *G. bemidjiensis, G. metallireducens,* and *G. sulfurreducens* (73). In support of this, at least 9 cytochromes can be identified, by TMBZ-stained SDS-PAGE, in ferric citrate grown cultures both before and after shearing of outer-surface cytochromes, while 5 are predicted to be outer-membrane or surface-exposed due to their detection within the lane corresponding to the sheared fraction (Figure 2.7). These cytochromes, and those identified within the genome, could serve to reduce soluble and insoluble electron acceptors, facilitate intracellular electron transfer, and enable the capacitor-like physiology of the *Geobacteraceae*.

2.7.7 *Extracellular polymeric substances*

G. ehrlichii strain SS015 was found to express an acidic EPS when stressed by antibiotics or when cultures were incubated outside of their optimal growth temperature (66). This EPS likely contributes to the gelatinous bags which are the namesake of the 'Bag City' hydrothermal vent system and, in *G. ehrlichii*, has been linked to growth on structural Fe(III) within phyllosilicate minerals (176). In addition, the expression of an EPS matrix alongside properly anchored *c*-type cytochromes has, in *G. sulfurreducens*, been shown to be essential for growth on insoluble oxides and in microbial fuel cells (90). As *G. ehrlichii* is known to interact with insoluble Fe(III) oxides (66), it was of interest to determine if the genes encoding the EPS of *G. ehrlichii* were similar to those of *G. sulfurreducens*.

Using the XapA-K genes from *G. sulfurreducens* as BLAST queries against the *G. ehrlichii* genome I was able to identify a gene cluster (peg.2850-2859) which is likely involved in EPS biosynthesis. As in *G. sulfurreducens* (76, 90), these genes follow a pilus-assembly gene cluster (peg.2833-2849) and, in addition, are followed by an additional cluster of non-redundant pilus-assembly genes (peg.2860-66) both of which have been discussed previously. Strong homologues could be found to XapA-E (peg.2853, peg.2850, peg.2851, peg.2852, and peg.2853; respectively). Two additional glycosyltransferase proteins (GT-B clan) (peg.2855-56), a membrane protein involved in the export of O-antigen/techoic acid/lipoteichoic acids (peg.2857), and an ADP-heptose--lipooligosaccharide heptosyltransferase II (peg.2859) were also found within the gene cluster. Thus, this EPS cluster may serve a similar purpose to that of the Xap operon in *G. sulfurreducens* and permit the anchoring of essential *c*-type cytochromes into an electroactive extracellular matrix to facilitate electron transfer to insoluble iron oxides (90).

2.8 *Conclusions*

G. ehrlichii strain SS015 is the only member of the *Desulfuromonadales* available in pure culture. This order contains the *Geobacteraceae* family, which has recently been proposed to be

split into the *Geobacteraceae* and the *Desulfuromonadaceae*, and the *Pelobacteraceae*. Genome sequences are available for a surprising number of members of these families, considering the lack of direct human impact these environmental isolates have. Yet, their use in bioelectronics, bioremediation, nanotechnology, and green energy has promoted great interest in the order. To date, members of the *Desulfuromonadales* have been isolated able to grow at psychrophilic, mesophilic, and thermophilic temperatures and, with the inclusion of the *Geoalkalibacter spp.* available in pure culture, a range of pH values. Thus, these extremophilic members of the family can provide interesting model systems to examine dissimilatory iron reduction under 'atypical' environmental conditions. *G. ehrlichii*, for example, was isolated as the first member of the family *Geobacteraceae* able to grow optimally at thermophilic temperatures. I have attributed this ability to an optimization of amino acid usage to function at elevated temperatures, a trend which is reversed in the psychrophile *G. electrodiphilus*. In addition, I have identified a gene cluster implicated in EPS production and secretion which may be used in a similar way to the Xap operon of *G. sulfurreducens.* Finally, I have identified numerous *c*-type cytochromes, a flagellum and associated genes to enable chemotaxis, and a type IV pilin and associated assembly genes within the genome of *G. ehrlichii* which are undoubtedly involved in its respiratory ability to grow on soluble and insoluble Fe(III) oxides. *G. ehrlichii* shares a number of physiological and genetic characteristics with the *Geobacteraceae*; however, its recent classification into the *Desulfuromonadaceae* is upheld within this work by the absence of an alpha chemotaxis gene cluster in *G. ehrlichii* and its phylogenetic position within the *Desulfuromonadales*. While the presence of genes of interest within the genome can be analyzed, any genes found lacking within this report may be artifactual due to the incomplete nature of the genome assembly. Efforts will continue in order to rectify this in the future to provide a high-quality closed genome for the only thermophilic *Desulfuromonadales* member available in pure culture.

CHAPTER 3. THE COMPLETE GENOME SEQUENCE AND EMENDATION OF THE HYPERTHERMOPHILIC, OBLIGATE IRON-REDUCING ARCHAEON *GEOGLOBUS AHANGARI* STRAIN 234^T

3.1 *Abstract*

Geoglobus ahangari strain 234^T is an obligate Fe(III)-reducing member of the *Archaeoglobales*, within the archaeal phylum *Euryarchaeota*, isolated from the Guaymas Basin hydrothermal system. It grows optimally at 88 °C by coupling the reduction of Fe(III) oxides to the oxidation of a wide range of compounds, including long-chain fatty acids, and also grows autotrophically with hydrogen and Fe(III). It is the first archaeon reported to use a direct contact mechanism for Fe(III) oxide reduction, relying on a single archaellum for locomotion, numerous curled extracellular appendages for attachment, and outer-surface heme-containing proteins for electron transfer to the insoluble Fe(III) oxides. Here I describe the annotation of the genome of *G. ahangari* strain 234^T and identify components critical to its versatility in electron donor utilization and obligate Fe(III) respiratory metabolism at high temperatures. The genome comprises a single, circular chromosome of 1,770,093 base pairs containing 2,020 protein-coding genes and 52 RNA genes. In addition, emended descriptions of the genus *Geoglobus* and species *G. ahangari* are described.

3.2 *Keywords*

Euryarchaeota; *Archaeoglobales;* hydrothermal vent; Guaymas Basin; Fe(III) respiration; extracellular electron transfer; autotroph.

3.3 *Introduction*

Geoglobus ahangari strain 234^T is the type strain and one of only two known members of the *Geoglobus* genus within the order *Archaeoglobales* and the family *Archaeoglobaceae*. It is an

obligate Fe(III)-reducing archaeon isolated from the Guaymas Basin hydrothermal system and grows at temperatures ranging from 65-90 °C, with an optimum at about 88°C (52). It was the first isolate in a novel genus within the *Archaeoglobales* and the first example of a dissimilatory Fe(III)-reducer able to grow autotrophically with H_2 (52), a metabolic trait later shown to be conserved in many hyperthermophilic Fe(III) reducers (177). *G. ahangari* can also couple the reduction of soluble and insoluble Fe(III) acceptors to the oxidation of a wide range of carbon compounds including long-chain fatty acids such as stearate and palmitate, which were previously not known to be used as electron donors by archaea (52). It was also the first hyperthermophile reported to fully oxidize acetate to CO_2, a metabolic function once thought to occur solely in mesophilic environments (112). Unlike the other two genera in the order *Archaeoglobales* (*Archaeoglobus* and *Ferroglobus*), which can utilize acceptors such as sulfate and nitrate (52, 53, 178–183), the two cultured members of the genus *Geoglobus* can only use Fe(III) as an electron acceptor (52, 178). The obligate nature of Fe(III) respiration in *Geoglobus* spp. makes the genus an attractive model to gain insights into the evolutionary mechanisms that may have led to the loss and/or gain of genes involved in the respiration of iron and other electron acceptors such as sulfur- and nitrogen-containing compounds within the *Archaeoglobales*.

G. ahangari strain 234^T also serves as a model organism for mechanistic studies of iron reduction at high (>85 °C) temperatures. Dissimilatory Fe(III) reduction has been extensively studied in mesophilic bacteria (reviewed in references (71, 84)). By contrast, little is known about the mechanisms that allow (hyper)thermophilic organisms to respire Fe(III) acceptors (113, 114, 139, 184–186). As previously observed in the thermophilic Gram-positive bacterium *Carboxydothermus ferrireducens* (114), *G. ahangari* also needs to directly contact the insoluble Fe(III) oxides to transfer respiratory electrons (139). In *G. ahangari,* cells are motile via a single archaellum, which could help in locating the oxides, and also express numerous curled extracellular appendages, which bind the mineral particles and position them close to heme-containing proteins on the outer surface of the cell to facilitate electron transfer (139). A direct

contact mechanism such as this is predicted to confer on these organisms a competitive advantage over other organisms relying on soluble mediators such as metal chelators (97) and electron shuttles (187, 188), which are energetically expensive to synthesize and are easily diluted or lost in the environment once excreted (102). This is particularly important in hydrothermal vent systems such as the Guaymas basin chimney where *G. ahangari* strain 234^T was isolated, as vent fluids in these systems can flow through at rates as high as 2 m/s (109). Here, I report the complete genome sequence of *G. ahangari* strain 234^T and summarize the physiological features that make this organism a good model system to study Fe(III) reduction in hot environments and to gain insights into the evolution of Fe(III) respiration in the family *Archaeoglobales*.

3.4 *Organism information*

3.4.1 *Classification and features*

Geoglobus ahangari strain 234^T is a euryarchaeon originally isolated from samples obtained from a hydrothermal chimney located within the Guaymas Basin (27° N, 111° W) at a depth of 2,000 m (52). The sequence of the single 16S rRNA gene found in its genome was 99% identical to the previously published 16S rDNA sequence (*AF220165*). The full length 16S rRNA gene (1,485 bp) was used to construct a phylogenetic tree in reference to 16S rRNA gene sequences from other hyperthermophilic archaea using two thermophilic bacteria ("*Aquifex aeolicus"* and *Pseudothermotoga thermarum*) as outgroups (Figure 3.1). The closest known relative was *Geoglobus acetivorans* (97% identical), the only other known member of the *Geoglobus* genus, which also is available in pure culture (178). Closest relatives outside the genus were other hyperthermophilic archaea within the family *Archaeoglobaceae* such as the sulfate-reducing *Archaeoglobus* species *A. fulgidus* and *A. profundus* (97% and 93% identical, respectively) and *Ferroglobus placidus* (94% identical), which can reduce Fe(III), thiosulfate, and nitrate (112, 179).

Cells of *G. ahangari* strain 234^T are regular to irregular cocci, 0.3 to 0.5 µm in diameter, and usually arranged as single cells or in pairs (Figure 3.2 and Table 3.1) (52). Cells are motile via a single archaellum (52), but also produce abundant extracellular curled filaments when grown with both soluble and insoluble Fe(III) (139). Though optimum growth occurs at *ca.* 88 °C, growth is observed between 65 °C and 90 °C (52). Furthermore, growth was supported at pH values between 5.0 and 7.6, with an optimum at pH 7.0, and with NaCl concentrations ranging from 9 to 38 g/L, with an optimum at 19 g/L (52).

A distinctive feature of the metabolism of *G. ahangari* strain 234^T is its obligate nature of Fe(III) respiration, with both soluble and insoluble Fe(III) species supporting growth but the insoluble electron acceptor being preferred (52). The obligate nature of Fe(III) reduction contrasts with the wide range of electron donors that *G. ahangari* can oxidize (52). Acetate, alongside a number of other organic acids (such as propionate, butyrate, and valerate), several amino acids, and both short-chain and long-chain fatty acids were completely oxidized to CO_2 to support growth during Fe(III) respiration (52, 112). Furthermore, *G. ahangari* strain 234^T was also able to grow autotrophically with H_2 as the sole electron donor and Fe(III) as the electron acceptor (52). The main physiological features of the organism are listed in Table 3.1.

3.5 *Genome sequencing and annotation*

3.5.1 *Genome project history*

Based on its unique physiological characteristics (52) and use as a model system for mechanistic investigations of Fe(III) reduction by hyperthermophilic archaea (139), *G. ahangari* strain 234^T was selected for sequencing. Insights from its genome sequence and annotation provide greater understanding of the evolution of respiratory metabolisms in the *Archaeoglobales*, and, in particular, about hyperthermophilic iron reduction within the *Archaea*. The genome project information is listed in the Genomes OnLine Database (Gp0101274) (189) and the complete

genome sequence has been deposited in GenBank (CP011267). A summary of the project information is shown in Table 3.2.

3.6 *Growth conditions and genomic DNA preparation*

G. ahangari strain 234^T was from our private culture collection and is available at the Deutsche Sammlung von Mikroorganismen und Zellkulturen (*DSM-27542*), the Japan Collection of Microorganisms (*JCM 12378*), and the American Type Culture Collection (*BAA-425*). The strain was grown in marine medium (52) with 10 mM pyruvate as the electron donor and 56 mM ferric citrate as the electron acceptor. Cultures were incubated under a N_2:CO_2 (80:20 %, v/v) atmosphere at 80 °C or 85 °C in the dark. Strict anaerobic techniques were used throughout the culturing and sampling experiments (125).

gDNA was extracted as previously reported for *F. placidus* (190). Alternatively, cells were lysed with an SDS-containing lysis buffer (5% SDS, 0.125 M EDTA, 0.5 M Tris, pH 9.4), as reported elsewhere for the preparation of whole cell extracts from *G. ahangari* (139), and gDNA was extracted using the MasterPure™ DNA Purification Kit (EPICENTRE® Biotechnologies), according to the manufacturer suggested guidelines.

3.7 *Genome sequencing and assembly*

The finished genome of *G. ahangari* strain 234^T (CP011267) was generated from Illumina (127) draft sequences generated independently at the Research Support and Training Facility at Michigan State University, the Deep Sequencing Core Facility at the University of Massachusetts Medical School, and the Genomics Resource lab at the University of Massachusetts-Amherst. Table 3.2 presents the project information.

The sequencing project at the University of Massachusetts facilities used gDNA suspended in 3 ml of sonication buffer (4.95 % glycerol, 10 mM Tris-HCl (pH 8.0), 1 mM EDTA) and sonicated for 10 min (2 min on, 30 sec off) using a 550 Sonic Dismembrator (Fisher Scientific).

The samples were then dispensed as equal volumes into 4 tubes and mixed with 150 µl TE buffer (10 mM Tris-HCl (pH 8.0), 1 mM EDTA), 100 µl ammonium acetate (5 M), 20 µl glycogen (5 mg/ml), and 1 ml of cold (-20 °C) isopropanol. Nucleic acids were precipitated at -30 °C for 1 h, as previously described (190) and suspended in EB buffer (Qiagen) before separating the DNA fragments in the sample by agarose gel electrophoresis. DNA fragments between 300-500 bp were then purified with the QiaQuick Gel Extraction Kit (Qiagen). All steps involved in end repair, 3' adenylation, adaptor ligation, and purification of Illumina products were performed using reagents supplied by the TruSeq DNA Sample Prep Kit (Illumina). This resulted in the construction and sequencing of five independent 100 bp paired-end Illumina shotgun libraries which generated 7,970,036, 7,970,182, 7,973,896, 7,966,671 and 3,144,785 reads totaling 3.50 Gbp. The Illumina draft sequences were assembled *de novo* with SeqMan NGen (DNASTAR) and Velvet (191) (version 1.2.10) and optimized with VelvetOptimiser (version 2.2.5). Reads were down-sampled to 500x coverage to increase the efficacy of the Velvet assembler while the complete depth of reads was used to verify the final genome assembly.

A total of 1,780,565 bp were assembled into 25 scaffolds ranging in size from 207 bp to 510,180 bp. The scaffolds were then connected by adaptor-PCR as previously described (192). *G. ahangari* gDNA was subsequently digested separately by four different restriction enzymes (*Eco*RI, *Bam*HI, *Bcl*I, and *Sal*I). After a 1.5-h incubation at 37 °C (or 50 °C for *Sal*I), the restriction digests were separated by agarose gel electrophoresis and fragments between 5-10 kb were isolated and purified with the QiaQuick gel extraction kit (Qiagen). Adaptor sequences with 3' overhangs generated by *Eco*RI, *Bam*HI, *Bcl*I, and *Sal*I at the phosphorylated 5' ends were then ligated with T4 DNA ligase to the fragments purified from the restriction digests of *G. ahangari* gDNA. The adaptor sequences used were: *Eco*RI adaptor AATTCCCTATAGTGAGTCGTATTAAC** (phosphorylated at 5' end); *Bcl*I and *Bam*HI adaptor GATCCCCTATAGTGAGTCGTATTAAC**; and finally the *Sal*I adaptor TCGACCCTATAGTGAGTCGTATTAAC**. Further assembly was performed with SeqMan Pro

(DNASTAR) and primers were designed targeting the 3' and 5' ends of the 25 scaffolds. The adaptor ligations were diluted 100-fold and 1 µl of the diluted sample was used in PCR reactions with AccuTaq™ LA DNA Polymerase (50 µl total volume) according to manufacturer specifications (Sigma-Aldrich). Fifty reactions were performed with *G. ahangari*-specific primers designed from the various Illumina scaffolds and a non-phosphorylated primer that complemented the adaptor sequence on the gDNA (GTTAATACGACTCACTATAGGG). All PCR products were purified with the Qiagen PCR purification kit and sent for sequencing at the University of Massachusetts (Amherst) sequencing facility. This process was repeated until a single contig was obtained using SeqMan Pro assembly software.

The assembly was then verified against a second, independent genome assembly generated at Michigan State University. Extracted gDNA was used to construct a single Illumina shotgun library using the Illumina DNAseq Library Kit, which was sequenced in two 150 bp paired-end runs with an Illumina MiSeq at the Research Support and Training Facility at Michigan State University. The sequencing project generated 1,233,811 and 796,056 reads totaling 304.5 Mbp. Reads were quality trimmed using a combination of fastq-mcf (193) (ea-utils.1.1.2-537, using default parameters) and ConDeTri (194) (v2.2, using default parameters with the exception of hq=33 and sc=33) to remove low-quality reads and over-represented sequences. High-quality paired and unpaired reads were assembled using Velvet (191) (v1.2.08 using default parameters and a kmer value of 63) to generate a new assembly (1.77 Mbp, 51 contigs ≥ 1,000 bp, and an N75 of 37,520 bp). The second assembly was then compared to the primary assembly to identify errors and low-coverage regions, which were subsequently resolved by PCR-amplifying and sequencing the regions of interest.

3.7.1 *Genome annotation*

Initial genome annotation was performed by the RAST server (131), the IGS Annotation Engine (195) at the University Of Maryland School Of Medicine, and the IMG-ER platform (196). The annotations were compared to manual annotations performed using GLIMMER (197) for

gene calls and DELTA-BLAST analysis to identify conserved domains and homology to known proteins. EC numbers and COG categories were determined with a combination of DELTA-BLAST analysis of each annotated gene and the IMG-ER platform. Pseudogenes were identified using the GenePRIMP pipeline (132). The data were used to create a consensus annotation before the final assembled genome was uploaded onto the IMG-ER platform. IMG-ER annotations were manually curated by comparison to the consensus annotation before submitting the final genome annotation.

Potential *c*-type cytochromes were selected based on the presence of *c*-type heme binding motifs (CXXCH) within the amino acid sequence as previously described (89). Predicted subcellular localization and the presence of signal peptides and/or an N-terminal membrane helix anchor (89) was investigated by PsortB (198), PRED-TAT (199), TMPred (200), and the TMHMM Server (v. 2.0) (135). Putative *c*-type cytochromes were then examined by BLAST analysis to determine homology to known *c*-type cytochromes in the NCBI database. The molecular weight of putative *c*-type cytochromes was estimated with the ExPASy ProtParam program (137). The weight of the signal peptide was then subtracted from the predicted weight and 685 daltons were added for each heme-binding motif to estimate the molecular weight of the mature cytochrome. The predicted molecular weight values and subcellular localization of the mature cytochromes were compared to the masses reported for mature heme-containing proteins present in whole cells and outer-surface protein preparations of *G. ahangari* (139).

3.8 *Genome properties*

The genome of *G. ahangari* strain 234^T comprises one circular chromosome with a total size of 1,770,093 bp and does not contain any plasmids. The genome size is within the range of those reported for other members of the *Archaeoglobales* [15, 33, 50–52, and NC_015320.1]. The mol percent G+C is 53.1 %, which is lower than the 58.7 % estimated experimentally via HPLC (52). Out of the total 2,072 genes annotated in the genome, 52 were identified as RNA

genes and 2,020 as protein-coding genes (Table 3.3). There are 47 pseudogenes, comprising 2.3 % of the protein-coding genes. Furthermore, 76.5 % of the predicted genes (1,557) are represented by COG functional categories. Distribution of these genes and their percentage representation are listed in Figure 3.3 and Table 3.4.

The preferred start codon is ATG (83.8 % of the genes), followed by GTG (10.4 %) and TTG (5.7 %). This distribution is similar to the start codon representation of the other member of the *Geoglobus* genus, *G. acetivorans* (79.4 % ATG, 11.6 % GTG, and 9.0 % TTG) (184) and the closely related archaeon *F. placidus* (82.5 % ATG, 10.2 % GTG, 6.1 % TTG, and 1.3 % other) (190). There is one copy of each of the rRNA genes but the genes are located in two different regions of the genome: the 16S rRNA (GAH_00462) and 23S rRNA (GAH_00460) genes are in the same gene cluster and separated by a span of 139 bp encoding a single tRNA whereas the 5S rRNA (GAH_02069) is located 205,273 bp away in a region with genes coding for proteins with functions unrelated to ribosome function and biogenesis.

Almost all origins of DNA replication identified in *Archaea* to date are located in close proximity to genes coding for a homologue of the eukaryotic Cdc6 and Orc1 proteins (204). Interestingly, I identified two genes encoding Orc1/Cdc6 family replication initiation proteins (GAH_00094 and GAH_00965) in the genome of *G. ahangari*, thus raising the possibility that the genome contains more than one functional origin of replication. Many archaeal replication origins consist of long intergenic sequences upstream of the *cdc6* gene containing an A/T-rich duplex unwinding element flanked by several conserved repeat motifs known as ORBs (205). A specific ORB could not be identified in the genome when compared to other archaeal origins of replication available in the DoriC database (206). However, the 320-bp long region upstream of GAH_00965, one of the Orc1/Cdc6 family replication initiation proteins, contains a long (111 bp) non-coding intergenic region with one AT-rich stretch and 8 direct repeats (3 TCGTGG, 3 CGTGGTC, and 2 GGGGATTA), which could function as a replication origin. Furthermore, the 580-bp region directly upstream of the other Orc1/Cdc6 family replication initiation protein (GAH_00094) lacks a non-

coding intergenic region and/or AT-rich span but contains 8 direct repeats (2 GGTTGAGAAG, 3 TGAGAAG, and 3 AACATCCCG) and several “G-string” elements analogous to *ori* sites reported for haloarchaeal species (207).

3.9 *Insights from the genome*

3.9.1 *Autotrophic growth with H_2 as electron donor*

G. ahangari strain 234^T was the first dissimilatory Fe(III)-reducing hyperthermophile shown to grow autotrophically with H_2 as an electron donor (52). In its genome, I identified genes required for the two branches of the reductive acetyl-CoA/Wood-Ljungdahl pathway (208–211), which other members of the Euryarchaeota (212), including most members of the *Archaeoglobales* (181, 203, 213–216), use for carbon fixation. A bifunctional carbon monoxide dehydrogenase/acetyl-CoA synthase complex (encoded by GAH_01139-01144, and two additional copies of the beta and maturation factors encoded by GAH_00919 and GAH_00306, respectively) are present within the genome, which could initiate carbon fixation. The bifunctional nature of this enzyme also allows it to link methyl and carbonyl branches and enable acetyl-CoA biosynthesis, as reported for methanogenic archaea (217). Complete enzymatic pathways for alternative means of carbon fixation were not identified.

The genome of *G. ahangari* also contains 29 genes encoding hydrogenase subunits, maturation proteins, and a cluster of genes (*hypA*, *hypB*, *hypC*, *hypD*, and *hypE*) involved in biosynthesis and assembly of Ni-Fe hydrogenases (GAH_00190-00195). Genes coding for the large, small, and *b*-type cytochrome subunits of a Ni-Fe hydrogenase I protein (GAH_00910-00912) were identified in the genome. I also found a gene cluster (GAH_00337-00347) encoding all subunits of a NADH-quinone oxidoreductase, which transfers electrons to the quinone membrane pool and may function as the primary generator of the proton-motive force (201). Another large cluster of hydrogenase genes (GAH_02036-02044) codes for all coenzyme F_{420} hydrogenase subunits and proteins involved in recycling coenzyme F_{420}, thus replenishing the

cofactor for the reductive acetyl-CoA pathway (216, 218–220). The presence of multiple hydrogenases is not unusual in iron-reducing microorganisms and allows them to diversify the paths used to transfer electrons derived from the oxidation of H_2 to their acceptors (221).

Autotrophic growth in methanogens can also be supported using reduced coenzyme F_{420} as an electron donor to produce methane (222). The distinctive fluorescence emission from this coenzyme has been detected in members of the *Archaeoglobales* (53, 181, 182, 213, 215) but not in the iron-respiring *F. placidus* (179) or in *G. ahangari* (52). Yet, the *G. ahangari* genome contains genes for all coenzyme subunits of the proteins coenzyme F_{420}-reducing hydrogenase (GAH_00337 and GAH_02036-02038), coenzyme F_{420}-dependent N^5,N^{10}-methylene tetrahydromethanopterin reductase (GAH_01605, GAH_01835), and F_O synthase (CofGH) (GAH_00662, GAH_00663) (223). Furthermore, although *G. ahangari* cannot produce methane when growing autotrophically (52), its genome codes for nearly all enzymes responsible for the reduction of CO_2 to methane (209). Similar to *A. fulgidus*, *F. placidus*, *A. sulfaticallidus*, and *G. acetivorans*, *G. ahangari* has genes encoding all proteins involved in the formation of 5-methyl-tetrahydromethanopterin and a gene coding for one of the 8 subunits (MtrH) of the enzyme responsible for the transfer of a methyl group to coenzyme M (GAH_01245). Yet, the genome is missing all four genes required for a functional coenzyme M reductase, the enzyme responsible for the final step of methane production by methanogenic archaea (209). The fact that *Archaeoglobale* genomes have nearly all of the genes involved in methanogenesis and the high level of homology that exists between genes from the reductive acetyl-CoA pathway in both *Archaeoglobales* and the methanogenic archaea suggests that the *Archaeoglobales* may have evolved from a methanogenic archaeon that lost its ability to reduce CO_2 and produce methane over time.

3.9.2 *Central metabolism*

Heterotrophic growth in *G. ahangari* is supported by a wide range of organic carbon compounds (52), which serve as electron donor for respiration while also providing carbon for

assimilation in the central pathways. Similar to other hyperthermophilic archaeal species (224), the *G. ahangari* genome contains a modified Embden-Meyherhof-Parnas glycolytic pathway (Figure 3.4). The initial step of glycolysis (glucose phosphorylation to glucose 6-phosphate) is carried out by an ATP-dependent archaeal hexokinase (GAH_00546) belonging to the ROK family of proteins. A gene coding for the phosphoglucose isomerase enzyme, which catalyzes the next reaction in the pathway (interconversion of the aldose in glucose 6-phosphate and the ketose in fructose 6-phosphate) was also identified (GAH_01135) and was most similar to cupin-type phosphoglucose isomerases from other anaerobic *Euryarchaeota*, including *Archaeoglobus fulgidus* (224).

In *A. fulgidus*, fructose 6-phosphate is phosphorylated to fructose 1,6-bisphosphate by an ADP-dependent phosphofructokinase protein (EC:2.7.1.11) (225). However, homologs of this enzyme were not present in the genomes of *G. ahangari* or any other *Archaeoglobale* species sequenced to date. Instead, the genome of *G. ahangari* contained two genes (GAH_00966 and GAH_01843) coding for proteins with pfkB-like domains and ATP-binding sites, which are consistent with the ATP-dependent phosphofructokinases (PFK-B) of other hyperthermophilic archaea such as *Aeropyrum pernix* and *Desulfurococcus amylolyticus* (226, 227). The genome also contains two genes (GAH_00357 and GAH_01437) encoding archaeal fructose 1,6-bisphosphatases, which catalyze the reverse reaction during gluconeogenesis but can also supply fructose 1,6-bisphosphate to the glycolytic pathway from dihydroxyacetone phosphate and *D*-glyceraldehyde 3-phosphate (228). Furthermore, a triosephosphate isomerase (GAH_00576) was identified in the genome to catalyze the isomerization of dihydroxyacetone phosphate to D-glyceraldehyde 3-phosphate. Alternatively, GAH_01502 and GAH_01751, which encode proteins homologous to archaeal type class I fructose 1,6-bisphosphate aldolase proteins, could catalyze the conversion of fructose 1,6-bisphosphate into *D*-glyceraldehyde 3-phosphate.

The next steps in the pathway involve the oxidation of *D*-glyceraldehyde 3-phosphate and formation of 3-phosphoglycerate. The *G. ahangari* genome contains a homolog (GAH_00413) of

a GAPOR, which in *A. fulgidus* and many other archaeal species catalyzes the irreversible oxidation of D-glyceraldehyde-3-phosphate to 3-phospho-D-glycerate bypassing the formation of the intermediate 1,3-bisphospho-*D*-glycerate (224). In addition, the genome of *G. ahangari* contains genes coding for an archaeal specific type II glyceraldehyde-3-phosphate dehydrogenase (GAH_01734) and a phosphoglycerate kinase (GAH_01571), which could catalyze the formation of 3-phosphoglycerate via the 1,3-diphosphoglycerate intermediate. These two enzymes are unidirectional and involved in formation of glyceraldehyde-3-phosphate from 3-phosphoglycerate during gluconeogenesis in most hyperthermophilic archaea (224).

As in *A. fulgidus* (229), *G. ahangari* has 2 genes coding for cofactor-independent phosphoglycerate mutase proteins (GAH_00739 and GAH_01116), which can catalyze the interconversion of 3-phospho-*D*-glycerate to 2-phospho-*D*-glycerate. Phosphoenolpyruvate is then formed by an enolase protein (GAH_00972), which is subsequently dephosphorylated to pyruvate by pyruvate kinase. Although a gene coding for the well-characterized pyruvate kinase protein is present in the close relative *F. placidus* (Ferp_0744), homologs were not identified in *G. ahangari* or any other *Archaeoglobale* species. Instead, the genomes of *G. ahangari* (GAH_00154) and all other sequenced *Archaeoglobales* species contain genes encoding PK_C superfamily proteins [15, 33, 50–52, and NC_015320.1], which have pyruvate kinase and alpha/beta domains and are homologous to an *A. fulgidus* enzyme with pyruvate kinase activity *in vitro* (230). Pyruvate can then be converted into acetyl-CoA via pyruvate synthase (GAH_01438-01441 and GAH_02021-02024).

As in the close relative *F. placidus* (190), *G. ahangari* lacks genes from the oxidative pentose phosphate pathway but is predicted to circumvent this limitation (231) via the use of a complete RuMP pathway (GAH_00051 and GAH_01859). The latter results in the accumulation of formaldehyde (231), which in *G. ahangari* could be removed by formaldehyde-activating enzymes (GAH_00575 and GAH_00673). Ribulose 5-phosphate formed in the RuMP pathway could then be converted into ribose-5-phosphate by a ribose 5-phosphate isomerase

(GAH_00131), and then into PRPP by ribose-phosphate pyrophosphokinase enzymes (GAH_00743 and GAH_00557). This supplies PRPP to various anabolic pathways such as the biosynthesis of histidine and purine/pyrimidine nucleotides.

Similar to other *Archaeoglobale* species, a complete TCA cycle is present within the *G. ahangari* genome. All enzymes involved in the formation of oxaloacetate from acetyl-CoA (GAH_00258, GAH_01703, GAH_01110, GAH_02012-02013, GAH_00784-00784, GAH_00779-00782, GAH_00526-00527, and GAH_00039), including putative aconitase proteins (GAH_00857-00858) (232), were identified in the genome. Also present is a phosphoenolpyruvate carboxylase (GAH_01652), which could catalyze the reversible carboxylation of phosphoenolpyruvate to oxaloacetate, a precursor metabolite of many amino acids.

3.9.3 *Fatty acids as electron donors*

G. ahangari strain 234^T was the first hyperthermophile reported to completely oxidize long-chain fatty acids anaerobically, an unsuspected capability of hyperthermophilic microorganisms prior to this discovery (52). Long-chain fatty acids are abundant in sedimentary environments where they accumulate as byproducts of the hydrolysis of complex organic matter and the anaerobic degradation of alkanes (233, 234). Long-chain fatty acids are also major components of crude oil (235), which is often present in environments inhabited by *Archaeoglobale* species (236). Consistent with the ability of *Archaeoglobale* members to oxidize long-chain fatty acids, the genomes of *G. ahangari* and other members of the family (*F. placidus*, *G. acetivorans*, *A. fulgidus*, and others) contain a large number of genes coding for β-oxidation pathway enzymes (184, 190, 201). The *A. fulgidus* genome, for example, contains 57 genes encoding the 5 core proteins (discussed below) involved in β-oxidation (201). All of these genes were used as BLAST queries against the genomes of *F. placidus* (190), *G. acetivorans* (184), and *G. ahangari* and identified 39 homologous proteins in the genomes of the *F. placidus* and *G. acetivorans* and 32 in the genome of *G. ahangari*.

Fatty acid degradation in the *Archaeoglobales* is thought to occur in a manner similar to bacteria and mitochondria (201), with the initial step involving activation of a long chain fatty acid to a fatty acyl CoA by a fatty acyl CoA synthetase/ligase. I identified seven genes in *G. ahangari* coding for fatty acid CoA synthetase proteins (GAH_00420, GAH_00623, GAH_01111, GAH_01124, GAH_01769, GAH_01899, and GAH_02051). The next step in the pathway involves the oxidation of the fatty acyl-CoA to a trans-2-enoyl-CoA by acyl-CoA dehydrogenase proteins, which in *G. ahangari* are putatively encoded by 11 genes (GAH_00179, GAH_00421, GAH_00484, GAH_00591, GAH_00629, GAH_00785, GAH_01331, GAH_01442, GAH_01601, GAH_01810, and GAH_02050). A water molecule is then added to trans-2-enoyl-CoA to form (3S)-3-hydroxyacyl-CoA in a reaction catalyzed by an enoyl-CoA hydratase, which in *G. ahangari* could be encoded by 4 genes (GAH_00487, GAH_00802, GAH_01332, and GAH_01602). Two of these genes (GAH_00487 and GAH_01602) are in fact hybrid proteins containing an enoyl-CoA hydratase domain fused to a 3-hydroxyacyl-CoA dehydrogenase domain. Hybrid enoyl-CoA hydratase/dehydrogenase proteins such as these have been identified in other archaeal species including the *Archaeoglobales* species *G. acetivorans*, *F. placidus*, and *A. fulgidus* (184, 190, 201).

The next step in the β-oxidation pathway leads to the formation of 3-oxoacyl-CoA in an oxidation reaction that generates NADH and is catalyzed by a 3-hydroxyl-CoA dehydrogenase protein, which in *G. ahangari* is likely encoded by several genes (GAH_00328**,** GAH_00487, GAH_01600, GAH_01602 – again noting the hybrid nature of GAH_00487 and GAH_01602). Finally, acetyl-CoA is removed from the 3-oxo-acyl-CoA molecule by an acetyl-CoA acetyltransferase and is free to enter the TCA cycle. There are 8 genes in the *G. ahangari* genome that could catalyze this reaction (GAH_00292, GAH_00485, GAH_00625, GAH_00626, GAH_01327, GAH_01328, GAH_01886, and GAH_02049). Additional proteins involved in fatty-acid metabolism include the alpha (GAH_01318) and beta (GAH_01319) subunits of a 3-oxoacid CoA-transferase. The large number of genes dedicated to β-oxidation in *G. ahangari* and other

species within the *Archaeoglobales* provides genomic evidence supporting the notion that long- and short-chain fatty acid oxidation is a conserved metabolic feature within the family.

3.9.4 *Degradation of aromatic compounds and n-alkanes*

F. placidus, a member of the *Archaeoglobales* closely related to *G. ahangari*, can couple the complete oxidation of aromatic hydrocarbons to Fe(III) reduction (237–239). The *G. ahangari* genome does not contain any benzoate degradation genes, further supporting the observation that it cannot utilize aromatic compounds as electron donors for growth (52). Interestingly, *G. acetivorans*, the other member of the *Geoglobus* genus, has homologues of all genes coding for proteins of the benzoyl-CoA ligation pathway present in *F. placidus*, yet as in *G. ahangari* growth on aromatic hydrocarbons has not been observed in *G. acetivorans* (178, 184).

Another member of the *Archaeoglobales*, *A. fulgidus*, can also couple the oxidation of n-alkanes and n-alkenes with sulfur respiration (240, 241). This archaeon uses an alkylsuccinate synthase and an activating protein (AssD/BssD; AF1449-1450) to oxidize saturated hydrocarbons (n-alkanes in the range of C_{10}-C_{21}) (241). I identified homologs of both of these proteins in the genome of *G. ahangari* (GAH_01645-01646) and *G. acetivorans* (Gace_0420-0421). *A. fulgidus* can also oxidize long chain n-alk-1-enes ($C_{12:1}$ to $C_{21:1}$) when thiosulfate is provided as the terminal electron acceptor (240). Although enzymes involved in the activation of alkenes by *A. fulgidus* have not been characterized, the genome of *A. fulgidus* contains a homologue of a Mo-Fe-S containing enzyme (AF0173-AF0176) (240), which in *Azoarcus sp. EBN1* anaerobically hydroxylates a branched alkene (242). The Mo-Fe-S enzyme consists of 4 subunits including a chaperonin-like protein, a membrane anchor heme-*b* binding subunit, an Fe-S binding subunit, and a molybdopterin-binding subunit (243). This gene cluster was identified in the genomes *of G. ahangari* (GAH_01285-01288) and *F. placidus* (Ferp_0121-0123), but not in the other member of the *Geoglobus* genus, *G. acetivorans*.

3.9.5 *Nitrogen compounds as electron acceptors*

Except for *F. placidus* (179, 215), all of the *Archaeoglobales*, including *G. ahangari* (52), are unable to use nitrate or nitrite as electron acceptors for respiration (53, 178, 180–183) (Table 3.5). Yet, surprisingly, the genome of *G. ahangari* contains several 4Fe-4S domain-containing nitrate and sulfite reductase proteins (GAH_01242 and GAH_02063) as well as all four subunits (NarGHIJ) of a nitrate reductase (GAH_01285-01288). A nitrate/nitrite transporter is also annotated in the genome (GAH_00501), though it does not cluster with genes involved in nitrate/nitrite respiration and thus may function in the transport of alternative compounds. In addition, I identified a gene in this region of the genome (GAH_01290) coding for an uncharacterized channel protein, which could potentially function as a nitrate transport protein. The presence of genes encoding both nitrate reductase proteins (NarGHIJ and NirA) combined with the inability of *G. ahangari* to use nitrate for respiration (52) suggests a role for these proteins in assimilatory, rather than dissimilatory, nitrate reduction (244).

Similar to *F. placidus*, the *G. ahangari* genome does not contain any *nir* or *nrf* genes (for the NADH- and formate-dependent nitrite reductase proteins, respectively), with the exception of several homologues of NirA (GAH_00501, GAH_00506, GAH_01242, and GAH_02063), a nitrite reductase protein that catalyzes the reduction of nitrite to ammonia and is involved in assimilatory nitrate reduction in other organisms (244). Also missing are genes coding for nitric and nitrous oxide reductase proteins, which the genome of *F. placidus* contains (190), again supporting the observation that *G. ahangari* is not capable of dissimilatory nitrate reduction (52). The lack of these enzymes helps explain the physiological separation of *G. ahangari* from its close phylogenetic relative *F. placidus,* which is capable of dissimilatory nitrate reduction to N_2O (215). Furthermore, it is unlikely that the reduction of nitrogen-containing compounds exerts any significant selective pressure on hydrothermal vent microorganisms, as concentrations of these compounds are often low in vent systems (245).

N_2 gas, on the other hand, is the largest reservoir of nitrogen in the ocean (245, 246) and nitrogen fixation supplies hydrothermal vent systems with nitrogen sources for assimilatory growth (245). Ammonium is particularly abundant in the heavily sedimented Guaymas Basin hydrothermal system (51), from which *G. ahangari* was isolated (52), and this could select for organisms with assimilatory rather than dissimilatory nitrogen metabolisms and inhibit nitrogen fixation. Not surprisingly, the annotated genome of *G. ahangari* and homology searches for the primary enzymes from the nitrogen fixation pathway (*nifH*, *nifD*, and *nifK*) provided no significant hits, as previously reported for other members of the *Archaeoglobales*.

The genome does contain genes coding for a glutamine synthetase (GAH_01658), a glutamate synthase (GAH_01667-01669), and a glutamate dehydrogenase (GAH_00573 and GAH_01931). The enzymes glutamine synthetase-glutamate synthase comprise the GS-GOGAT pathway, and together with the GDH pathway, function as the two major paths for ammonium assimilation in archaea (244). While the GDH pathway does not use ATP as an energy source, as the GS-GOGAT pathway does, it has a lower affinity for ammonium (244). The presence of these enzymes and two ammonium transporter proteins (GAH_00438 and GAH_01767) for the formation of 2-oxoglutarate and glutamate from ammonium, is consistent with the notion that *G. ahangari* is under pressure to assimilate ammonium for anabolic processes.

3.9.6 *Sulfur compounds as electron acceptors*

Most members of the *Archaeoglobales* are dissimilatory sulfate-reducing organisms and able to use several sulfur-containing compounds as electron acceptors to fuel their metabolism (53, 179–183) (Table 3.5). By contrast, *G. ahangari* cannot couple the oxidation of electron donors that supported Fe(III) reduction to the respiration of commonly considered sulfur-containing electron acceptors such as sulfate, thiosulfate, sulfite, or S^0 (52). Interestingly, the genome of *G. ahangari* contains two genes (GAH_02067 and GAH_01481) coding for sulfate adenylyltransferase, which can initiate the first step in both the dissimilatory and assimilatory sulfate reduction pathways by catalyzing the formation of APS from ATP and inorganic sulfate.

The enzyme is also present in the genome of *F. placidus* which, like *G. ahangari*, is unable to respire sulfate (179) (Table 3.5). APS can then be used as substrate in the assimilatory (247–250) or dissimilatory (251, 252) pathway, depending on the needs and capabilities of the microorganism (249). The assimilatory pathway converts APS to the intermediate PAPS in a reaction catalyzed by an adenylsulfate kinase, which in *G. ahangari* is encoded by GAH_01478. The genome of *G. ahangari* contains genes coding for both the alpha and beta subunits of adenylsulfate reductase (GAH_02065-02066), an FAD dependent oxidoreductase protein that reduces APS to sulfite in the dissimilatory pathway. However, the genome lacks genes coding for a dissimilatory sulfite reductase (*dsrAB*), which catalyzes the reduction of sulfite to hydrogen sulfide in the final step of the dissimilatory sulfate reduction pathway (253). Strong matches could not be found even when the alpha (AAB17213.1) and beta (AEY99618.1) subunits of the sulfite reductase from *A. fulgidus* were used as queries in manual searches.

It is interesting to note that, despite the absence of *dsrAB* genes in the genome, *G. ahangari* does have a nitrite and sulfite reductase 4Fe-4S domain-containing protein (GAH_02063) located in a cluster of genes involved in sulfur metabolism (GAH_02063-02067). Whether these genes code for functional proteins of the dissimilatory pathway, perhaps with electron donor/acceptor pairs not tested yet, remains to be elucidated. *F. placidus*, for example, has homologs of all of these genes, except for *dsrAB*, and it grows with thiosulfate as the sole electron acceptor when hydrogen is provided as an electron donor (179). This capability may be due to the presence of several molybdopterin oxidoreductase proteins within the genome of *F. placidus* that show high similarity to a predicted thiosulfate reductase (NP_719592.1) from *Shewanella oneidensis*. However, strong homologs of this protein were not present in the genome of *G. ahangari.*

3.9.7 *Fe(III) as the sole electron acceptor for respiration*

The most distinctive physiological feature of *G. ahangari* strain 234^T is its dependence on Fe(III) as an electron acceptor for respiration (52). Both insoluble Fe(III) oxides and soluble

species of Fe(III), such as Fe(III) citrate, support growth, though the original isolate did not grow readily with the soluble electron acceptor and required prolonged adaptation under laboratory conditions to grow in its presence (52). Key to the ability of *G. ahangari* to respire the insoluble Fe(III) oxides is the ability of the cells to locate the oxides, attach to them, and position electron carriers of the outer surface close enough to favor the transfer of electrons (139). Hence, I examined the genome of *G. ahangari* for genes that code for cellular components that could be involved in motility and attachment and extracellular electron transfer.

Motility in this organism is enabled by a single flagellum (52), which in archaea is designated as an archaellum to reflect its distinct evolutionary origin (254). Archaeal flagellar genes can be organized into one of two very well conserved clusters (*fla*1 and *fla*2) based on the type and order of genes in the cluster: *flaBC(D/E)FGHIJ* in *fla*1 and *flaBGFHIJ* in *fla*2 (255). The *fla*1 clusters are exclusively found in *Euryarchaea* while *fla*2 clusters are generally associated with the *Crenarchaea*, which includes the *Desulfurococcales* and *Sulfolobales* orders, and are also present within the *Euryarchaeal* order *Archaeoglobales* (255). Interestingly, the *Archaeoglobales* have members with both types. I identified, for example, a *fla*1 gene cluster in the genome of *G. ahangari* (GAH_01994-02001), as in *F. placidus* (Ferp_1456-1463) (190), while the flagellar genes of *Archaeoglobus spp.* [15, 33, 50–52, and NC_015320.1] and *G. acetivorans* (184) were of the *fla*2 type. It has been suggested that a horizontal gene transfer (HGT) event occurred in the *Ferroglobus* lineage after divergence from the *Archaeoglobus* and *Geoglobus* lineages (184). Yet, the presence of a *fla*1 gene cluster in the flagellated and motile *G. ahangari* (52), when compared to the *fla*2 gene cluster found in the non-motile and non-flagellated *G. acetivorans* (178), would lend credence to a possible second HGT event within the family.

The genome of *G. ahangari* also encodes several glycosyltransferase genes (GAH_00218**,** GAH_00870, and GAH_01279) and an oligosaccharyltransferase (GAH_01455), which could glycosylate the growing archaellum (256) and post-translationally modify surface proteins, as is commonly observed in the *Archaea* (257). However, chemotaxis proteins, which

are present in nearly all sequenced members of the *Archaeoglobales* [15, 33, 50, 51, and NC_015320.1], with the exception of *A. sulfaticallidus* (203), and are typically found immediately upstream or downstream of the *fla* gene cluster, were absent in *G. ahangari*. The lack of chemotaxis genes in *G. ahangari* contrasts with their presence in most *Archaeoglobales* genomes, including *G. acetivorans* (184), the other member of the genus. Both *Geoglobus* species were isolated from hydrothermal vent chimneys: *G. acetivorans* from the Ashadze field on the Mid-Atlantic Ridge at a depth of 4,100 m (178) and *G. ahangari* from a Guaymas Basin chimney at a depth of 2,000 m (52). The hydrothermal fluids spewed from chimneys within the Guaymas Basin system are likely enriched in nutrients after passage through the 300-400 m thick, organic-rich sediments underneath (110). Furthermore, hydrothermal circulation at this site is high (109), which would rapidly replenish nutrients, both electron donors and fresh Fe(III) oxides, and thus organisms living in this environment may not need to utilize chemotactic mechanisms to seek out these nutrients. By contrast, hydrothermal fluids from offshore spreading systems, such as the Ashadze field, flow through thin sediment layers before reaching the chimney (110). This likely increases the selective pressure on resident microbes to evolve chemotactic mechanisms to locate nutrients.

The genome of *G. ahangari* also encodes proteins potentially involved in the assembly of extracellular protein appendages such as pili. I identified, for example, a prepilin peptidase (GAH_00760), numerous type II secretion system proteins (GAH_01195-01196, GAH_00173, GAH_00290, GAH_01412-01413), and a putative twitching motility pilus retraction ATPase (GAH_00960). Homologous genes are also present in the genomes of *G. acetivorans* (184), *F. placidus* (190), and *A. fulgidus* (201). In addition, *G. ahangari* has two genes encoding proteins with DUF1628 or DUF1628-like domains (GAH_01202, GAH_01671), which are associated with previously described archaeal pilin proteins (258) and present in all sequenced members of the *Archaeoglobales* [15, 33, 50–52, and NC_015320.1]. Any of these proteins could be involved in the assembly of the curled extracellular appendages that *G. ahangari* produces to attach to Fe(III)

oxides and facilitate the transfer of electrons from electron carriers located on the outer surface to the insoluble electron acceptor (139).

G. ahangari uses heme-containing proteins to transport electrons across the cell envelope and to the insoluble Fe(III) oxides (139). The most common heme-containing proteins used by mesophilic Fe(III) reducers for extracellular electron transport are *c*-type cytochromes (259). Archaea are known to have a variant form of the cytochrome *c* maturation (Ccm) system, whereby the CcmE protein has a CXXXY-type motif, rather than the HXXXY motif found in eukaryotic and most bacterial *c*-cytochromes, and CcmH is absent (89). Similar to other sequenced *Archaeoglobales*, *G. ahangari* has an archaeal-type CcmE protein (GAH_01977), a CcmC protein (GAH_00620) with a tryptophan-rich motif (WG[S,T][F,Y]WNWDPRET), a CcmF protein (GAH_01976 and GAH_01093) with the motif WGGXWFWDPVEN, and a gene coding for a CcmB homolog (GAH_00449) lacking the conserved FXXDXXDGSL motif. Although previously reported archaeal cytochrome maturation pathways do not contain CcmH (89), I identified two putative CcmH proteins in the genomes of not only *G. ahangari* (GAH_01092 and GAH_01094), but also in *G. acetivorans* (GACE_2070 and GACE_2068) and *F. placidus* (Ferp_1362 and Ferp_1364). All of these proteins contain cysteine-rich motifs consisting of LX[S,N]C[E,D,H]C but lack the LRCXXC motif characteristic of most CcmH proteins. However, they all flank a duplicate CcmF-encoding gene found only in *G. ahangari* (GAH_01093), *G. acetivorans* (184), and *F. placidus* (190).

In addition to having a distinct cytochrome *c* biogenesis pathway, the iron-reducing *Archaeoglobales*, *Geoglobus* and *Ferroglobus* species, also have more *c*-type cytochromes than any other archaeon, and many of these *c*-type cytochromes have multiple heme groups (113, 184, 190). The genome of *G. ahangari* contains 21 genes (Table 3.6) encoding putative *c*-type cytochromes, 7 of which have more than 5 heme groups; *F. placidus* has 30 *c*-type cytochromes (12 with more than 5 heme groups); and *G. acetivorans* has 16 *c*-type cytochromes (8 with more than 5 heme groups). By contrast, *Archaeoglobus* species, which do not use Fe(III) electron

acceptors (Table 3.5), have significantly fewer *c*-type cytochromes. Within this genus, the greatest number of *c*-type cytochrome encoding genes was found in the genome of *A. veneficus*, which has 16 *c*-type cytochromes (3 with more than 5 hemes). Other species such as *A. profundus* and *A. sulfaticallidus* have only 1 monoheme *c*-type cytochrome and *A. fulgidus* has 3 *c*-type cytochromes (none of which have more than 5 heme groups).

The subcellular localization of the putative *c*-type cytochromes of *G. ahangari* was also investigated. The ExPASy TMPred program (137) revealed that a majority (62%) of the *c*-type cytochromes have at least 1 transmembrane helix, consistent with their association to the cytoplasmic membrane. One of these *c*-type cytochrome proteins (GAH_00504) was predicted to be extracellular. I also identified several *c*-type cytochromes (GAH_01306, GAH_00286, GAH_01534, and GAH_01253) with predicted sizes once in mature form (46.3, 39.1, 18.5, and 16.9 kDa, respectively) matching those reported for outer-surface heme-containing proteins required for the reduction of insoluble Fe(III) oxides, but not soluble Fe(III) citrate, by *G. ahangari* (139) (Table 3.6). Hence, these 4 *c*-type cytochromes likely function as the terminal electron carriers between the cells and the oxides.

In addition to *c*-type cytochromes, I identified other potential electron carriers such as quinones, flavoproteins, and various Fe-S proteins (*i.e.* ferredoxins). I identified a number of uniquinone/menaquinone biosynthesis proteins in the genome of *G. ahangari* (Table 3.7), which could create a quinone pool in the membrane to promote electron transfer. The genome also contains a great number of Fe-S binding domain proteins and ferredoxins, which could participate in electron transfer pathways (Table 3.8). Fe-S proteins and ferredoxins were also abundant in the genome of *G. acetivorans* and *F. placidus,* which, like *G. ahangari,* also utilize Fe(III) respiration as their primary metabolism. Fe-S proteins and ferredoxins are regarded as some of the most ancient of electron transfer carriers (260) and also have high thermostability (261), which is critical to ensure maximum rates of electron transfer in the hot hydrothermal vent systems. Thus, the abundance of electron carrier proteins, some known to have increased thermostability,

and *c*-type cytochromes, some of them localized to the outer surface, is consistent with a mechanism evolved for efficient extracellular electron transfer in hot environments.

3.10 *Conclusions*

G. ahangari strain 234^T is only one of three members of the *Archaeoglobales* capable of dissimilatory Fe(III) respiration. Furthermore, it is an obligate Fe(III) reducer that grows better with insoluble than soluble Fe(III) species. Consistent with this, the genome contains a large number of *c*-type cytochromes within and on the cell surface, as well as other redox-active proteins such as thermostable ferredoxin and Fe-S proteins. The paucity of *c*-type cytochromes within non-Fe(III) respiring members of the *Archaeoglobales* (*Archaeoglobus* species) is consistent with the physiological separation between these archaea and *F. placidus, G. acetivorans,* and *G. ahangari*, which can gain energy for growth from the reduction of Fe(III) electron acceptors. Additionally, some genes required for both dissimilatory sulfate and nitrate metabolisms are absent in *G. ahangari* and *G. acetivorans.* This supports the physiological separation of *Geoglobus spp.* from *F. placidus*, which is capable of Fe(III)-, thiosulfate-, and nitrate respiration, and from *Archaeoglobus* species which are primarily sulfur-respiring organisms. Genomic data also support the reported physiological similarities between *G. ahangari* and other *Archaeoglobales* such as autotrophic growth with H_2 via the reductive acetyl-CoA/Wood-Ljungdahl pathway and the use of similar electron donors, including short- and long-chain fatty acids. Noteworthy is the fact that genomic evidence supports the synthesis of the methanogenic coenzyme-F_{420} in *G. ahangari* which is responsible for the characteristic fluorescence detected in all *Archaeoglobus spp.* except for *G. ahangari* or *F. placidus*. Hence, the genome sequence of *G. ahangari* provides valuable insights into its physiology and ecology as well as into the evolution of respiration within the *Archaeoglobales*.

3.11 *Taxonomic note*

The initial publication (52) of the *Geoglobus* genus and *Geoglobus ahangari* species was accepted for publication with extenuating circumstances at several culture-collection agencies. Thus, upon the original publication *G. ahangari* strain 234^T was accepted only at a single agency. In addition, the G+C mol% determined from the complete genome sequence (53.1 mol%) differs from that originally published (58.7 mol%), representing a discrepancy of over 5 mol%. This publication thus warrants an emended description of the genus *Geoglobus* and the type species, *Geoglobus ahangari*.

3.12 *Emended description of* Geoglobus *Kashefi et al. 2002*

The description of the genus *Geoglobus* is the one provided by Kashefi *et al.* 2002 (52), with the following modifications. In addition to the single monopolar flagellum, numerous curled filaments can be seen per cell (139). The G+C content of the genomic DNA of the type species is 53.1 mol%.

3.13 *Emended description of* Geoglobus ahangari *Kashefi et al. 2002*

The description of the species *Geoglobus ahangari* is the one provided by Kashefi *et al.* 2002, with the following modifications. The type strain is strain 234^T and has been deposited at three culture collection agencies which include the Deutsche Sammlung von Mikroorganismen und Zellkulturen (*DSM-27542*), the Japan Collection of Microorganisms (*JCM 12378*), and the American Type Culture Collection (*BAA-425*). Thereby, *Geoglobus ahangari* is now a validly published species name.

CHAPTER 4. EXTRACELLULAR ELECTRON TRANSFER TO FE(III) OXIDES BY THE HYPERTHERMOPHILIC ARCHAEON *GEOGLOBUS AHANGARI* VIA A DIRECT CONTACT MECHANISM

4.1 *Abstract*

The microbial reduction of Fe(III) plays an important role in the geochemistry of hydrothermal systems yet it is poorly understood at the mechanistic level. Here I show that the obligate Fe(III)-reducing archaeon *Geoglobus ahangari* uses a direct contact mechanism for the reduction of Fe(III) oxides to magnetite at 85 ˚C. Alleviating the need to directly contact the mineral with the addition of a chelator or the electron shuttle anthraquinone-2,6-disulfonate (AQDS) stimulated Fe(III) reduction. By contrast, entrapment of the oxides within alginate beads to prevent cell contact with the electron acceptor prevented Fe(III) reduction and cell growth unless AQDS was provided. Furthermore, filtered culture supernatant fluids had no effect on Fe(III) reduction, ruling out the secretion of an endogenous mediator too large to permeate through the alginate beads. Consistent with a direct contact mechanism, electron micrographs revealed cells in intimate association with the Fe(III) mineral particles, which once dissolved revealed abundant curled appendages. The cells also produced several heme-containing bands. Some of them were detected among proteins sheared from the cell's outer surface and were required for the reduction of insoluble Fe(III) oxides but not for the reduction of the soluble electron acceptor Fe(III) citrate. The results thus support a mechanism in which the cells directly attach and transfer electrons to the Fe(III) oxides using redox-active proteins exposed on the cell surface. This strategy confers on *G. ahangari* a competitive advantage for accessing and reducing Fe(III) oxides under the extreme physical and chemical conditions of hot ecosystems.

4.2 *Introduction*

The accumulation of Fe(III) in hot sediments surrounding marine hydrothermal vents and the availability of electron donors for microbial growth, such as H_2 and acetate (31), provide ideal conditions to support the growth and activity of dissimilatory Fe(III)-reducing microorganisms at elevated (>80 °C) temperatures (262). Fe(III) reduction is, in fact, a conserved metabolic capability of deeply-branching hyperthermophilic microorganisms (32) and the advent of isolation methods using Fe(III) oxides as the sole electron acceptors have enabled the recovery, in pure culture, of many novel hyperthermophilic Fe(III) reducers with previously unsuspected metabolic capabilities (reviewed in (177)). Evidence to date also indicates that the reduced Fe(III) minerals produced by dissimilatory Fe(III) reducers have distinctive signatures (263–266) which could serve as geological markers for Fe(III) biomineralization in hot ecosystems.

Despite the critical role that Fe(III) biomineralization has in the geochemistry of hydrothermal systems, its underlying mechanisms remain largely unknown. By contrast, Fe(III) biomineralization has been extensively studied in moderate temperature environments. In general, mesophilic, dissimilatory metal-reducing bacteria, both Gram-negative and Gram-positive, rely on *c*-type cytochromes to transfer metabolic electrons to the outer surface (185, 259, 267). Some transfer the electrons directly from the cell surface electron carriers to the Fe(III) oxides or indirectly via the secretion of soluble redox mediators, such as electron shuttles and/or metal chelators (reviewed in (84)). Recent studies in the thermophilic Gram-positive bacterium *Carboxydothermus ferrireducens* have also provided evidence for a direct contact mechanism for the reduction of Fe(III) oxides at moderately elevated temperatures (65 °C) (114). Mesophilic Fe(III) reducers can also transfer electrons to exogenous electron shuttles such as dissolved humic substances (187) and solid phase humics (188) generated during the degradation of organic matter. Both humic forms can be recycled through cycles of microbial reduction and abiotic reoxidation by the Fe(III) oxides, thus stimulating the rates of Fe(III) reduction in sediments (96, 188, 268). A third mechanism involving conductive extracellular appendages or ‘nanowires’

has also been proposed in species of *Geobacter* and *Shewanella*, which use a direct and an indirect strategy for Fe(III) reduction, respectively (91, 94, 269).

The finding that Fe(III) reducers with a direct contact mechanism predominate over those producing endogenous shuttles and chelators in a wide variety of subsurface environments (270–273) has led to the proposal that a direct strategy may confer on microorganisms a competitive advantage for reducing insoluble Fe(III) oxides (102). This is because these microorganisms do not divert energy towards the synthesis of endogenous soluble mediators, which often need to be replenished due to their loss to diffusion and advection in the bulk fluid and their adsorption onto redox-inactive solid phases (102). Such losses could be more pronounced in areas of high fluid circulation such as in hydrothermal environments, where seawater seeps down through fissures of the volcanic bed and is pushed back up again through the volcanic rock once heated by the underlying magma (31). However, mechanistic understanding of microbial Fe(III) reduction in hydrothermal environments is lacking.

Hence, I investigated the mechanism used by the model hyperthermophilic archaeon *Geoglobus ahangari* to reduce Fe(III) oxides. *G. ahangari* is an obligate Fe(III)-reducing archaeon isolated from the Guaymas Basin hydrothermal system at a depth of 2,000 m that grows at temperatures between 65 and 90ºC, with an optimum at ca. 85-88 °C (52). It was the first isolate in a novel genus within the *Archaeoglobales* and the first example of a dissimilatory Fe(III)-reducer growing autotrophically on H_2 (52), a metabolic trait later found to be conserved in many hyperthermophilic Fe(III) reducers (177). In addition to H_2, it oxidizes a wide range of organic acids, amino acids and long-chain fatty acids for the reduction of Fe(III). Here I show that *G. ahangari* reduces Fe(III) oxides with a direct contact mechanism and I identify cellular components necessary for the cell to establish electronic contact with the oxide minerals. To the best of our knowledge, this is the first mechanistic study of Fe(III) reduction by a hyperthermophilic archaeon and provides novel insights into the microbial adaptive responses that contribute to Fe(III) mineralization in hydrothermal systems.

4.3 *Materials and Methods*

4.3.1 *Bacterial strains, culture conditions and mineral characterization*

G. ahangari strain 234^T (JCM 12378^T, ATCC BAA-426^T) was routinely grown anaerobically in modified marine (MM) medium (52) with pyruvate (10 mM) as electron donor and free poorly-crystalline Fe(III) oxides (100 mM for routine transfers or 50 mM for experiments with free Fe(III) oxides) or soluble Fe(III) citrate (50 mM) as electron acceptor. Incubations were in the dark and at 85°C. These nominal concentrations of electron donor and acceptor were selected so the electron donor was provided in excess supply of electrons (one molecule of pyruvate, 10 electrons) to yield the full reduction of the electron acceptor (1/3 of the Fe(III) in Fe(III) oxides and all the Fe(III) in Fe(III) citrate). The cultures were transferred (5% (v/v)) into fresh medium when ca. 1/3 (Fe(III) oxides) or 2/3 (Fe(III) citrate) of the Fe(III) had been reduced (early stationary phase and late-exponential phase, respectively). The extent of Fe(III) oxide reduction in the cultures was periodically monitored by extracting the Fe(II) from the mineral phase with 0.5 N HCl (274) (HCl-extractable Fe(II)) and measuring it with the ferrozine method (275). When indicated, soluble Fe(II) was also measured in filtered (0.22 μm) culture supernatant fluids with the ferrozine method. The supernatant fluids were also treated with hydroxylamine hydrochloride under acidic conditions to reduce soluble Fe(III) to Fe(II) (276) and the total soluble Fe content was measured with the ferrozine method. The difference between the total Fe content and the Fe(II) fraction was used to estimate the amount of soluble Fe(III). When indicated, the reduced Fe(III) oxide mineral was characterized by harvesting the mineral particles from early stationary phase cultures by centrifugation, drying the sample with N_2 gas, and examining it by electron diffraction using a JEOL 2000 FX MARK II, 200kV transmission electron microscope.

4.3.2 *Assays for endogenous mediators*

The secretion of low-molecular-weight mediators by *G. ahangari* was investigated using Fe(III) oxides entrapped in alginate beads (12-kDa pore size, 3-mm diameter), prepared as previously described (277, 278) and modified for Fe(III) oxides (98). The bead-entrapped Fe(III)

oxides were subjected to 30 cycles of pressurization with N_2 gas followed by aspiration to vacuum to remove any residual oxygen trapped in the beads and were then dispensed at 50 mM concentrations in tubes with 10 ml of MM medium with 10 mM pyruvate. Tubes were periodically sacrificed to measure the extent of Fe(III) reduction in the beads as HCl-extractable Fe(II). The beads were first washed with autoclaved, anaerobic marine wash buffer (NaCl, 19.0 g/L; $MgCl_2 . 6H_2O$, 9.0 g/L; $CaCl_2 . 2H_2O$, 0.3 g/L; KCl, 0.5 g/L; pH to 7.0) and the Fe(II) in the beads was then extracted with 0.5 N HCl for 12 h and measured with the ferrozine method (275). Cell growth was also monitored by counting the number of acridine orange-stained cells in the culture supernatant fluids by fluorescence microscopy, as described previously (279).

The secretion of endogenous mediators larger than the bead pore size was investigated by measuring the effect of culture supernatant fluids on the reduction of free Fe(III) oxides (10 mM) by washed cell suspensions, using a protocol adapted from a previously published procedure (98). The supernatant fluids were harvested from 200-ml cultures grown with 10 mM pyruvate and 50 mM Fe(III) oxide until ca. 1/3 of the Fe(III) was reduced. After being filtered and oxidized as previously described (98), the supernatant fluids were concentrated 100-fold in an Ultracel® YM-10 centrifugal filter unit (Millipore, 10 kDa nominal molecular weight limit), made anaerobic by gassing with N_2:CO_2 (80:20) for 20 min and diluted 100-fold in MM medium supplemented with 10 mM pyruvate and, when indicated, 10 µM AQDS. Approximately 9.7 ml of these supernatant fluids were dispensed anaerobically into culture tubes. Tubes with 9.7 ml of MM medium were also used as controls. These tubes were inoculated with cells harvested by centrifugation (8,000 x *g*, 10 min, 20 °C) from 100 ml Fe(III) citrate (50 mM) cultures grown to mid-exponential phase (ca. 25 mM Fe(III) reduced). After washing them twice with autoclaved, anaerobic marine wash buffer, the cells were suspended in 5 ml of MM medium and flushed with N_2:CO_2 (80:20) gas for 20 min. Approximately 0.1 ml of this cell suspension (~ 0.6 mg of total cell protein) was inoculated into each tube containing 9.7 ml of concentrated supernatant fluids or fresh medium.

4.3.3 *Microscopy*

Acridine orange-stained cells were routinely examined and counted using a Zeiss Axioskop 20 phase-contrast microscope using an oil-immersion objective x 100/1.25, equipped with an UV lamp, an excitation filter (LP 420) and a red-attenuation filter (BG 38). Cells from stationary-phase cultures grown with free Fe(III) oxides or Fe(III) citrate were also fixed with 2.5% (w/w) glutaraldehyde, adsorbed onto Formvar-coated nickel grids (200-mesh, Electron Microscopy Sciences) for 15 min, washed with ddH_2O, and negatively stained with 1% uranyl acetate for 15 min. Negatively stained cells were then examined by Transmission Electron Microscopy (TEM) using a JEOL100 CXII TEM operated at 75 mV. When indicated, the culture samples were first treated with an oxalate solution for 15 min at room temperature to dissolve any cell-associated iron deposits before fixing and staining them for TEM analyses.

The biofilms associated with the bead-entrapped Fe(III) oxides were examined by Confocal Laser Scanning Microscopy (CLSM) using an inverted Olympus FluoView 1000 LSM equipped with a UPlanFLN 40x objective. Prior to CLSM, the beads were washed with PBS buffer and stained with the BacLight^{TM} viability kit (Invitrogen) for 5 min, following manufacturer's recommendations. After another wash with PBS, the beads were transferred to a glass bottom 35-mm microwell dish (MatTek Co.) and imaged. The fluorescence from the SYTO9 dye (green, live cells) was detected with a 488 nm argon line using a 505-525 band-pass filter, whereas the fluorescence from the propidium iodide dye was detected with a 560 long-pass filter. Images were collected at 1.0-µm increments.

4.3.4 *Denaturing Polyacrylamide Gel Electrophoresis (SDS-PAGE) and heme staining*

Cultures with 10 mM pyruvate and 50 mM Fe(III) citrate were grown to late-exponential phase at 85 °C and treated with oxalate (52) for 15 min to remove Fe precipitates that formed around the cells. The oxalate-treated cells were harvested by centrifugation (8,000 x *g*, 30 min, 25°C), washed once with marine wash buffer, and incubated at 37 °C for 30 min in iron extraction buffer, prepared as previously described (280) but containing 100 mM EDTA. The cells were

harvested by centrifugation and stored as a pellet at -20 °C until use. Loosely-bound proteins were mechanically sheared off the cell's outer surface by repeated (20 x) passages through a 23G needle (91). The cells were pelleted by centrifugation (453 x *g*, 60 min, 25 °C) and the supernatant containing the soluble, sheared protein fraction was removed and concentrated using an Amicon Ultra-15 centrifugal filter unit equipped with a 100-kDa vertical membrane (Millipore). The protein sample was then washed repeatedly with ddH_2O, re-suspended in 10 mM Tris buffer (pH 8.0), and stored at -20 °C until use. All protein samples were mixed with an equal volume of a 2X Laemmli Sample Buffer (Bio-Rad Laboratories, Inc.) and subjected to SDS-PAGE. Reducing agents were omitted from the SDS-sample buffer and the samples were loaded onto the gel without boiling to prevent the loss of heme groups (138). The protein samples were separated by SDS-PAGE in a 4-20 % Tris-Glycine Mini-PROTEAN gel (Bio-Rad Laboratories, Inc.) at 250 V for 30 min. Heme staining after SDS-PAGE was performed as previously described (138). The heme-stained gels were then de-stained (138) and stained with Coomassie Brilliant Blue G (Acrōs Organics) to visualize all the proteins in the samples.

4.3.5 *Effect of mechanical shearing of outer surface proteins on Fe(III) reduction*

The role of exposed outer surface redox proteins in electron transfer to poorly crystalline Fe(III) oxides was examined by testing the ability of cells subjected to mechanical shearing (as described above) or untreated cells to resume Fe(III) oxide reduction. All culture manipulations were performed inside a glove bag (Coy laboratories) containing a H_2:CO_2:N_2 (7:10:83) atmosphere and all the cultures were prepared in MM medium (pH 6.8) lacking sodium bicarbonate to minimize pH drops during exposure to the glove bag atmosphere. Untreated or sheared cells grown with 10 mM pyruvate and 50 mM Fe(III) citrate were harvested by centrifugation (8000 x *g*, 10 min, 25 °C) when approximately 2/3 of the Fe(III) had been reduced. After being washed anaerobically with the same medium, the cell pellets were gently resuspended with a Pasteur pipette into tubes containing 10 ml of MM medium supplemented with 10 mM

pyruvate as the electron donor and 100 mM Fe(III) oxides or 50 mM Fe(III) citrate as the electron acceptor. Incubation was at 85 °C in the dark.

4.4 *Results and discussion*

4.4.1 *Stimulation of Fe(III) reduction by exogenous mediators*

As shown in Figure 4.1A, *G. ahangari* coupled the oxidation of pyruvate to the reduction of poorly crystalline Fe(III) oxide at 85 °C with doubling times for three independent experiments, each containing at least triplicate samples, ranging from 4.3 to 5.2 h, which is within the ranges previously reported for the growth of the original isolate at optimum temperatures (52). The reduced mineral harvested from stationary phase cultures was black and magnetic and contained 20 (± 2) mM of HCl-extractable Fe(II). This contrasts with the less than 4 mM Fe(II) produced in controls lacking the electron donor (Figure 4.1A), which accounts for any extractable Fe(II) produced abiotically by reducing agents in the medium such as cysteine and $FeCl_2$ or carried over in the inoculum. Thus, 16 (± 2) mM of the Fe(II) extracted from the reduced mineral was generated during the biological reduction of the Fe(III) oxides. This Fe(II) concentration is approximately 1/3 of the nominal concentration of poorly crystalline Fe(III) oxides (50 mM) provided as electron acceptor, consistent with the formation of a mixed valence mineral such as magnetite, which has 1/3 Fe(II) and 2/3 Fe(III). To further confirm this, I analyzed the electron diffraction pattern of the reduced magnetic mineral generated by *G. ahangari*. As shown in the inset in Figure 4.1A, the electron diffraction analyses showed the characteristic diffuse ring electron diffraction pattern of magnetite (281).

I also gained insights into the mechanism of Fe(III) reduction by *G. ahangari* in experiments in which an exogenous electron shuttle was added to partially alleviate any need of the cells to directly contact the Fe(III) oxides. Addition of low (50 µM) concentrations of the humics analog anthraquinone-2,6-disulfonate (AQDS) stimulated the reduction of Fe(III) oxides over that observed in controls without AQDS, as evidenced by the increased rate of accumulation of HCl-

extractable Fe(II) over time (Figure 4.1A). Extracellular quinones such as AQDS function as electron shuttles between the cell and the Fe(III) oxides (282). The cells reduce AQDS to anthrahydroquinone-2,6-disulfonate (AHQDS), which then abiotically reduces Fe(III) to Fe(II), thus regenerating the quinone and making it available for a new cycle of biotic reduction and abiotic oxidation. This partially alleviates the need for the cell to directly contact the insoluble electron acceptor and stimulates the rates of Fe(III) reduction (282).

The stimulatory effect of AQDS on Fe(III) reduction was not dose-dependent. As shown in Figure 4.1B, concentrations of AQDS up to 100 µM stimulated growth, as indicated by the decreases in doubling times, whereas 200 µM concentrations did not significantly affect the doubling times. By contrast, doubling times were ca. two-fold higher in the presence of 500 µM concentrations of AQDS. This suggests that AQDS is toxic to *G. ahangari* above relatively low threshold concentrations and provides a plausible explanation for the cell's reported inability to respire AQDS when provided as sole electron acceptor for growth, which requires mM concentrations of the humic analog in the medium (52). High (10 mM) concentrations of AQDS also inhibited the growth of the mesophilic Fe(III)-reducing bacterium *Shewanella oneidensis* (283). However, *S. oneidensis* reduced and respired AQDS at 1 mM concentrations (283). The higher threshold of AQDS toxicity in *S. oneidensis* has been linked to the activity of the outer membrane protein TolC, which functions as a pump to extrude the AQDS (283). The increased sensitivity to AQDS noted in *G. ahangari* could be due to the absence of an outer membrane in its cell envelope, which has the characteristic archaeal structure composed of a cytoplasmic membrane and an S layer (52). Consistent with this, the rate of Fe(III) reduction at 100 °C by resting cell suspensions of another hyperthermophilic archaeon *Pyrobaculum islandicum* was highest at 200 µM concentrations of AQDS, but decreased at 500 µM concentrations (284).

As with AQDS, the addition of the synthetic metal chelator nitrilotriacetic acid (NTA, 4 mM) also stimulated the reduction of Fe(III) oxides by *G. ahangari* (Figure 4.1A). NTA solubilizes Fe(III) from the Fe(III) oxides and provides a soluble, chelated form of Fe(III) as an electron acceptor for

its microbial reduction (96, 285). As a result, NTA partially alleviates any need of the cell to directly contact the Fe(III) oxides and stimulates Fe(III) reduction (96, 285). Consistent with this, Fe(III) oxide cultures supplemented with NTA solubilized 3-times more Fe than cultures with no additions and most of the soluble Fe species were in the reduced form (Fe(II)) (Figure 4.1C).

4.4.2 *G. ahangari does not secrete endogenous mediators for Fe(III) reduction.*

I further investigated the mechanism of Fe(III) reduction in *G. ahangari* by growing the cells with Fe(III) oxides that had been entrapped in microporous alginate beads. As with the experiments with free Fe(III) oxides, the nominal concentration of entrapped Fe(III) oxides per tube was 50 mM and there was little variability between replicates (49.8 ± 1.8 mM of entrapped Fe(III) per tube). As shown in Figure 4.2A, *G. ahangari* produced 3.9 (± 0.9) mM Fe(II) over the course of 72 h in cultures with the entrapped Fe(III) oxide. This amount is approximately 7.8 (± 1.8) % of the total Fe(III) entrapped in the alginate beads, which corresponds well with the amount of Fe(III) (10 %) that is exposed on the beads surface (98). This suggests that only the Fe(III) oxide exposed on the surface of the beads was accessible for microbial reduction. As a result, cell growth was limited in these cultures (Figure 4.2A). By contrast, addition of 50 µM AQDS stimulated Fe(III) reduction and cell growth (Figure 4.2A). AQDS is small enough to pass through the pores of the alginate beads and can, therefore, shuttle electrons between the cell and the entrapped oxides (98).

Approximately one third (17 ± 1.0 mM) of the Fe(III) entrapped in the beads was reduced to Fe(II) in the cultures supplemented with AQDS (Figure 4.2A), consistent with the complete reduction of the entrapped Fe(III) oxide to the mixed-valence (Fe[II]:Fe[III], 1:2) mineral magnetite. This yield of HCl-extractable Fe(II) is 13 mM higher than in the cultures without AQDS, which were about 4 mM. The discrepancy between the amount of Fe(III) reduced in the presence of AQDS (13 mM) and the electron-accepting capacity of the AQDS provided (50 µM) indicates that the AQDS molecules underwent several (ca. 260) cycles of microbial reduction and abiotic oxidation until all the entrapped Fe(III) oxides had been reduced to magnetite. By stimulating the

reduction of the entrapped Fe(III), AQDS also supported the concomitant growth of a planktonic population (Figure 4.2A). Thus, AQDS alleviated, at least partially, the need of the cells to directly contact the insoluble Fe(III) oxides. Biofilms also grew on the bead surface in cultures supplemented with AQDS (Figure 4.2B). This contrasted with the cultures lacking AQDS, which only contained a few live and dead cells attached to the bead surface (Figure 4.2B, inset). This is because the ability of AQDS to serve as an electron shuttle also facilitates long-range electron transfer across multilayered biofilms (286). By contrast, the synthetic metal chelator NTA did not stimulate the reduction of the entrapped Fe(III) oxides (1.6 ± 0.3 mM Fe(II) produced over 72 h). This is because although NTA is small enough to permeate through the bead pores, it solubilizes Fe(III) at rates too slow to support cell growth (98).

The alginate beads experiments ruled out the secretion by *G. ahangari* of electron-shuttling compounds with molecular weights smaller than the pore size of the microporous beads. However, they cannot rule out the presence of larger mediator molecules or molecules. To bypass this limitation, I also tested the ability of cell-free culture supernatants obtained from stationary phase cultures grown with free Fe(III) oxides to stimulate Fe(III) reduction by washed cell suspensions of *G. ahangari*. Concentrated filtered supernatant fluids did not stimulate Fe(III) reduction compared to cell suspensions in fresh medium unless supplemented with AQDS (Figure 4.2C). These results further suggest that *G. ahangari* does not produce endogenous mediators to reduce Fe(III) oxides.

4.4.3 *Cellular components involved in Fe(III) reduction in G. ahangari*

In the absence of mediators, cells need to directly contact the Fe(III) oxides in order to reduce them. Consistent with this, TEM micrographs of *G. ahangari* cells from cultures with free Fe(III) oxide revealed cells densely coated by Fe(III) oxide particles (Figure 4.3A). Treatment of the cells with oxalate to dissolve most of the Fe(III) oxide particles revealed abundant filaments (Figure 4.3B). Similar appendages were also present in cells grown with Fe(III) citrate and were associated with mineral particles, presumably Fe precipitates as they were easily dissolved with

oxalate (Figure 4.3C). The cell's single polar flagellum (52) was easily distinguishable from abundant curled, thin appendages (Figure 4.3C). The production of a flagellum and the tumbling motility exhibited by this microorganism in cultures with Fe(III) oxides (52) provide a mechanism for locating the Fe(III) oxides, similar to what has been observed in mesophilic Fe(III) reducers (102). On the other hand, the production of the curled appendages associated with the Fe(III) oxides suggests a mechanism for binding the mineral particles close to the cell.

Close association between the cells and the insoluble Fe(III) oxides is necessary to directly transfer electrons from reduced proteins on the cell's outer surface to the Fe(III) oxides. Most of the redox-active proteins catalyzing this last step of electron transfer in mesophilic Fe(III) reducers are heme-containing, *c*-cytochromes (267). These proteins are especially suited for electron transfer at high temperatures because the covalent attachment of heme groups to proteins stabilizes their secondary structure and increases their thermal stability (287). However, dithionite-reduced versus air-oxidized spectral analyses of resting cell suspensions of *G. ahangari* failed to identify the spectral signatures characteristic of *c*-type cytochromes (52). Similarly, cytochromes were not detected by redox-difference spectroscopy in mesophilic metal-reducing bacteria from the genus *Pelobacter* (288–290). Yet, when whole-cell proteins from cells of *Pelobacter carbonolicus* were concentrated and subjected to electrophoresis on an SDS-PAGE gel and heme-stained, three bands were detected and identified as cytochromes by peptide mass fingerprinting (291). Following a similar approach, I detected several heme-stained bands in whole cell extracts of *G. ahangari* (Figure 4.4A and B). At least 4 of these bands (with relative molecular masses of 46, 38, 19 and 16 kDa) were also present in protein fractions that had been mechanically sheared from the cell surface (Figure 4.4A and B).

The presence of heme-containing bands in the sheared protein fraction is consistent with redox-active proteins having sufficient exposure on the cell's outer surface to interact directly with the insoluble Fe(III) oxides (166). To further test this, I investigated the ability of cells missing these outer surface proteins after mechanical shearing to resume growth and reduce Fe(III)

oxides. Shearing the outer surface proteins prevented the cells from reducing insoluble Fe(III) oxides (Figure 4.4C), although the cells still produced the curled appendages (Figure 4.4D). Furthermore, shearing did not compromise cell viability, as indicated by the fact that these cells did not have a growth defect when the soluble electron acceptor Fe(III) citrate was provided as the electron acceptor for growth (Figure 4.4E). This is analogous to the mesophilic Fe(III) reducer *Geobacter sulfurreducens*, which requires *c*-cytochromes exposed on the outer surface to reduce insoluble metal oxides but not Fe(III) citrate (166), and is consistent with their role in the direct transfer of electrons to the mineral. This is because their exposure minimizes the distance with the Fe(III) oxides and facilitates the direct tunneling of electrons between the heme groups and the mineral surface (292).

4.5 *Conclusions*

The results presented above demonstrate that *G. ahangari* uses a direct contact mechanism to reduce Fe(III) oxides, strongly associating with the mineral particles to promote electron transfer between redox-active proteins exposed on the outer surface and the mineral. TEM micrographs of other hydrothermal vent isolates consistently show cells in intimate association with the Fe(III) oxide particles (65, 293, 294), suggesting that this may be a widespread mechanism for Fe(III) reduction in these environments. A direct contact mechanism is likely to confer on these microorganisms a competitive advantage over microorganisms relying on mediators. Fluid circulation is especially high in hydrothermal systems (31), which limits the bioavailability of soluble electron shuttles and favors the growth of microorganisms that can directly contact the oxides. Colonization of the mineral surface can also lead to the formation of biofilms, as shown for *G. ahangari*, thus providing a microenvironment for the absorption and concentration of nutrients, including soluble electron shuttles. Solid phases of humic acids are also abundantly produced during the degradation of organic matter and can serve as an electron acceptor to support the growth of dissimilatory Fe(III)-reducing microorganisms (188). The

insoluble nature of the humic phases and their co-association with Fe(III) oxides in sediments is likely to also select for direct contact mechanisms.

Like *G. ahangari*, most hyperthermophilic Fe(III) reducers isolated to date are flagellated and motile (177). Flagellar motility is especially advantageous to these organisms as it provides a mechanism to access Fe(III) oxides freshly deposited in the hot sediments. The heated waters that exit the vents dissolve minerals from the volcanic rock and deposit them in the nearby sediments. As a result, reactive ferric minerals are continuously being deposited as a dispersed layer on top of the hot sediments around hydrothermal vents and could be accessible to motile microorganisms. Energy expenditure for flagellar synthesis and operation is relatively modest (about 2 % and 0.1 %, respectively, of the total energy expenditure of the cell during normal growth (295)), yet yields high returns, as it enables microorganisms to rapidly access nutrients and increases their chances of survival (296). Hence, motility and direct contact mechanisms for the reduction of Fe(III) oxides are likely to have coevolved to maximize the fitness of microorganisms growing under the extreme physical and chemical conditions of hydrothermal systems.

CHAPTER 5. MICROBIAL NANOWIRES: A CONSERVED MECHANISM OF EXTRACELLULAR ELECTRON TRANSFER

5.1 *Abstract*

Microbial nanowires have been identified in only two genera of mesophilic iron reducers, *Geobacter* and *Shewanella*. Here I demonstrate the presence of conductive filaments isolated from both the bacterium *Geothermobacter ehrlichii* and the archaeon *Geoglobus ahangari* which are predicted to be essential for iron respiration at (hyper)thermophilic temperatures. CP-AFM analysis of the motility structures (flagella and putative archaella, respectively) and the putative nanowires (type IV pili and pilus-like filaments, respectively) obtained by mechanical shearing demonstrated that the motility structures were insulating while the pili or pilus-like filaments were conductive under the same conditions. These data were reproduced using exhaustively-purified filaments, again demonstrating their conductivity. Since these organisms are both able to grow at extreme temperatures, it was of interest to determine if these novel nanowires exhibited increased thermal stability over those of mesophilic *Geobacter* species. A Sypro Orange thermal shift assay was carried out and whole-cell extracts from these organisms presented the appropriate trends. Unfortunately, sufficient data could not be generated for the highly-purified filaments. However, the available data support a mechanism whereby microbial nanowires function in thermophilic and hyperthermophilic organisms to avoid the use of soluble compounds which could be lost to the surrounding environment, and to increase the surface area available for extracellular electron transfer.

5.2 *Introduction*

Iron is the fourth most abundant element in the Earth's crust, and as such it represents a significant electron sink for surface and subsurface microorganisms (84). Yet, iron presents a challenge as, unlike the electron acceptors used by the majority of organisms on the Earth's surface (*i.e.* oxygen), it is unable to enter the cell in its most common form (84). At circumneutral

pH, iron is insoluble and exists as an oxidized (Fe(III)) or reduced (Fe(II)) solid-phase mineral (84). Still, numerous microorganisms are able to utilize these insoluble oxides (84). The most commonly studied dissimilatory iron-respiring microorganisms are *Geobacter sulfurreducens* (74) and *Shewanella oneidensis* (297). While these bacteria can solve the problem of reducing an insoluble electron acceptor, they accomplish this goal with different mechanisms.

S. oneidensis has the ability to utilize a range of extracellular electron transfer mechanisms to reduce insoluble Fe(III) oxides (94, 298, 299). Chelation of iron into a soluble form is known to assist in the reduction of Fe(III) oxides (84, 100). A weak chelator is produced by *S. oneidensis*, while the rate of solubilization has been shown to be too low to permit the demonstrated growth rates (300). The predicted metal chelator, an endogenously-produced flavin, instead serves as an electron shuttle (100). This flavin, in addition to any exogenously supplied shuttles, facilitates growth on Fe(III) oxides and within microbial electrochemical cells (MECs) (300). If produced in a MEC, cells remain planktonic and electrons are passed to the electrode surface via the excreted flavin (286). If no electron shuttle is present, a biofilm is formed on the electrode surface (286). In addition, a unique microbial nanowire can be produced by *S. oneidensis* (94). These “nanowires” are produced by the rapid extension of the cell membrane, forcing any cytochromes present in the periplasm or on the membrane outward (95).

Studies on *G. sulfurreducens* have resulted in a range of proposed mechanisms for iron respiration (see (103) for review), and even after 20 years (74) a consensus has not been reached. However, after extensive study, reproducible assays were developed to permit mechanistic studies on this organism and others (97, 113, 114, 139). It is now firmly cemented that *G. sulfurreducens*, the model of the *Geobacteraceae*, is an obligate direct-contact reducer of insoluble Fe(III) oxides (91, 164–166). If an electron shuttle or a chelator is available, the cells will utilize this more readily-available electron acceptor (96, 187), but they are unable to produce shuttles themselves (164, 301, 302).

These two model systems thus demonstrate that multiple pathways exist to enable direct-contact respiration (see (84) for review). The simplest of these mechanisms is the expression of a terminal reductase on the cell surface (84, 114). In dissimilatory iron-reducing microorganisms these terminal reductases are commonly *c*-type cytochromes (72). Via their expression on the outer surface of the cell, they are placed into close proximity with the mineral surface and enable electron transfer from the cell interior to the extracellular electron acceptor (84, 86, 166, 303, 304). Facilitating this interaction could be the expression of an extracellular polysaccharide (EPS) matrix to maintain a biofilm on the mineral surface (90), production of a motility apparatus to locate or maintain proximity to the electron acceptor (102), and/or the production of filaments to attach and bind to the mineral surface (91). Yet, the inadequacy of these mechanisms is that the cell surface has a limited area, and as such the amount of contact with the mineral is restricted (91).

The extension of the surface area for reduction can be accomplished by the secretion or loss of outer-surface cytochromes into an EPS matrix (90) or by the production of conductive filaments (91, 95). Deletion of an operon (Xap) encoding the EPS of *G. sulfurreducens* generated strains that were unable to reduce Fe(III) oxides. This phenotype was attributed to the loss of EPS-associated cytochromes from the biofilm matrix (90). Cytochromes, however, are not the sole reductase of iron in *G. sulfurreducens.* The first proposed mechanism for the extension of the electroactive cell surface was based on the discovery that the type IV pili of *G. sulfurreducens* were conductive and able to transfer respiratory electrons to the cell surface and beyond (91). These ‘microbial nanowires’ resemble typical type IV pili with one important distinction. These ‘geopilins’ lack the conserved globular head domain and have therefore a lower subunit molecular weight (91). The loss of this domain alters the function of the pilus away from typical type IV pili functions, such as motility and attachment, and towards being a conduit for metabolic electrons to exit the cell (91, 118).

Dissimilatory iron respiration is also found outside of the mesophiles. In fact, the majority of thermophiles and hyperthermophiles are able to respire Fe(III) oxides as a terminal electron

acceptor when examined by cell-suspension assays (32). Yet, little attention has been spent on the diversity of thermophilic iron reducers until recently (113, 114, 126, 139, 184). Genome evidence demonstrating the presence of *c*-type cytochromes, flagella, and other filament morphologies is available for several (hyper)thermophilic bacteria and archaea (190, 201, 305). The first thermophile to have an elucidated iron-respiration mechanism was the bacterium *Carboxydothermus ferrireducens*, with a T_{opt} of 65 °C (306). This bacterium was capable of using exogenous electron shuttles or chelators, but produced none of its own (114). Thus, a mechanism based on *c*-type cytochromes, flagella for motility, and pili for attachment was proposed (114). Another thermophilic bacterium, *Thermincola potens,* has been studied and *c*-type cytochromes expressed on the cell surface are predicted to be the terminal reductase (186). Similar studies have also been performed within the *Archaea.* The hyperthermophilic archaeon *Geoglobus ahangari* (52), presented within this work (Chapter 4), belongs to the archaeal family *Archaeoglobaceae* and similarly lacks endogenously produced mediators and contains an archaellum, pilus-like filaments, and numerous *c*-type cytochromes (139). This physiology is conserved within the *Archaeoglobaceae,* as both *Ferroglobus placidus* (179) and *Geoglobus acetivorans* (178) have both been shown to rely on the same strategy for iron respiration (113, 184, 190).

Thus, all of the thermophilic and hyperthermophilic organisms, regardless of their kingdom (18), appear to forego the use of excreted compounds in favor of direct contact with the mineral surface. Due to the presence of both pilus-like filaments and *c*-type cytochromes (113, 114, 126, 139, 184, 190), however, it is difficult to speculate which is (or are) the terminal reductase(s) of iron in these organisms. Therefore, the next step is to determine if the filaments are conductive under physiologically-relevant conditions (307). If the filaments produced are conductive, it would indicate that microbial nanowires are a wide-spread mechanism for dissimilatory iron reduction. To this end, *G. ahangari* and the only thermophilic relative of the *Geobacteraceae*,

Geothermobacter ehrlichii, were selected for biochemical and electrochemical characterization of their extracellular filaments.

5.3 *Materials and Methods*

5.3.1 *Bacterial strains and culture conditions*

G. ahangari strain 234^T (JCM 12378^T, ATCC BAA-426^T) was grown anaerobically in a modified marine (MM) medium with pyruvate (10 mM) as electron donor and soluble Fe(III) citrate (50 mM) as electron acceptor. Incubations were in the dark and at 85 °C (18). *G. ehrlichii* strain SS015 (ATCC BAA-635, DSM 15274) was grown anaerobically in MM medium with malate (10mM) as the electron donor and soluble Fe(III) citrate (50mM) as the electron acceptor (Chapter 2). Incubations were in the dark and at 55 °C (66). Cultures were transferred (10% (v/v)) into fresh medium when $^2/_3$ of the Fe(III) had been reduced (late-exponential phase). The extent of Fe(III) oxide reduction by growing cultures was monitored by extracting the Fe(II) from the mineral phase with 0.5 N HCl (23) and measuring the extracted Fe(II) by the ferrozine method (46).

5.3.2 *Isolation and purification of extracellular filaments*

Both a rapid and exhaustive method were developed for the purification of the extracellular filaments of *G. ehrlichii* and *G. ahangari.* The rapid preparation was developed to produce filament preparations containing both the pilus-like filaments and archealla of *G. ahangari,* and both the pili and flagella of *G. ehrlichii*. This protocol involves repeated mechanical shearing, via a 23G needle (10 passages), of the filaments from the cell surface followed by centrifugation (20 min, 3,220 x *g*, RT) to remove whole cells and cell debris. Culture supernatant, containing the sheared filaments, was concentrated via a 30 kDa Centriprep centrifugal filter (Millipore) and washed with an oxalate solution (52), an iron extraction buffer (139), and a final wash with MMWB (139). By utilizing the preparatory cell gel electrophoresis (prep-cell) protocol developed in our lab (92), it was possible to use the SDS-insolubility of the pili of *G. ehrlichii* and the pilus-like filaments of *G. ahangari* to purify these filaments to homogeneity.

5.3.3 *Thermostability measurements by thermal shift assay*

Thermal shift assay protocols are derived from those in (308–310). *G. sulfurreducens* strain PCA, *G. ehrlichii* strain SS015, and *G. ahangari* strain 234^T were used to represent mesophilic (74), thermophilic (66), and hyperthermophilic (52) dissimilatory iron reducers with direct-contact mechanisms involving microbial nanowires ((91, 139) and Chapter 2). Whole-cell preparations, which were washed as per the culture supernatant above to remove residual iron, were lysed by repeated (3 x) sonication (duty cycle = 50, time = 1 min, output = 1, on ice) of cell pellets from late-exponential stage ferric citrate cultures. Cell debris was removed by centrifugation (20 min, 3,220 x *g*, RT) and the soluble protein fraction was collected. Sypro Orange (Sigma-Aldrich) was diluted to a 10 x stock (from 5,000 x) and 5 µl were added to 40 µl of the desired pH buffer. The buffers used were 50 mM sodium acetate (pH 4.0), 50 mM HEPES (pH 7.0), and 50 mM CHES (pH 9.4). Finally, 5 µl of the desired sample was added to the well and mixed. To create the appropriate blank for each condition, 5 µl of 10x Sypro Orange was placed in 45 µl of the appropriate buffer. Samples, including the soluble fraction of whole-cell lysate and purified filaments, were placed into an iQ 96-Well PCR Plate (Bio-Rad Laboratories, Inc.) and covered with iCycler iQ optical tape (Bio-Rad Laboratories, Inc.) before being placed in the iQ5 multicolor real-time PCR detection system (Bio-Rad Laboratories, Inc.). The thermal cycler was ramped from 25 to 99 °C in 0.5 °C increments with a hold time of 30 seconds per step. Fluorescence measurements were performed using an excitation wavelength of 545 nm while the emission of the dye was measured at 585 nm. Due to limited preparations, protein quantification was foregone. Two biological replicates and three technical replicates were performed for each organism and the average and standard deviation of each T_m was calculated from these replicates. T_m was calculated as the median temperature obtained between the trough and the peak fluorescence. However, calculations could not be performed on the prep-cell purified pilus or pilus-like filaments under investigation as these samples failed to produce sufficient fluorescence data using the experimental parameters discussed above.

5.3.4 *Conductive probe – atomic force microscopy*

Mechanically-sheared samples obtained from both *G. ehrlichii* or *G. ahangari* were immobilized onto independent highly oriented pyrolytic graphite (HOPG) surfaces, thoroughly dried under a stream of N_2 gas, and imaged by a Cypher atomic force microscope (Asylum Research). Topographic scans by atomic force microscopy (AFM) were performed at a 4.88 Hz scan rate or a 2.44 Hz scan rate, for scans below 2 µm, using an AC240TS tip (Asylum Research). Upon location of an appropriate area for conductivity measurements, one containing a number of diffuse fibers, the tapping tip was exchanged for a conductive tip (ASYELEC01) (Asylum Research) and the instrument was reengaged for conductive probe atomic force microscopy (CP-AFM). When possible, multiple points (2-4) were selected across 1-2 filaments per frame, including points on both thick and thin areas, representing bundled and what I believe to be less aggregated filaments. Analysis of current/voltage (I/V) output was performed within the Igor software suite (WaveMetrics). Averages were taken for measurements at each bias voltage and these values were smoothed using a Savitzky-Golay algorithm (311) with the end points considered using the 'bounce' option. Following this, the slope across the midpoint was calculated and averaged. Finally, resistance was calculated as $1 \; x \; \text{slope}^{-1}$ and compared to the resistance obtained from the other filaments under investigation.

5.3.5 *Elemental analysis of purified filament preparations*

Quantitative elemental analysis of purified filament preparations are awaiting additional sample preparations, as the prep-cell protocol yield is low, yet will proceed as previously described (92) by inductively coupled plasma – atomic emission spectrometry (ICP-AES). Analyses will be performed at the Chemical Analysis Laboratory at the University of Georgia (Athens, GA) using a Thermo Jarrell-Ash Enviro 36 Inductively Coupled Argon Plasm. In brief, samples obtained from each microorganism under investigation will be resuspended in 10 mM CHES buffer (pH 9.5, 1 mM EDTA) and this same buffer will be used as a reference during the experimental procedure. In order to obtain a value for the number of elemental atoms per filament

subunit it will be important to quantify the samples before submission. As previously stated, the quantification of filament samples from these organisms is difficult, but will be performed on three prep-cell samples per organism to create an average per preparatory gel. Thus, I can use this concentration and the data from the ICP-AES protocol to calculate the number of elemental atoms per filament subunit. For *G. ahangari*, where the molecular weight of the nanowire subunit is unknown, it will be possible to calculate the number of elemental atoms per microgram of protein while the predicted molecular weight of pilin of *G. ehrlichii* (peg.2848) is estimated (137) to be 6.95 kDa, or 1.15×10^{-11} µg.

5.3.6 *Examination of the curli-like nature of G. ahangari nanowires*

Methods for the identification of amyloid-fibril forming filaments include microscopic analysis of fibril formation after incubation at 4 °C in a pH neutral buffer, Congo Red binding, and Thioflavin T binding (312). Preparations of sheared pilus-like filaments from *G. ahangari* were incubated (4 °C, pH 7.0) for 72 h before examination by transmission electron microscopy on a JEOL CXII transmission microscope (operated at 75 mV) to qualitatively determine if the number of individual filaments decreased and if there was an increase in the amount of fibrils formed. Samples before and after incubation were placed on Formvar-coated 300-mesh copper grids (Electron Microscopy Supplies), washed twice with ddH_2O and stained with 1% ammonium molybdate.

Additionally, while not yet performed, Thioflavin T (ThT) binding assays will be performed on sheared samples from *G. ahangari*. These will be incubated for 24 h in a range of buffers (pH 4.0, 7.0, and 9.4) and mixed with ThT and examined for the increased fluorescence of the bound dye (313). ThT binding was chosen over that of Congo Red due to the specificity of ThT for amyloid fibrils (312, 313). Sheared samples will be of a lesser purity than those purified via the prep-cell, yet have the advantage in that they exhibit decreased amounts of bundling and aggregation (see Figure 5.1) when compared to the exhaustive 3-day protocol performed on the prep-cell samples. This aggregation will likely block ThT binding and lessen the efficacy of the

assay (312). ThT binding will be performed on the pilus-like filaments of *G. ahangari* (as per (312)) using the QuantaMaster spectrometer (Photon Technology International) available at Michigan State University. In tandem, the nanowires of *G. ehrlichii*, which are presumed to not be curli-like in nature, will be used as a negative control to assess the accuracy of the protocol within (hyper)thermophilic filaments from dissimilatory iron-reducing microorganisms.

In addition to these biochemical studies, DELTA-BLAST analysis was conducted using curli-associated proteins from *Escherichia coli* against the genome of *G. ahangari*. CsgA (CDU39169.1), CsgB (ACB59306.1), CsgC (ACB59308.1), CsgD (ACB59305.1), CsgE (ACB59297.1), CsgF (ACB59303.1), and CsgH (ACB59302.1) from *E. coli* were used as queries.

5.4 *Results and discussion*

5.4.1 *Isolation and purification of filaments*

Rapidly-purified samples from *G. ehrlichii* and *G. ahangari*, prior to the iron-cleanup steps of oxalate and IEB treatment, appear visually to contain a significant amount of insoluble iron oxide particles, which are presumed to be iron clays (139). In most cases, the sheared filaments at the end of the rapid protocol, even following the iron-cleanup steps, appear from faint orange to black, depending on the extent of iron remaining in the preparation that was resilient to the iron-cleanup steps. This is unlike the majority of samples acquired from the prep-cell protocol. In most cases these samples, from either organism, contain small black filaments which are visible to the naked eye and occasionally a fine white precipitate. Both of these remain following the vigorous cleanup steps after the preparatory electrophoresis setup runs. The black filaments are presumed, as in *G. sulfurreducens*, to be bundles of highly-purified filaments while the fine white precipitate is presumed to be acrylamide particles released from the surface of the gel during collection of the protein filaments.

TEM micrographs of filaments purified from *G. ehrlichii* by the rapid method clearly show both the bacterial flagella and the type IV pili (Figure 5.2A and B). The bacterial flagella produced

by *G. ehrlichii* appear morphologically similar, *i.e.* relatively straight with an average diameter of 30 nm, to those reported in other members of the *Desulfuromonadaceae* (107, 108, 116, 147) and flagellated members of the *Geobacteraceae* (73, 102, 314, 315). While reportedly rare within the extremophilic members of the *Desulfuromonadaceae* (108, 116, 147), type IV pili (*ca.* 2.5 nm in diameter) were purified by both purification protocols (Figure 5.2B-D). Thereby, their SDS-insolubility, like the pili of *G. sulfurreducens* (92), was confirmed. These filaments appear morphologically similar by TEM to the geopili present in *Geobacteraceae* species and, based on previous alignments of the pilin sequence to other members of the *Geobacteraceae,* are predicted to be most similar to the pili of *G. metallireducens* (Chapter 2).

TEM micrographs of filaments purified, by the rapid method, from *G. ahangari* clearly show both the archaellum and numerous pilus-like filaments (Figure 5.1A). The archaella of *G. ahangari* exhibited the same structure as seen by TEM (139), *i.e.* relatively straight with an average diameter of 4 – 6 nm. The pilus-like filaments (139) again appear smaller than the archaella (*ca.* 2.5 nm in diameter) and exhibit a curled structure resembling the amyloid-fibril forming curli of several mesophilic organisms (316, 317). These filaments are also seen in the iron-respiring members of the *Archaeoglobales*, *F. placidus* (113) and *G. acetivorans* (184). The pilus-like filaments remained intact throughout both purification procedures (Figure 5.1A and B), indicating their SDS-insolubility and resistance to depolymerization, while the archaella were only present within the rapidly-purified sample preparations. These pilus-like filaments are thus morphologically and physiologically similar to the curli of several mesophilic isolates in that they appear curled or kinked and are resistant to stressors that would denature or depolymerize the majority of extracellular appendages (316, 317). However, without additional studies this behavior may be proven to be circumstantial and/or related to the predicted thermal and chemical stability of these filaments.

5.4.2 *G. ehrlichii expresses multiple filaments while only the Geopili are conductive*

As expected, when examined by AFM, the filaments of *G. ehrlichii* exhibited the same structure as seen by TEM (Figure 5.3A). In preliminary CP-AFM experiments, performed with Dr. Sanela Lampa-Pastirk (Reguera lab), sheared pili from *G. ehrlichii*, while shown to be conductive, were covered in an insulating layer of what was presumed to be EPS (Figure 5.3A). This EPS layer made measurements difficult, yet an average resistance was calculated for the sheared pili and was determined to be ca. 37,458 (± 9,381) MOhms (Figure 5.3B and when compared to graphite (Figure 5.3B, insert)). The flagella, visualized within the same preparation, were found to be insulating (Dr. Lampa-Pastirk, personal communication). These results were expected, as the flagella are used primarily as motility structures (52, 66) and the relatedness of *G. ehrlichii* to members of the *Geobacteraceae* (66, 73, 107, 108) suggests their pili may function similarly to those of *G. sulfurreducens* inasmuch as they are produced to increase the electroactive surface area of the cell and permit the reduction of metal oxides at a distance (91).

Conductivity measurements by CP-AFM were repeated on an additional biological replicate of purified pili from *G. ehrlichii* purified using the prep-cell protocol. The resistance was found to be dependent on the location of measurement (Figure 5.4A) and the bias voltage sweep that was performed. At a 1 V sweep (from -1.0 to 1.0), two spots were analyzed. The first, Position 4, was located within a bundled, or globular, region of the micrograph while the second, Position 3, was located on a thinner, more pilus-like filament section. The calculated resistance at Position 4 was 3,775 (± 2,088) MOhms while the resistance at Position 3 was calculated as 454 (± 64) MOhms. These values can be compared to the resistance of the HOPG surface (Position 1) analyzed within the same micrograph (45.8 ± 21.6 MOhms) (Figure 5.4A). This trend, of Position 4 being more insulating than any of the less-bundled positions, was replicated at 0.6 V, 0.3 V, and 0.1 V sweeps (Figure 5.4C). The resistance of Position 4 at 0.6 V was 5,905 (± 2,205) MOhms while Positions 3, 6, and 7 averaged a resistance of 127 (± 20) MOhms. Yet, the resistance of graphite remained approximately the same at 51 MOhms (n=1 within this micrograph). This trend

further continued at lower bias voltage sweeps, with Position 4 being more insulating than Position 3. However, sample resistances begin to approach those of graphite at these lower bias voltage sweeps, and as such will not be reported. The pili of *G. ehrlichii* thus represent the first nanowires identified within a thermophile and demonstrate that microbial nanowires are likely a conserved structure within the *Geobacteraceae.*

5.4.3 *G. ahangari expresses multiple filaments while only the smaller, pilus-like filaments are conductive*

Both filament morphologies in *G. ahangari* exhibited the same structure as seen by TEM (139) (Figure 5.5A and B). Preliminary experiments on the filaments of *G. ahangari*, with Dr. Sanela Lampa-Pastirk, were performed on sheared preparations and prep-cell samples (Figure 5.5C and D). The sheared samples, possibly containing residual metal ions, had a resistance of 266 ± 147 MOhms. The archaella, in comparison, were found to be insulating; an average resistance was calculated and determined to be 465,825 ± 84,953 MOhms. The conductivity of purified pili, by the prep-cell protocol, was also assessed at the time and the resistance (993 ± 405 MOhms) was determined to be higher than those from the sheared preparations, yet still far lower than the insulating archaella (Figure 5.5C and D).

Conductivity measurements were again performed on the pilus-like filaments of *G. ahangari*, purified using the prep-cell protocol, and confirmed the conductive nature of the pilus-like filaments (Figure 5.6B and C). Initial measurements, performed at a range of forces (8 - 15 nN) and voltage sweeps (0.3, 0.6, and 1 V) on two different positions (Figure 5.6A) showed that the pilus-like filaments were less conductive than previously found (18,338 ± 9,799 MOhms) while the large standard deviation indicates substantial variability (Figure 5.6C). However, after repeated measurements and dithering of the CP-AFM tip on the graphite surface, to remove any insulating material on the tip, it was possible to break through this insulating layer and, I believe, examine the true conductivity of the pilus-like filaments. Averaged resistance values were calculated from 2 independent positions (Position 3 and Position 4) (Figure 5.6A) and over the full

assessed range of bias voltages. As opposed to the nanowires of *G. ehrlichii*, as bias voltages narrowed (1.0, 0.6, and 0.3 V) an increase in resistance was seen (292, 497, and 731 MOhms, respectively), although this trend was not as drastic as in *G. ehrlichii*. The average resistivity after the removal of the insulating layer, over a total of 13 measurements, was 540 ± 246 MOhms (Figure 5.6C).

As the archaella are structurally and genetically similar to type IV pili (318), it was predicted that these filaments would be conductive. Yet, the abundance of the curled filaments on the cell surface (139) makes them physiologically more similar to bacterial nanowires. However, the identification of protein nanowires in this organism is the first report of such nanowires in the *Archaea* and in a hyperthermophile. Based on the shared metabolic capabilities and phylogenetic relatedness between *G. ahangari, G. acetivorans,* and *F. placidus,* the conductivity of the pilus-like filaments from these species should be assessed to determine if they too could function as microbial nanowires. Identification of additional microbial nanowires among other hyperthermophiles, due at least in part to their proposed relatedness to the last common ancestor (32), would permit speculation regarding the antiquity of this strategy for iron respiration.

5.4.4 *Thermostability of soluble cell extracts and thermophilic nanowires*

Soluble fractions of whole-cell extracts from *G. sulfurreducens, G. ehrlichii,* and *G. ahangari* (representing a mesophile, a thermophile, and a hyperthermophile; respectively) were examined via the Sypro Orange thermal shift assay. As expected, the T_m of the soluble cell fraction increased from 57.2 (± 2.9), to 64.6 (± 1.5), to 81.6 (± 2.3) °C as the growth temperature of the organism increased (Figure 5.7). These temperatures match the approximate upper limit of growth temperatures for each organism (52, 66, 74), with the exception of *G. ahangari*. Thus, cessation of cell growth at their upper temperature limit, in most cases, is due to an overall instability of protein and thereby reduced function at increased temperatures. In addition, increasing (9.4) or decreasing (4.0) the pH away from a neutral (7.0) buffer negatively affected the T_m, as expected for proteins derived from neutrophilic microorganisms (52, 66, 74) (Figure

5.7A-C). Thus, the presence of stabilizing proteins and solutes in the cell interior, especially in the case of *G. ahangari*, likely functions to increase the *in vivo* stability of these proteins, which is lost upon their release from the cell.

Thus, while the soluble protein fractions demonstrate an increased thermal stability, the thermal stability of the nanowires themselves must be assessed to evaluate their use in nanodevices or biomimetic interfaces (307, 319) in which this stability is desired or required. The majority of proposed uses for these filaments, including electroactive nanobrushes for contaminant removal (307, 319), require the filaments to remain functional under conditions that would destabilize mesophilic proteins (17). Thermal stability has been linked to increased overall stability (17), and as such these thermophilic nanowires will likely exhibit increased resistance to a number of stressors. As the stability of the nanowires of mesophilic *Geobacter* species has never been assessed, it was also important to identify conditions and temperatures which would result in the denaturation of these, in addition to the (hyper)thermophilic nanowires. While the pili of *G. sulfurreducens* are being developed into nanodevices at Michigan State University (Chemical Engineering and Materials Science department), the pili of *G. metallireducens* were chosen to compare to those of *G. ahangari* and especially *G. ehrlichii* due to the phylogenetic relatedness of the pili of *G. metallireducens* to those of *G. ehrlichii* (Chapter 2).

Sypro Orange binding to the highly-purified filaments, *i.e.* the T_m, was expected to be dependent on the pH of the incubating buffer. However, after repeated attempts to obtain thermostability data for these filaments I was unable to obtain any useable results (Figure 5.8). Initial samples were introduced in low quantities and produced no increase in fluorescence, indicating no Sypro Orange binding to exposed hydrophobic domains. Subsequent attempts were made with increased relative protein concentrations, including an entire prep-cell sample being loaded, and the experiment was again unsuccessful. Of the samples which produced a fluorescence peak, each was present at the same temperature, regardless of organism or buffer pH (see Figure 5.8, *G. ahangari* for example). This is unlike sheared samples which were

introduced into the Sypro Orange assay. These samples, like the whole cells, reflected changes in the growth temperature of the organism and the incubating buffer. However, these matched the results obtained for whole-cell extracts and thus, the results were deemed to be acquired from contaminant, non-filament proteins. One additional possibility for the failure of prep-cell samples to provide sufficient fluorescence could be the presence of residual acrylamide from the purification protocol. Acrylamide is a well-known fluorescence quenching compound (320–322), and as such may interfere with the Sypro Orange fluorescence. Further attempts will be made to assess the chemical and thermal stability of these nanowires in comparison to those of mesophilic strains, primarily *G. sulfurreducens*. This may include further Sypro Orange assays on filaments not purified using acrylamide, or circular dichroism after filament incubation in a range of chemical and pH stressors.

5.4.5 *Pilus-like filaments from G. ahangari demonstrate curli-like behavior*

Amyloid fibrils produced by the curli of mesophilic bacteria, primarily within the *Enterobacteriaceae* (see (316, 317) for review), raised the exciting possibility of studying amyloid-fibril formation in a non-eukaryotic system. If an archaeal system, which would potentially be phylogenetically more related to systems in eukaryotes (18), was identified it could lead to major breakthroughs in the study of amyloid-based diseases such as Huntington's and Alzheimer's (317). The smaller, pilus-like filaments from *G. ahangari* are superficially similar to the curli of several mesophilic bacteria by both transmission electron microscopy and atomic force microscopy, as previously described (Figure 5.9A and B). Upon shearing of the pilus-like filaments from the cell and incubation at 4 °C, the filaments did function to enable the formation of amyloid-like bundles (Figure 5.9C and D). However, this alone is insufficient to permit speculations regarding the curli-like nature of these filaments. A definitive test is the incubation of sheared cell preparations with the amyloid-specific (323, 324) dye Thioflavin T. This dye, upon the switch from alpha helix to beta-pleated sheet, binds to the amyloid-like protein and alters its fluorescence. ThT fluorescence increase was seen in biofilms of the archaeon *Haloferax volcanii* (325),

indicating that functional amyloids may be present within archaeal biofilms, as they are in bacterial.

The next step in the identification of the first reported amyloid-forming filaments in the *Archaea* would be to determine if incubations of filament preparations from *G. ahangari* strain 234^T bind Thioflavin T. Sheared filament preparations using the rapid protocol from *G. ahangari* and *G. ehrlichii*, which will serve as the negative control, will be incubated at pH 4.0, 7.0, and 9.4, and in the presence of denaturing agents. A negative result, indicating that amyloid fibrils are not formed, would indicate that the morphological similarity of the pilus-like filaments from *G. ahangari* to bacterial curli is coincidental and that the aggregates formed after incubation at 4 °C are artifactual or non-amyloid aggregates. This finding would be supported by genome evidence. Homology searches conducted using the curli-associated Csg genes of *E. coli* against the genome of *G. ahangari* resulted in no homologous proteins; with the exception of the master regulator, CsgD, which provided weak hits to CheY and other response regulators within the genome. The probability that such proteins would be homologous across kingdoms is low, so this alone is not sufficient evidence to disprove the presence of curli-like filaments in *G. ahangari*. If I do see an increase in ThT fluorescence, indicating the presence of amyloid-like bundles, it would be the first report of amyloid fibrils forming in an archaeon outside of a biofilm environment.

5.5 *Conclusions*

Previous results demonstrate that both *G. ehrlichii* and *G. ahangari* use direct contact mechanisms to reduce insoluble Fe(III) oxides in the laboratory. The numerous *c*-type cytochromes identified within both genomes, and via SDS-PAGE, were speculated to be the terminal reductases of Fe(III) oxides. This indicated that the flagellar structures from both organisms were primarily used for motility and that the pili or pilus-like filaments were for attachment to the mineral surface (Chapters 2 and 3). A similar strategy is proposed for the thermophilic bacteria *C. ferrireducens* (114) and *T. potens* (186) and the hyperthermophilic

archaea *F. placidus* (113) and *G. acetivorans* (184) based on mechanistic and genomic evidence. Thus, based on available evidence, this was proposed to be a conserved mechanism for iron respiration at thermophilic and hyperthermophilic temperatures.

However, with the inclusion of the evidence presented within this chapter, it may be possible that these proposed mechanisms were missing one important consideration. The conductivity measurements presented within this chapter for *G. ehrlichii* and *G. ahangari* indicate that both of the hyper(thermophilic) nanowires under investigation are conductive (127 and 540 MOhm, respectively). While possibly fortuitous, the identification of nanowires in two physiologically- and geographically-distinct iron reducers suggests that microbial nanowires are more widespread than initially thought. TEM micrographs of other hydrothermal vent isolates able to grow on iron oxides show cells in direct contact with the mineral surface (15-17), and this may be linked to the presence of extracellular filaments. A thorough investigation of the prevalence of microbial nanowires has yet to be performed in mesophilic iron reducers, and as such this represents the first manuscript to provide data from a multi-species approach to examine the diversity of microbial nanowires. In addition, these represent the first microbial nanowires functioning outside of the mesophilic bacteria and the first report of microbial nanowires within the *Archaea*.

The development of a genetic system for either *G. ehrlichii* or *G. ahangari* would facilitate additional studies of these nanowires and their involvement in iron reduction. The pilus-like filaments from *G. ahangari* are predicted to be produced by GAH_01202 and/or GAH_01671, yet this is solely based on the presence of a DUF1628 domain, which has been found in pilin proteins throughout the archaea (258). The development of a genetic system for this model organism would permit mutagenesis assays and gene knockouts to help identify the gene(s) responsible for the production of these pilus-like filaments. However, given the sequence similarity between the pilin subunit sequences of *G. ehrlichii* and the *Geobacteraceae* (Chapter 2), it is likely that the mechanism present within the *Geobacteraceae* extends to the closely related

Desulfuromonadales. This similarity presents a unique opportunity for the *G. ehrlichii* pilin sequence to be heterologously expressed within apiliated strains of *G. sulfurreducens* (91) or *G. metallireducens* (82) and examined for their ability to transfer electrons to iron oxides or the anode of a microbial electrochemical cell.

Thus, the use of the nanowires of *G. ehrlichii* and *G. ahangari* may serve as a better developmental system for the future of microbial nanowires if I can determine their thermal and chemical stability. The Sypro Orange thermal shift assay presented here is ineffective due to the reasons discussed above, yet other assays may be performed. Determination of the stability of these proteins under a range of stressors would allow for the customization of nanodevices, employing one of the known microbial nanowires. Environmental sites where the use of nanowire-based nanodevices has been proposed have a range of stressors including pH, surfactants, and temperature (326). Similarly, the differences in resistance of these nanowires could be utilized for further customization.

An additional point of interest regarding these thermophilic and hyperthermophilic nanowires is the fact that they are operational at temperatures 30 – 60 °C below the temperature optimum of the organisms from which they were purified (52, 66). Enzymatic studies demonstrate increased reaction rates at increasing temperatures (17). If this trend holds true for the nanowires under investigation, conductivity measurements performed at thermophilic or hyperthermophilic temperatures on the nanowires of *G. sulfurreducens*, *G. ehrlichii*, and *G. ahangari* may provide further insight into their pathway for electron transfer and its stability at elevated temperatures. *G. sulfurreducens* nanowires, being mesophilic, may show an increase in resistance while those of the (hyper)thermophiles, being thereby closer to their optimal temperature, may increase in conductivity.

The finding that microbial nanowires are a conserved mechanism by which both the *Bacteria* and the *Archaea* can interact with and reduce insoluble Fe(III) oxides is of great interest to the field. This suggests that these conductive filaments are an ancestral mechanism, rather

than a recent acquisition by the *Geobacteraceae.* Evolution of extracellular appendages from attachment structures to conductive filaments would have been an efficient way for (hyper)thermophiles living in a biofilm environment (29) to extend their electroactive surface area and ensure the availability of electron acceptors to support growth.

CHAPTER 6. CONCLUSIONS AND FUTURE DIRECTIONS

6.1 *Review of project*

Dissimilatory iron reduction has been intensively studied in mesophilic microorganisms, primarily those residing within the bacterial genera *Shewanella* and *Geobacter*. Other models for iron reduction are available, yet until recently ((113, 114, 184–186) and (139) presented within this work) there has been no study of thermophilic and hyperthermophilic bacteria and archaea. The relatedness of these organisms to the last common ancestor has been established in the literature (32). Thus, the study of these microorganisms represents a unique opportunity to study the origins of one of the earliest forms of respiration (32) and of life on Earth (5, 20). These organisms, most often found surrounding geothermally-heated sites, can be a challenge to sample and culture due to their stringent growth requirements and low growth yields (34).

Yet, much can be learned from the study of hyperthermophiles. The fields of genetics, microbiology, and genomics owe much to a single species – *Thermus aquaticus*. This bacterium was isolated in 1969 from Yellowstone National Park (Wyoming) and grows at temperatures between 40 °C and 79 °C, with an optimum of 70 °C (327). Studies on *T. aquaticus* led to the identification and development of a number of enzymes which are still at the forefront of research in many fields (17, 328); foremost of which is the DNA polymerase from *T. aquaticus* which is lovingly named “Taq polymerase” or “Taq” for short. Since its discovery (329), this enzyme has revolutionized the field of genetics and a number of other fields (17, 330).

T. aquaticus demonstrates the power of thermophilic studies, and their ability to shape our world (17, 328, 331, 332). If I apply this same formula to other systems it may be possible to reach new heights in almost any field. The general formula which applies, regardless of what enzyme or property is being utilized, proceeds as follows: 1) identify, characterize, and sequence the product of interest within a (hyper)thermophilic organism, 2) heterologously express the

thermostable product in a mesophilic organism which is easy to culture and reaches high density (*i.e. E. coli*), and 3) verify that the properties sought for are still present for the heterologously-expressed product (330). Applying this same technique to almost any gene product could enable the expression and mass production of thermostable gene products.

Within this project I have proceeded through the initial stages of this workflow. Selection of potential model organisms was a key initial step. Following the selection of *G. ehrlichii* and *G. ahangari* as potential models for thermophilic and hyperthermophilic iron reduction it was possible to examine their mechanisms of iron reduction by both physiological and genomic studies. Finally, key proteins were identified which can, in the future, be applied to bioelectronic devices in development at Michigan State University to replace or augment the use of homologous, mesophilic, proteins.

6.1.1 *Review of* Geothermobacter ehrlichii *genome studies*

The genome of *G. ehrlichii* strain SS015 was targeted for sequencing based on its phylogenetic position (66), within the *Desulfuromonadaceae* yet close to the well-studied *Geobacteraceae* family (108), and due to its phylogenetically-unique ability to grow at thermophilic temperatures (66). A high-quality draft genome was constructed from a single Illumina library and contains 3.27 Mbp across 84 contigs. Present within these contigs are 3,059 protein-coding genes, 53 RNA genes, and a predicted 60 missing genes. This genome, while not complete, enabled the identification of key components which differentiate *G. ehrlichii* from the rest of the *Desulfuromonadales* and others which cement its inclusion within the order. A phylogenetic tree was created using the complete small subunit rRNA from the genome and populated with the increased diversity within the order, provided key insights into the diversity of the *Geothermobacter* genus and its position within the *Desulfuromonadales*. The thermophilic nature of *G. ehrlichii* was attributed to the increased usage of thermostable amino acids and the decreased usage of thermolabile residues. These trends were in opposition to those for the psychrophile *G. electrodiphilus*.

Central metabolic pathways within the genome were identified and a near-complete glycolytic and a complete gluconeogenic pathway were encoded. In addition, a complete TCA cycle was identified within the genome and contained the conserved eukaryotic citrate synthase (156). A near complete non-oxidative phase of the pentose phosphate pathway was also identified within the genome while the oxidative phase was absent. *G. ehrlichii* is unable to respire sulfur-containing compounds to support growth (66). However, a near complete dissimilatory pathway was discovered within the genome in addition to the identified assimilatory pathway. Nitrate reduction has been identified in *G. ehrlichii* and, based on the work presented here, may proceed in a manner similar to *G. metallireducens* (77, 333) where nitrite is produced by the identified NarGHI gene cluster and immediately consumed, although the enzyme for this could not be definitively determined.

Mechanistic studies of dissimilatory iron reduction have been ongoing for years within the *Geobacteraceae* (103). Thus, it was essential to this project to identify, within the *G. ehrlichii* genome, proteins involved in the respiration of insoluble Fe(III) oxides. A bacterial flagellum was identified and this, combined with the presence of numerous chemotaxis gene clusters, may be involved in chemotaxis to iron (102). In addition, 34 putative *c*-type cytochromes were identified in the genome which likely function as in *Geobacter spp*. to enable the capacitor-like physiology of the order (174). Finally, a type IV pilus and associated genes were identified within the genome. This Geopilus is most similar, by sequence similarity, to that of *G. metallireducens* and is predicted to be involved in binding or electron transfer to insoluble metal oxides. Finally, an EPS gene cluster was discovered between the type IV pilus gene clusters which may function as in *G. sulfurreducens* to facilitate the inclusion of *c*-type cytochromes into an EPS matrix to facilitate extracellular electron transfer (90).

6.1.2 *Review of* Geoglobus ahangari *genome studies*

G. ahangari was chosen for genomic sequencing due to its obligate iron-reducing nature and its phylogenetic position within a family, the *Archaeoglobaceae* (52), which predominantly

respire sulfur-containing compounds (334). *G. ahangari* (52), *G. acetivorans* (178), and *F. placidus* (179) are the only members of the *Archaeoglobales* able to respire insoluble Fe(III) oxides. A complete and finished genome was constructed from Illumina sequences, in collaboration with researchers at Western New England University. This genome, available at GenBank (CP011267), contains 1.77 Mbp, 2,072 genes, 52 RNA coding genes, and a predicted 47 pseudogenes.

Numerous hydrogenases were identified within the genome and these, combined with a near-complete methanogenesis pathway for carbon fixation, provides genomic evidence for the ability of *G. ahangari* to grow autotrophically with hydrogen as an electron donor (52). A modified Embden-Meyerhof-Parnas glycolytic pathway was identified in the genome and, based on the available sequence data, gluconeogenesis is expected to function. As in *F. placidus*, the incomplete nature of the oxidative pentose phosphate pathway is predicted to be overcome by the use of the RuMP pathway (231). In addition, a complete TCA cycle is present within the genome of *G. ahangari*, as is conserved among the *Archaeoglobales* (335). *G. ahangari* was the first anaerobic hyperthermophile reported to utilize long-chain fatty acids and completely oxidize them to CO_2 (52). 39 proteins were identified within the *G. ahangari* genome that encode for β-oxidation pathway proteins and likely enable this metabolism.

Proteins likely to be involved in extracellular electron transfer, with a focus on *c*-type cytochromes and cellular components involved in motility and attachment to iron oxides, were also identified in the genome of *G. ahangari*. An archaeal *fla1* gene cluster (255) was identified within the genome of *G. ahangari* to enable the production of an archaellum. This is surprising, as the majority of the family contains *fla2* gene clusters (255), including the only other member of the *Geoglobus* genus available in pure culture (184). Two putative pilus proteins, GAH_01202 and GAH_01671, were identified within the genome by the presence of a DUF1628 domain (258). These pilus proteins likely work in conjunction with the 21 genes encoding putative *c*-type cytochromes to enable extracellular electron transfer by *G. ahangari*.

6.1.3 *Review of* Geoglobus ahangari *iron-respiration mechanism*

Within this work I was able to demonstrate that *Geoglobus ahangari* employs a direct-contact mechanism for the reduction of insoluble Fe(III) oxides. This reduction results in the production of fine-grain magnetite, as shown by electron diffraction data. Addition of metal chelators or electron shuttles to the culture media stimulated the reduction of the Fe(III) oxides. No electron shuttles or chelators were produced by the cells. Thus, growth was not supported using alginate-entrapped Fe(III) oxides as the sole electron acceptor unless an exogenous electron shuttle was added. The addition of AQDS, the electron shuttle, enabled growth on these entrapped oxides and resulted in the accumulation of a biofilm on the bead surface in addition to supporting a planktonic population. The presence of a large electron shuttle, which would be unable to enter the pores in the alginate beads, was disproven by spent culture supernatant having no spurring effect on freshly inoculated *G. ahangari* cultures. In addition, no significant chelation of the Fe(III) oxides was shown in culture tubes unless an exogenous chelator was provided. Thus, I proposed that a direct-contact mechanism was employed by *G. ahangari* to enable the respiration of insoluble metal oxides.

Consistent with the proposed direct contact mechanism is the presence of numerous proteins which could facilitate extracellular electron transfer. Transmission electron microscopy analysis of cultures of *G. ahangari* show cells in direct contact, and encased in many cases, with Fe(III) oxides. Dissolution of the metal oxides revealed two different morphologies of extracellular filaments. One, the archaellum identified in the genome (Chapter 3), is predicted to function solely for motility. In contrast, numerous curled pilus-like filaments were found on soluble and insoluble Fe(III) oxide grown cultures. *G. ahangari* cells also, identified by a heme-stained SDS-PAGE gel, produced a number of heme-containing bands, several of which were able to be sheared from the outer surface of the cell. Mechanical shearing of outer-surface proteins, including the predicted outer-surface *c*-type cytochromes, resulted in the inability of cells to grow on insoluble,

but not soluble, Fe(III) oxides. These data thus supported the proposed mechanism that the archaellum provides a motility apparatus to locate iron oxides in the environment, the pilus-like filaments facilitate attachment and electron transfer, and the cytochromes act as the terminal reductase.

6.1.4 *Review of (hyper)thermophilic microbial nanowires*

Previous data suggested that a direct-contact mechanism permitted the respiration of Fe(III) oxides in both *G. ehrlichii* and *G. ahangari.* Due to the presence of extracellular filaments in these organisms their biochemical properties and contributions to extracellular electron transfer were assessed. Mechanical shearing of both species produced crude purifications of extracellular filaments. Both the motility apparatus and the putative nanowires were purified in this matter, concentrated, and visualized by both TEM and AFM. The pili of *G. ehrlichii* were numerous and *ca.2*- 2.5 nm in diameter while the flagella were much larger, *ca.* 30 nm. The pilus-like filaments from *G. ahangari,* which were again the more numerous of the filament morphologies, were *ca.* 2.5 nm in diameter and present a curli-like morphology as seen by TEM and AFM. Incubation of these curli-like filaments at 4 °C produced, after 72 h, protein aggregates which are hypothesized to be amyloid in nature. The archaella produced by *G. ahangari* are relatively straight and have a diameter of *ca.* 4 nm. The use of a preparatory gel (92) to purify these filaments to homogeneity resulted in highly-purified samples containing only the pilus and pilus-like filaments, demonstrating their SDS insolubility.

These purification techniques provided sufficient sample to determine if, like *G. sulfurreducens*, these filaments functioned as microbial nanowires in *G. ehrlichii* and *G. ahangari.* From the mechanical shearing protocol it was determined that the motility structures from both organisms were insulating. This provided an internal control to ensure that contaminant metals were not contributing significantly to the conductivity of the putative nanowires. When the more numerous cellular filaments were assayed by CP-AFM both of these filaments were shown to be conductive (37,458 and 266 MOhms for *G. ehrlichii* and *G. ahangari*, respectively). Purified

samples obtained from the prep-cell protocol retained their conductivity (127 and 540 MOhms for *G. ehrlichii* and *G. ahangari*, respectively). This indicates that contaminant metal ions and proteins were not the cause of the detected conductivity, and, in the case of *G. ehrlichii,* contaminants caused an insulating effect. These filaments are predicted to increase the electroactive surface area available to the cell (91), an ability thought to be evolutionarily beneficial in biofilm and subsurface environments where soluble compounds could easily be lost (102, 139).

Discovery of additional microbial nanowires expands our knowledge regarding the diversity of this mechanism of extracellular electron transfer. Additionally, due to the increased growth temperatures of both *G. ehrlichii* (66) and *G. ahangari* (52), the thermal stability of cell proteins and the filaments was assessed by the Sypro Orange thermal shift assay. Unfortunately, the thermal and chemical stability of the nanowires under investigation, in addition to the pili of *G. metallireducens*, could not be assessed due to limited fluorescent output attributed to fluorescence quenching, protein aggregation, or low protein concentrations. However, soluble cell extracts were produced from the mesophile *G. sulfurreducens* in addition to the two (hyper)thermophilic species under investigation and provided reproducible results. As expected, the thermal stability of these cell extracts approximately matched the upper limit of growth temperatures for these organisms, with the exception of *G. ahangari* which is expected to stabilize its proteins *in vivo*.

6.2 *Future directions*

6.2.1 *Geoglobus ahangari*

As discussed in Chapter 3, the protein-coding gene(s) for the pilus-like filaments of *G. ahangari* has been hypothesized but has not been confirmed by biochemical methods. Pending the development of a genetic system for this archaeon, a method to depolymerize the nanowires into their individual subunits must be elucidated. If taken from prep-cell samples, which are assumed to be comprised solely of the nanowires, a single band may be obtained by SDS-PAGE

analysis and stained using a high-sensitivity protein stain such as the Pierce™ Silver Stain Kit (Life Technologies). Yet, the predicted thermal stability of these filaments, which must also be successfully assessed, combined with their proposed curli-like nature will likely cause difficulties with their depolymerization (17, 316). If this can be overcome, it may be possible to obtain the protein sequence of the subunit and, due to the availability of the sequenced genome, match peptide fragments obtained by matrix-assisted laser desorption/ionization (MALDI-TOF) of trypsin-digested subunits to proteins encoded within the genome.

The production of protein aggregates after extended incubation at 4 °C by the pilus-like filaments of *G. ahangari* is a promising preliminary result to identifying the first amyloid-forming protein in an archaeon. However, the available data, which include their curled appearance by TEM and AFM, do not provide sufficient evidence to definitively make this claim. Within this work, the use of Congo Red and Thioflavin T as amyloid dyes has been proposed. These dyes, when bound to amyloid-like beta sheets, exhibit altered spectra (317). Incubation of the pilus-like filaments from *G. ahangari* at 4 °C for 72 h, as previously demonstrated to be sufficient for aggregates to form, in the presence of these dyes would provide sufficient evidence to cement the curli-like nature of these filaments.

6.2.2 *Geothermobacter ehrlichii*

Due to the phylogenetic and physiological similarities between *G. ehrlichii* and the intensely studied members of the *Geobacteraceae* (66), there exist a staggering number of possibilities for future studies in *G. ehrlichii*. Heterologous expression of the pilin gene in *G. sulfurreducens*, for example, would enable comparison of current production in microbial electrochemical cells, where the contribution of the pilus is expected to be important for electron transfer. Changes in current production would indicate that the pili of *G. ehrlichii* are more or less conductive than those of *G. sulfurreducens* when expressed heterologously. In addition, a similar strategy could be employed to determine if the EPS operon identified in the *G. ehrlichii* genome could complement the lack of the Xap operon of *G. sulfurreducens* when grown on insoluble

Fe(III) oxides. In addition to these studies, the thermal and chemical stability of the pili must be assessed.

While the genome of *G. ehrlichii* presented within this work has been sufficient to identify complete metabolic pathways and components critical to iron respiration, it is not closed or finished. Genome reconciliation attempts by Minimus2 (130) have been successful, but must continue. In addition, additional sequencing must be attempted by next-generation sequencing technologies or using the primer-based approach that is currently underway. The closure of the genome, while not essential, would strengthen the use of *G. ehrlichii* as the model thermophile within the *Desulfuromonadales*.

6.3 *Looking forward*

While the data presented within this work have shed light on a possible mechanism for the origins and evolution of ancient (hyper)thermophiles able to grow on and respire insoluble Fe(III) oxides, this has been discussed in depth previously. Looking forward, instead of back in time to early Earth, these nanowires may be critical components in the next generation of biomimetic nanodevices. Following successful heterologous expression in a mesophilic strain which is able to produce the nanowires in high numbers, as is in process for the pilus nanowires of *G. sulfurreducens*, it will be possible to examine their biochemical and electrochemical capabilities with greater ease. Self-assembly of the nanowires into films or as an assembly would permit their use in all systems being developed for *G. sulfurreducens*. While not expressly proven within this work, these thermophilic filaments are expected to have increased thermal and chemical stabilities over those currently in use. Thus, if they can be introduced into the current nanodevice framework, these nanowires will likely have a broader range of applicability in bioremediation sites where conditions are often far from pH 7.0 and 25 °C. Such applications are beyond the scope of this work, but researchers are only now beginning to scratch the surface in terms of applications

for these novel nanowires. The future is bright, and may someday be powered by (hyper)thermophiles and microbial nanowires.

APPENDICES

APPENDIX A

TABLES

Table 2.1. Classification and general features of *G. ehrlichii*

MIGS ID	Property	Term	Evidence code[a]
	Current classification	Domain *Bacteria*	TAS (18)
		Phylum *Proteobacteria*	TAS (121)
		Class *Deltaproteobacteria*	TAS (122, 123)
		Order *Desulfuromonadales*	TAS (123)
		Family *Desulfuromonadaceae*	TAS (108)
		Genus *Geothermobacter*	TAS [1]
		Species *Geothermobacter ehrlichii*	TAS [1]
		Type strain SS015	TAS [1]
	Cell shape	Rod	TAS [1]
	Motility	Motile	TAS [1]
	Sporulation	Non-sporulating	NAS
	Temperature range	35-65 °C (optimum 55 °C)	TAS [1]
	Salinity range	5.0-8.0 (optimum 6.0)	TAS [1]
	Salinity	5.0-50 g/L (optimum 19 g/L)	TAS [1]
MIGS-22	Oxygen requirement	Anaerobe	TAS [1]
	Carbon source	Organic acids, CO_2	TAS [1]
	Energy metabolism	chemoorganotrophic	TAS [1]
MIGS-6	Habitat	Marine geothermally heated areas	TAS [1]
MIGS-15	Biotopic relationship	Free-living	TAS [1]
MIGS-14	Pathogenicity	None	NAS
	Biosafety level	1	NAS
	Isolation	“Bag City” hydrothermal vent	TAS [1]

Table 2.1 (cont'd)

MIGS-4	Geographic location	Axial Seamount - Juan de Fuca Ridge	TAS [1]
MIGS-5	Isolation time	Unknown	
MIGS-4.1	Latitude	46° N	TAS [1]
MIGS-4.2	Longitude	130° W	TAS [1]
MIGS-4.3	Depth	1400 m	TAS [1]
MIGS-4.4	Altitude	Not applicable	

a) Evidence codes – IDA: Inferred from Direct Assay; TAS: Traceable Author Statement (i.e., a direct report exists in the literature); NAS: Non-traceable Author Statement (i.e., not directly observed for the living, isolated sample, but based on a generally accepted property for the species, or anecdotal evidence). These evidence codes are from the Gene Ontology project (124). Classification and general features are according to the MIGS recommendations (120).

Table 2.2. Genome sequencing project information for the genome of *G. ehrlichii*

MIGS ID	**Property**	**Term**
MIGS-31	Finishing quality	High-quality draft
MIGS-28	Libraries used	2 independent 100 bp paired-end Illumina shotgun libraries, and 1 Pacific Biosciences library run on a single SMRT cell
MIGS-29	Sequencing platforms	Illumina MiSeq, PacBio
MIGS-31.2	Sequencing coverage	300 × coverage (Illumina libraries), 600 × coverage (Pacific Biosciences library)
MIGS-30	Assemblers	Velvet, Minimus2
MIGS-32	Gene calling method	RAST
	INSDC ID	N/A
	Genbank Date of Release	N/A
	GOLD ID	N/A
	NCBI project ID	N/A
MIGS-13	Source material identifier	ATCC *BAA-635*, DSMZ *DSM-15274*
	Project relevance	Phylogenetic diversity, biotechnology, metal respiration in thermophiles, and microbial nanowires

Table 2.3. Assembly reconciliation statistics for the *G. ehrlichii* genome

	1S + 2S	2S + PacBio	1S + PacBio	(1S + 2S) + PacBio
# contigs (>= 0 bp)	38	23	21	19
# contigs (>= 1000 bp)	37	23	21	19
Total length (>= 0 bp)	2,997,257	3,307,005	3,254,057	3,070,722
Total length (>= 1000 bp)	2,996,328	3,307,005	3,254,057	3,070,722
# contigs	38	23	21	19
Largest contig	386,328	676,668	721,357	782,787
Total length	2,997,257	3,307,005	3,254,057	3,070,722
GC (%)	61.9	61.75	61.8	61.87
N50	121,299	228,051	227,920	234,024
N75	92,840	128,803	128,724	126,606
L50	7	5	5	4
L75	13	9	9	8
# N's per 100 kbp	2.64	1.15	2.09	2.77

Table 2.4. Primers used for gap closure of the *G. ehrlichii* genome

Primer	Sequence (5'-3')	Amplification
Geh_A+H_01_S	CTG CCA TCA CCA AGG TTC TT	Off of the 5' end of contig 1
Geh_A+H_02_S	TGA TCC CCA TGT ATC TGC TG	Off of the 5' end of contig 2
Geh_A+H_03_S	GTT TCG GTC ACC TTC TGC TG	Off of the 5' end of contig 3
Geh_A+H_04_S	CGG ACG GTA ACC TTT GAA GA	Off of the 5' end of contig 4
Geh_A+H_05_S	ACC GAC ACC AAC AGC AAA GT	Off of the 5' end of contig 5
Geh_A+H_06_S	GCA GTT GTT GGC GTA GAG AG	Off of the 5' end of contig 6
Geh_A+H_07_S	GGC AAC ATC CTC TGC TAC ATC	Off of the 5' end of contig 7
Geh_A+H_08_S	GTG TTG AAA GCA CGA CCA AA	Off of the 5' end of contig 8
Geh_A+H_09_S	GTC ACC GGC GTC TAC TAT CC	Off of the 5' end of contig 9
Geh_A+H_10_S	AGG GTG ACG AAC AAC AGC TT	Off of the 5' end of contig 10
Geh_A+H_11_S	ATC AGG CTC CAG GTC TCC TT	Off of the 5' end of contig 11
Geh_A+H_12_S	ATG ACC TTC AGC TCG GTC AG	Off of the 5' end of contig 12
Geh_A+H_13_S	AGA AAA TTT GGC AGC CTT CA	Off of the 5' end of contig 13
Geh_A+H_14_S	CCT GCG GTG TAA GAT GTG TG	Off of the 5' end of contig 14
Geh_A+H_15_S	GGC CAA CAA GTT CAA AGA GC	Off of the 5' end of contig 15
Geh_A+H_16_S	CGC CTT ACT CTT TGG TGC TC	Off of the 5' end of contig 16
Geh_A+H_17_S	ACA ACA GCG TCA GGA GGA CT	Off of the 5' end of contig 17
Geh_A+H_18_S	AGA CCG TAC TTG GCC TTG TG	Off of the 5' end of contig 18
Geh_A+H_19_S	CAC CGC AAC GAT TTC ATC AT	Off of the 5' end of contig 19
Geh_A+H_20_S	GAA GAG ATC CGG GAG GAA GT	Off of the 5' end of contig 20
Geh_A+H_21_S	CAG ATC GCT CTC TTC GAT CC	Off of the 5' end of contig 21
Geh_A+H_22_S	CCT CTA GTC ATC CCT GGC TTT	Off of the 5' end of contig 22

Table 2.4 (cont'd)

Geh_A+H_23_S	GGC CTC GTC CAC TAT CTT GA	Off of the 5' end of contig 23
Geh_A+H_01_E	TCA TCG AGG GGA TCA AGA AG	Off of the 3' end of contig 1
Geh_A+H_02_E	AAA ACC AAC GCC TGA AAA TG	Off of the 3' end of contig 2
Geh_A+H_03_E	AGG TCG CAA GCA AAA TCA AA	Off of the 3' end of contig 3
Geh_A+H_04_E	GTT CAA GGC CTT TGA CCA GA	Off of the 3' end of contig 4
Geh_A+H_05_E	CCT GGC TTC ATC GAA CAC TT	Off of the 3' end of contig 5
Geh_A+H_06_E	AAG CTC GAA GCT GAA CCA AA	Off of the 3' end of contig 6
Geh_A+H_07_E	GTT CAT CAC CCC CGG ATA CT	Off of the 3' end of contig 7
Geh_A+H_08_E	GGG GAT GAA CCG ATT TCT TT	Off of the 3' end of contig 8
Geh_A+H_09_E	GTT GAT CGC CAG GAT GAA GT	Off of the 3' end of contig 9
Geh_A+H_10_E	TTT GAA GAA CGG GGT GTG AC	Off of the 3' end of contig 10
Geh_A+H_11_E	AGG TCG CAA ACC ATC AAA AG	Off of the 3' end of contig 11
Geh_A+H_12_E	AAA GTC GCT GTA TGC CAG GT	Off of the 3' end of contig 12
Geh_A+H_13_E	GAT CGA AGA GAG CGA TCT GG	Off of the 3' end of contig 13
Geh_A+H_14_E	GCC ATC GAC GGC AAT ATC	Off of the 3' end of contig 14
Geh_A+H_15_E	CGA GAA CCA GGA GAA TGA GC	Off of the 3' end of contig 15
Geh_A+H_16_E	CGG TTT TGC TTT TGA TGG TT	Off of the 3' end of contig 16
Geh_A+H_17_E	GGG GCT TCT GGT AGT GTT GA	Off of the 3' end of contig 17
Geh_A+H_18_E	CGA GTG CAT CAG CAC CAC	Off of the 3' end of contig 18
Geh_A+H_19_E	CTG GCT GTT GGT GTG CAG	Off of the 3' end of contig 19
Geh_A+H_20_E	CAG ACC TTC GTG GCA GAA AT	Off of the 3' end of contig 20
Geh_A+H_21_E	CAA GGT GGT TGT CGA GGT CT	Off of the 3' end of contig 21
Geh_A+H_22_E	TTG GGC ACT GTC TCA ACA AG	Off of the 3' end of contig 22
Geh_A+H_23_E	GAT CAA CAC CGA CCC TGA AG	Off of the 3' end of contig 23

Table 2.5. Nucleotide content and gene count levels of the *G. ehrlichii* genome

Attribute	**Value**	**% of total[a]**
Size (bp)	3,276,179	100.0%
Coding region (bp)	2,845,273	86.8%
G+C content (bp)	2,022,946	61.8%
Number of replicons	1	
Extrachromosomal elements	0	
Total genes	3,112	100.0%
RNA genes	53	1.7%
rRNA operons	1	
Protein-coding genes	3,059	100.0%
Pseudogenes	115	3.7%
Genes with function prediction	2,289	74.8%
Genes assigned to KEG pathways	1,580	51.7%
Genes assigned Pfam domains	2,496	81.6%
Genes with signal peptides	206	6.7%
Genes with transmembrane helices	709	23.2%
CRISPR repeats	2	

a) The total is based on either the size of the genome in base pairs or the total number of protein coding genes in the annotated genome.

Table 2.6. Number of genes within *G. ehrlichii* associated with the 27 subsystem categories in RAST

Value	%age[a]	Description
296	9.7%	Amino acids and derivatives
265	8.7%	Protein metabolism
259	8.5%	Cofactors, vitamins, prosthetic groups, and pigments
219	7.2%	Carbohydrates
177	5.8%	Respiration
156	5.1%	RNA metabolism
118	3.9%	Membrane transport
108	3.5%	Motility and chemotaxis
105	3.4%	Fatty acids, lipids, and isoprenoids
102	3.3%	DNA metabolism
94	3.1%	Stress response
86	2.8%	Virulence, disease, and defense
79	2.6%	Cell wall and capsule
72	2.4%	Nucleosides and nucleotides
33	1.1%	Cell division and cell cycle
33	1.1%	Phosphorus metabolism
28	0.9%	Nitrogen metabolism
27	0.9%	Miscellaneous
21	0.7%	Sulfur metabolism
19	0.6%	Potassium metabolism
19	0.6%	Regulation and cell signaling

Table 2.6 (cont'd)

4	0.1%	Secondary metabolism
4	0.1%	Metabolism of aromatic compounds
3	0.1%	Dormancy and sporulation
1	0.0%	Iron acquisition and metabolism
0	0.0%	Photosynthesis
0	0.0%	Phages, prophages, transposable elements, and plasmids
731	23.9%	Not in subsystems

a) The total is based on the total number of protein coding genes in the genome

Table 2.7. Putative *c*-type cytochromes identified in the genome of *G. ehrlichii*

Feature id	Best hit by BLAST	Heme motifs	Final MW (kDa)
peg.33	Cytochrom_c3 superfamily protein	5	21.6
peg.301	Cytochrom_c7 superfamily protein	9	72.9
peg.357	Hypothetical protein	2	16.9
peg.481	Cytochrome *c* oxidase	1	14.2
peg.491	Cytochrome *c* family protein	1	8.9
peg.499	DUF3365 family protein	1	19.1
peg.569	Decaheme *c*-type cytochrome / Lipoprotein cytochrome *c*	1	77
peg.622	Hydroxylamine reductase / Cytochrome *c* family protein	13	104
peg.623	Hydroxylamine reductase / Cytochrome *c* family protein	10	35
peg.652	Cytochrome *c* family protein	1	15.7
peg.707	Cytochrome *c* family protein	3	13.1
peg.810	Cytochrome *c* family protein	23	83.4
peg.812	Cytochrome *c* family protein	8	38.8
peg.814	Cytochrome *c* family protein	4	23.6
peg.874	Hydroxylamine oxidoreductase	8	53.2
peg.1066	Cytochrome *c* family protein	4	22.4
peg.1403	Cytochrome *c* family protein	4	30.4
peg.1404	Cytochrome *c* family protein	7	43.1
peg.1443	Cytochrome *c* family protein	11	57.5

Table 2.7 (cont'd)

peg.1444	Cytochrome *c* family protein	5	18.3
peg.1570	Hydroxylamine reductase	9	51.6
peg.1636	Cytochrome *c* peroxidase	1	10.4
peg.1714	Cytochrome *b*	1	9.6
peg.2110	Cytochrome *c* family protein	9	32
peg.2155	Cytochrome *c* family protein	19	244.2
peg.2156	Cytochrome *c* family protein	57	310.5
peg.2157	Cytochrome *c* family protein	4	29.6
peg.2276	Cytochrome *cbb*3	1	15.3
peg.2316	Hypothetical protein	1	16.3
peg.2495	Octaheme tetrathionate reductase	8	54.5
peg.2497	Cytochrome *c* family protein	1	10.4
peg.2725	Hypothetical protein / DnaJ	4	11.6
peg.2734	Cytochrome *cbb*3	2	29.8
peg.2766	Cystathione beta synthase	7	31.6

Table 3.1. Classification and general features of *G. ahangari*

MIGS ID	Property	Term	Evidence code[a]
	Current classification	Domain *Archaea*	TAS (18)
		Phylum *Euryarchaeota*	TAS (18, 336)
		Class *Archaeoglobi*	TAS (337)
		Order *Archaeoglobales*	TAS (335)
		Family *Archaeoglobaceae*	TAS (334)
		Genus *Geoglobus*	TAS (52)
		Species *Geoglobus ahangari*	TAS (52)
		Type strain 234^T	TAS (52)
	Gram stain	Variable	NAS
	Cell shape	Irregular coccus	TAS (52)
	Motility	Motile	TAS (52)
	Sporulation	Non-sporulating	NAS
	Temperature range	65-90 °C	TAS (52)
	Optimal temperature	88 °C	TAS (52)
	pH range; Optimum	5.0-7.6 (optimum 7.0)	TAS (52)
	Carbon source	CO_2	TAS (52)
	Energy metabolism	Chemolithoautotrophic, chemolithotrophic, chemoorganotrophic	TAS (52)
MIGS-6	Habitat	Marine geothermally heated areas	TAS (52)
MIGS-6.3	Salinity	9.0-38 g/L NaCl	TAS (52)
MIGS-22	Oxygen requirement	Anaerobe	TAS (52)

Table 3.1 (cont'd)

MIGS-15	Biotopic relationship	Free-living	TAS (52)
MIGS-14	Pathogenicity	Non-pathogen	NAS
	Isolation	Hydrothermal vent chimney	TAS (52)
MIGS-4	Geographic location	Guaymas Basin hydrothermal system	TAS (52)
MIGS-5	Sample collection time	Unknown	NAS
MIGS-4.1	Latitude	27° N	TAS (52)
MIGS-4.2	Longitude	111° W	TAS (52)
MIGS-4.3	Depth	2000 m	TAS (52)
MIGS-4.4	Altitude	Not applicable	

a) Evidence codes – IDA: Inferred from Direct Assay; TAS: Traceable Author Statement (i.e., a direct report exists in the literature); NAS: Non-traceable Author Statement (i.e., not directly observed for the living, isolated sample, but based on a generally accepted property for the species, or anecdotal evidence). These evidence codes are from the Gene Ontology project (124). Classification and general features are based on the MIGS recommendations (120).

Table 3.2. Genome sequencing project information of *G. ahangari*

MIGS ID	Property	Term
MIGS-31	Finishing quality	Finished
MIGS-28	Libraries used	5 independent 100 bp paired-end Illumina shotgun libraries, 150 bp paired-end Illumina shotgun library
MIGS-29	Sequencing platforms	Illumina MiSeq
MIGS-31.2	Sequencing coverage	1,977 × coverage (100 bp libraries) 100 × (150 bp library)
MIGS-30	Assemblers	SeqMan NGen, Velvet, SeqMan Pro
MIGS-32	Gene calling method	JGI-ER, GLIMMER
	INSDC ID	CP011267
	Genbank Date of Release	May 11, 2015
	GOLD ID	Gp0101274
	NCBI project ID	258102
MIGS-13	Source material identifier	ATCC *BAA-425*, DSMZ *DSM-27542*, JCM *JCM 12378*
	Project relevance	Phylogenetic diversity, biotechnology, evolution of metal respiration in hyperthermophiles, and anaerobic degradation of hydrocarbons

Table 3.3. Nucleotide content and gene count levels of the *G. ahangari* genome

Attribute	**Value**	**% of total[a]**
Size (bp)	1,770,093	100.0%
Coding region (bp)	1,662,832	93.9%
G+C content (bp)	940,071	53.1%
Number of replicons	1	
Extrachromosomal elements	0	
Total genes	2072	100.0%
RNA genes	52	2.5%
rRNA operons	2	
Protein-coding genes	2020	100.0%
Pseudogenes	47	2.3%
Genes with function prediction	1677	83.0%
Genes in paralog clusters	1406	69.6%
Genes assigned to COGs	1470	72.8%
Genes assigned Pfam domains	1667	82.5%
Genes with signal peptides	55	2.7%
Genes with transmembrane helices	409	20.2%
CRISPR repeats	7	

a) The total is based on either the size of the genome in base pairs or the total number of protein coding genes in the annotated genome.

Table 3.4. Number of genes in *G. ahangari* associated with the 25 general COG functional categories

Code	Value	%age[a]	Description
J	155	7.6%	Translation, ribosomal structure and biogenesis
A	2	0.1%	RNA processing and modification
K	68	3.3%	Transcription
L	58	2.9%	Replication, recombination and repair
B	6	0.3%	Chromatin structure and dynamics
D	20	1.0%	Cell cycle control, Cell division, chromosome partitioning
Y	0	0.0%	Nuclear structure
V	7	0.3%	Defense mechanisms
T	24	1.2%	Signal transduction mechanisms
M	35	1.7%	Cell wall/membrane biogenesis
N	15	0.7%	Cell motility
Z	0	0.0%	Cytoskeleton
W	0	0.0%	Extracellular structures
U	23	1.1%	Intracellular trafficking and secretion
O	57	2.8%	Posttranslational modification, protein turnover, chaperones
C	160	7.9%	Energy production and conversion
G	37	1.8%	Carbohydrate transport and metabolism
E	139	6.8%	Amino acid transport and metabolism
F	49	2.4%	Nucleotide transport and metabolism
H	103	5.1%	Coenzyme transport and metabolism
I	55	2.7%	Lipid transport and metabolism

Table 3.4 (cont'd)

P	86	4.2%	Inorganic ion transport and metabolism
Q	16	0.8%	Secondary metabolites biosynthesis, transport and catabolism
R	244	12.0%	General function prediction only
S	198	9.7%	Function unknown
-	477	23.5%	Not in COGs

a) The total is based on the total number of protein coding genes in the genome

Table 3.5. Terminal electron acceptors in the *Archaeoglobales*

	Electron acceptors				
Organism	**Sulfate**	**Sulfite**	**Thiosulfate**	**Nitrate**	**Fe(III)**
Geoglobus spp.	**-**	**-**	**-**	**-**	**+**
Ferroglobus placidus	-	-	+	+	+
Archaeoglobus spp.	+/-	+	+	-	-

Table 3.6. Putative *c*-type cytochromes in *G. ahangari*

Gene ID:	Annotation:	# of heme binding motifs:	Calculated molecular weight:	TM domains:
GAH_00015	Hypothetical protein	4	58.4	0
GAH_00283	Cytochrome c7	4	21.2[a]	1
GAH_00286	Nitrate/TMAO reductases, membrane-bound tetraheme cytochrome c subunit	12	39.1	0
GAH_00301	Putative redox-active protein (C_GCAxxG_C_C)	2	31.5	3
GAH_00504	Hypothetical protein	10	54.5	1
GAH_00505	Hypothetical protein	4	26.8	2
GAH_00506	Cytochrome c3	9	48.6	0
GAH_00507	Cytochrome c7	4	27.4[a]	1
GAH_00508	Hypothetical protein	5	28.5	1
GAH_00510	Hypothetical protein	4	27.3	1
GAH_00817	Seven times multi-haem cytochrome CxxCH	8	53.7	1
GAH_01091	Hypothetical protein	1	11.7	1
GAH_01235	Hypothetical protein	5	21.5	0
GAH_01236	Hypothetical protein	5	22.3[b]	0
GAH_01253	Hypothetical protein	4	16.9	0
GAH_01256	NapC/NirT cytochrome c family, N-terminal region	10	43.6[a]	1

Table 3.6 (cont'd)

GAH_01296	Cytochrome c family protein	4	17.2	1
GAH_01297	Seven times multi-haem cytochrome CxxCH	8	61.0	1
GAH_01306	Class III cytochrome C family	8	46.3	0
GAH_01534	Hypothetical protein	1	18.5	1
GAH_01700	Hypothetical protein	3	9.9	0

a) No signal peptide detected

b) Signal peptide detected by PRED-SIGNAL

Table 3.7. Uniquinone and menaquinone biosynthesis proteins in *G. ahangari*

Protein name	**Abbreviation**	**Homologs in *G. ahangari***
1,4-dihydroxy-2-naphthoate octaprenyltransferase	MenA	GAH_01919
Naphthoate synthase	MenB	GAH_01602, GAH_00487, GAH_01332
Chorismate dehydratase	MqnA	GAH_00872
Cyclic dehypoxanthinyl futalosine synthase	MqnC	GAH_00873, GAH_00871, GAH_00663
1,4-dihydroxy-6-naphthoate synthase	MqnD	GAH_02003
Aminodeoxyfutalosine synthase	MqnE	GAH_00871, GAH_00873, GAH_00663
4-hydroxybenzoate polyprenyltransferase	MbiA	GAH_00304, GAH_00157
Phenylphosphate carboxylase subunit beta	UbiD	GAH_01625, GAH_00517
4-hydroxy-3-polyprenylbenzoate decarboxylase	UbiD	GAH_01570
UbiD family decarboxylase	UbiD	GAH_01625
Demethylmenaquinone Methyltransferase	UbiE/MenG	GAH_00100, GAH_01336, GAH_00796

Table 3.8. Fe-S binding domain proteins and ferredoxins within the genome of *G. ahangari*

Locus Tag	Gene Product Name
GAH_00040	Ferredoxin-like domain protein
GAH_00110	Uncharacterized Fe-S oxidoreductase
GAH_00113	Fe-S oxidoreductase
GAH_00114	Predicted Fe-S oxidoreductases
GAH_00137	Fe-S oxidoreductase
GAH_00138	Fe-S oxidoreductase
GAH_00140	Iron-sulfur cluster-binding protein
GAH_00158	Ferredoxin-like domain protein
GAH_00165	Predicted Fe-S oxidoreductases
GAH_00413	Aldehyde:ferredoxin oxidoreductase
GAH_00488	Electron transfer flavoprotein beta
GAH_00537	Heterodisulfide reductase, subunit A and polyferredoxins
GAH_00538	Iron-sulfur cluster-binding oxidoreductase
GAH_00570	Pyruvate ferredoxin oxidoreductase
GAH_00615	Uncharacterized Fe-S protein PflX
GAH_00622	Radical SAM domain iron-sulfur cluster-binding oxidoreductase with cobamide-binding-like domain
GAH_00678	Predicted Fe-S-cluster oxidoreductase
GAH_00684	Ferredoxin
GAH_00822	Fe-S oxidoreductase
GAH_00845	Ferredoxin
GAH_00886	Fe-S oxidoreductase

Table 3.8 (cont'd)

GAH_00924	Ferredoxin
GAH_01011	Indolepyruvate ferredoxin oxidoreductase
GAH_01136	4Fe-4S binding domain/Putative Fe-S cluster
GAH_01180	Iron-sulfur cluster-binding oxidoreductase
GAH_01225	Ferredoxin
GAH_01254	Fe-S-cluster-containing hydrogenase
GAH_01276	Fe-S oxidoreductase
GAH_01286	Fe-S-cluster-containing hydrogenase
GAH_01295	Fe-S-cluster-containing hydrogenase
GAH_01344	Predicted Fe-S oxidoreductase
GAH_01351	Uncharacterized Fe-S center protein
GAH_01440	Ferredoxin
GAH_01646	Ferredoxin
GAH_01669	Ferredoxin
GAH_01685	Rubredoxin
GAH_01686	Uncharacterized flavoproteins
GAH_01728	Aldehyde:ferredoxin oxidoreductase
GAH_01737	Predicted Fe-S oxidoreductases
GAH_01738	Aldehyde:ferredoxin oxidoreductase
GAH_01822	Aldehyde:ferredoxin oxidoreductase
GAH_01856	Aldehyde:ferredoxin oxidoreductase
GAH_01866	Ferredoxin-thioredoxin reductase

Table 3.8 (cont'd)

GAH_01870	Fe-S oxidoreductase
GAH_01921	Dehydrogenases (flavoproteins)
GAH_01948	Ferredoxin
GAH_01960	Ferredoxin
GAH_01981	Fe-S oxidoreductase
GAH_02012	Pyruvate ferredoxin oxidoreductase
GAH_02033	Heterodisulfide reductase, subunit A

APPENDIX B

FIGURES

Figure 1.1. Geologic timescale of the Precambrian Supereon

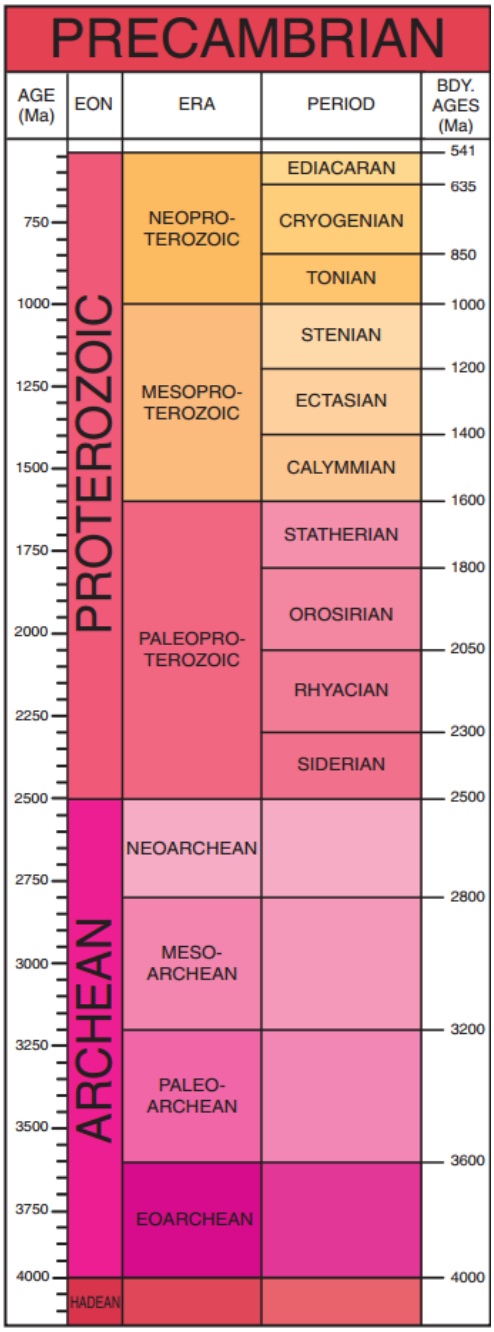

Taken from the Geological Society of America® and can be found at the following web address:

http://www.geosociety.org/science/timescale/timescl.pdf

Figure 1.2. Location of the Axial Seamount and the layout of the Axial Seamount caldera

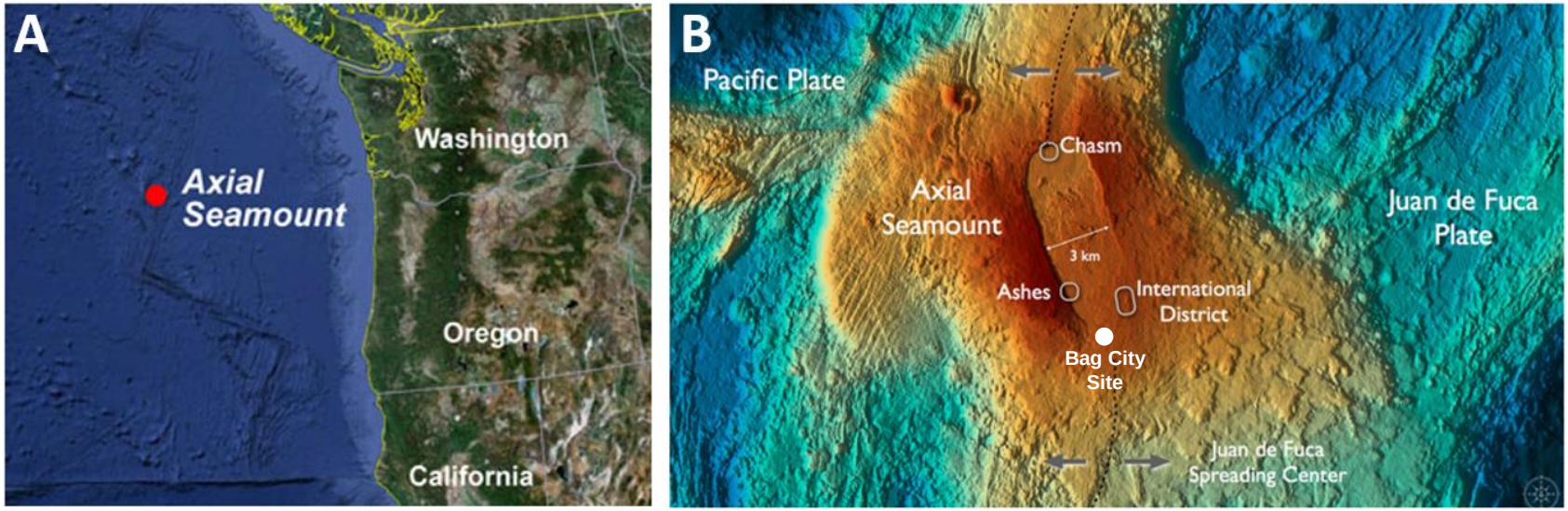

Location of the Axial Seamount in relation to the continental United States (A) and the layout of the Axial Seamount caldera (B). Image A is taken from the Monterey Bay Aquarium Research Institute and can be found at the web address http://www.mbari.org/news/homepage/2012/axial-mapping/axial-locationmap-350.jpg. Image B is taken from the Interactive Oceans website and can be found at the web address http://www.interactiveoceans.washington.edu/files/axial.seamount.webcopy_med.jpg and has been altered to include the approximate location of the Bag City site.

Figure 1.3. Location of the Guaymas Basin

Location of the Axial Seamount in relation to the continental United States, the Baja Peninsula, and Mexico. Image taken from the University of California Museum of Paleontology and can be found at the web address http://www.ucmp.berkeley.edu/images/science/profiles/guaymas.jpg

Figure 2.1. Phylogenetic tree of *G. ehrlichii*

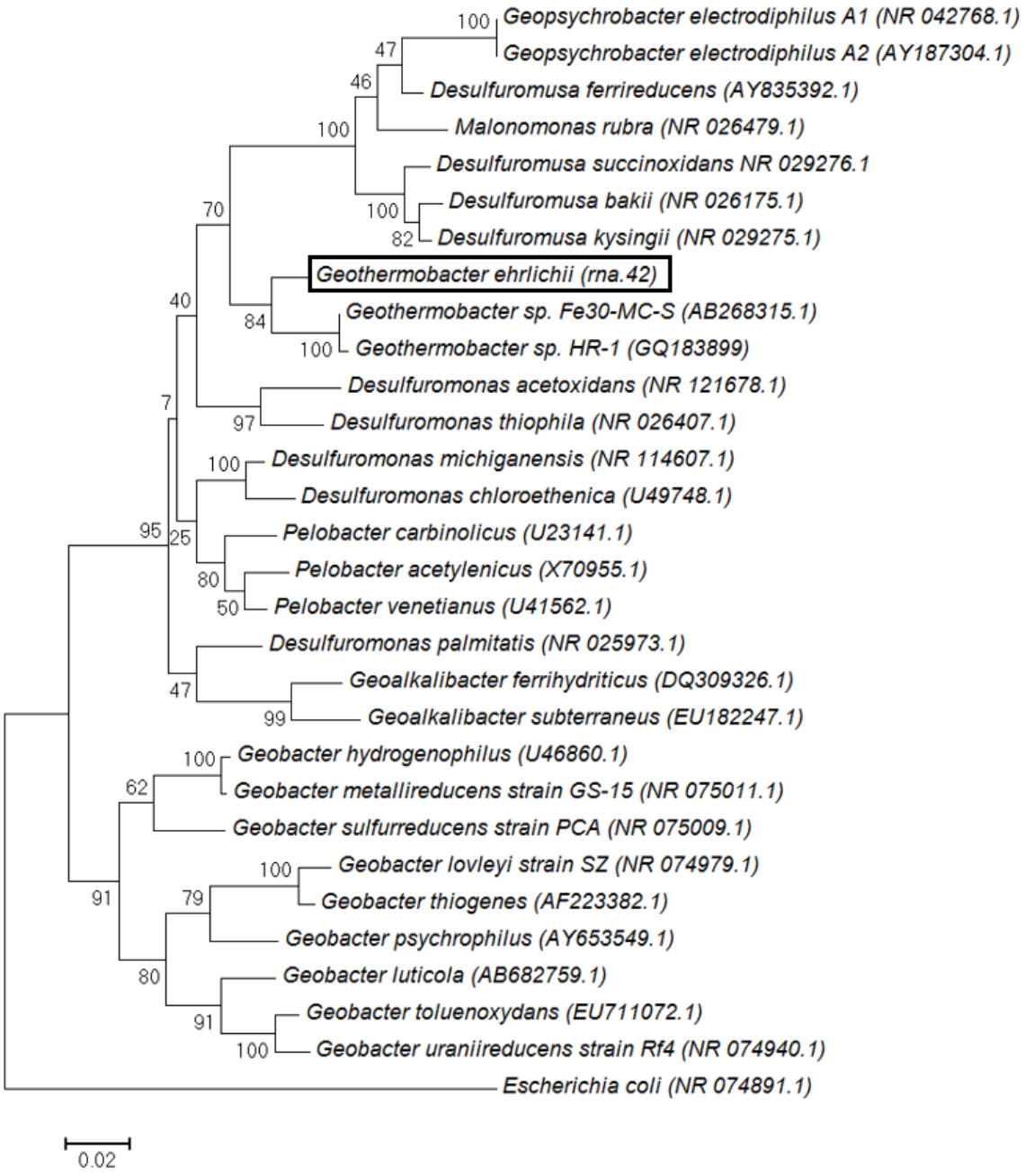

Tree constructed with the maximum likelihood algorithm comparing the 16S rRNA gene sequence from *G. ehrlichii* strain SS015 to other members of the Desulfuromonales. Bootstrap values were determined from 100 replicates and *Escherichia coli* was used as an outgroup.

Figure 2.2. Transmission electron micrograph of *G. ehrlichii*

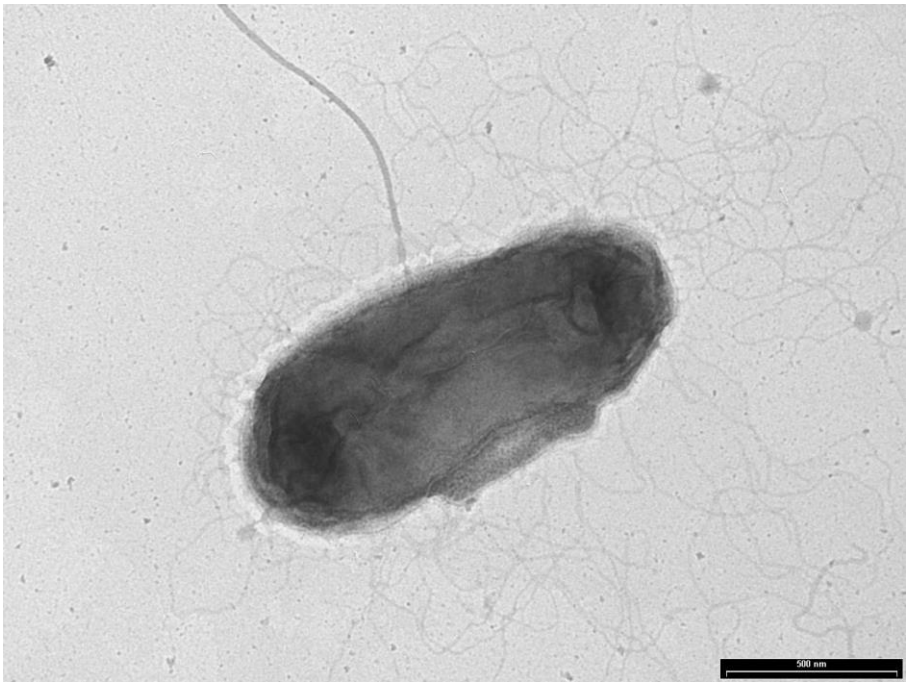

Cultures were grown on soluble Fe(III) oxides. Bar, 500 nm.

Figure 2.3. Amino acid usage of *G. ehrlichii* and *G. electrodiphilus* in comparison to mesophilic members of the *Geobacteraceae*

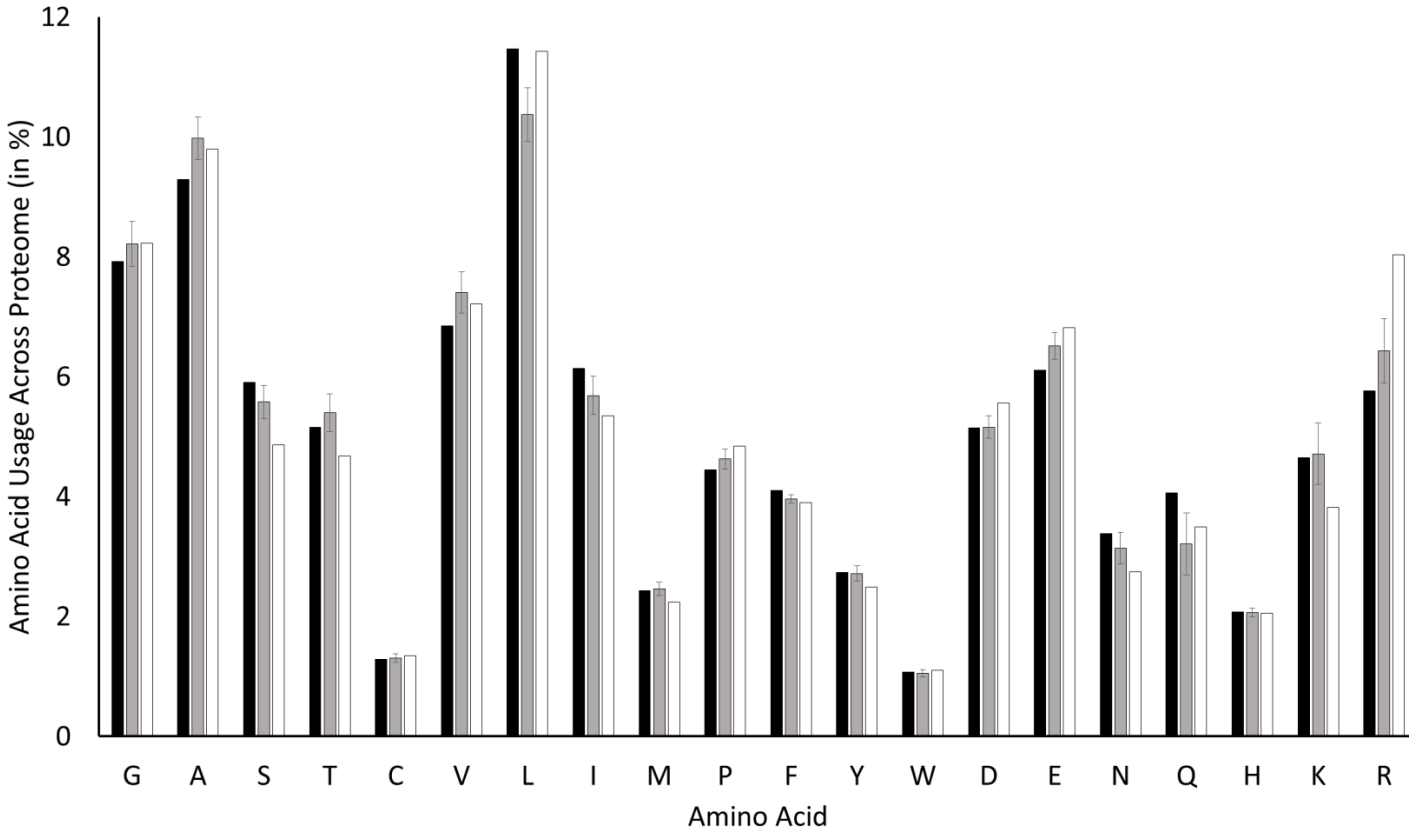

Amino acid usage of the psychrophile G. *electrodiphilus* (white) and the thermophile *G. ehrlichii* (black) compared to the averaged amino acid usage of examined mesophilic *Geobacter spp* (gray). Protein sequences were obtained from NCBI. Solid bar at bottom indicates amino acids which are implicated in increasing thermal stability while those indicated by the dashed line indicate amino acids implicated in reducing thermal stability.

Figure 2.4. Ratio of charged to polar amino acids from *G. ehrlichii, G. electrodiphilus,* and mesophilic members of the *Geobacteraceae*

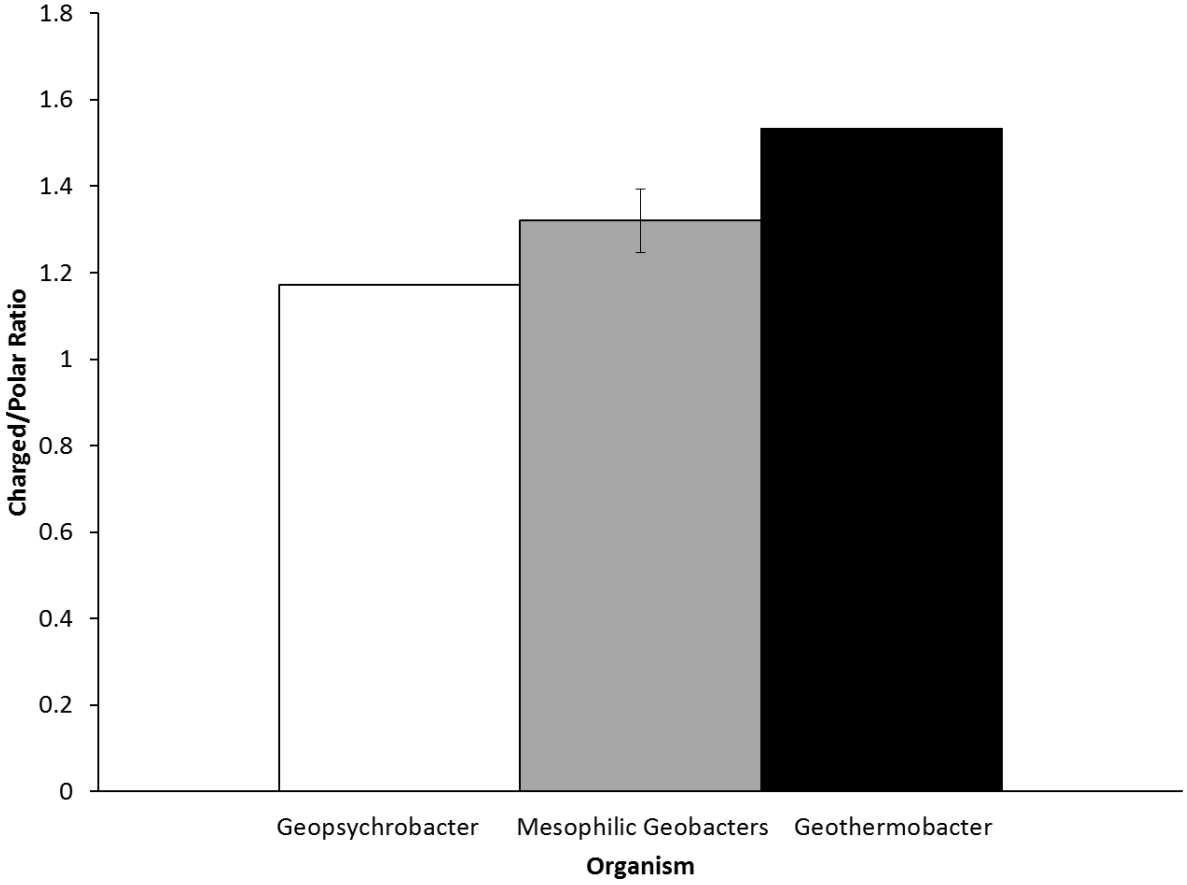

Charged to polar amino acid ratios of the psychrophile G. *electrodiphilus* (white) and the thermophile *G. ehrlichii* (black) compared to the averaged ratio of mesophilic *Geobacter spp* (gray). Protein sequences were obtained from NCBI.

Figure 2.5. Central metabolism in *G. ehrlichii*

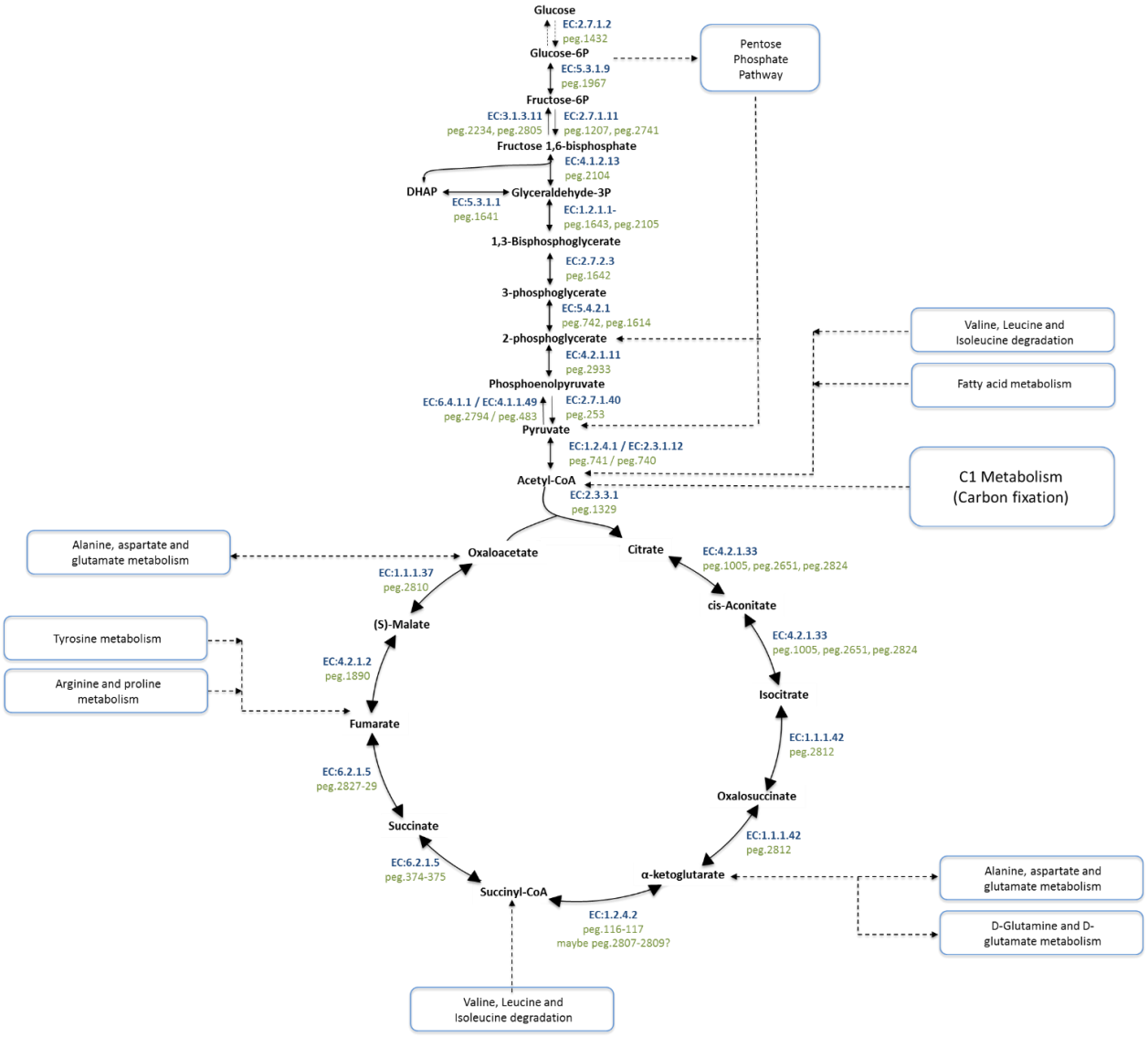

Figure 2.6. Sequence relatedness of the pilin subunit protein to members of the *Desulfuromonadales*

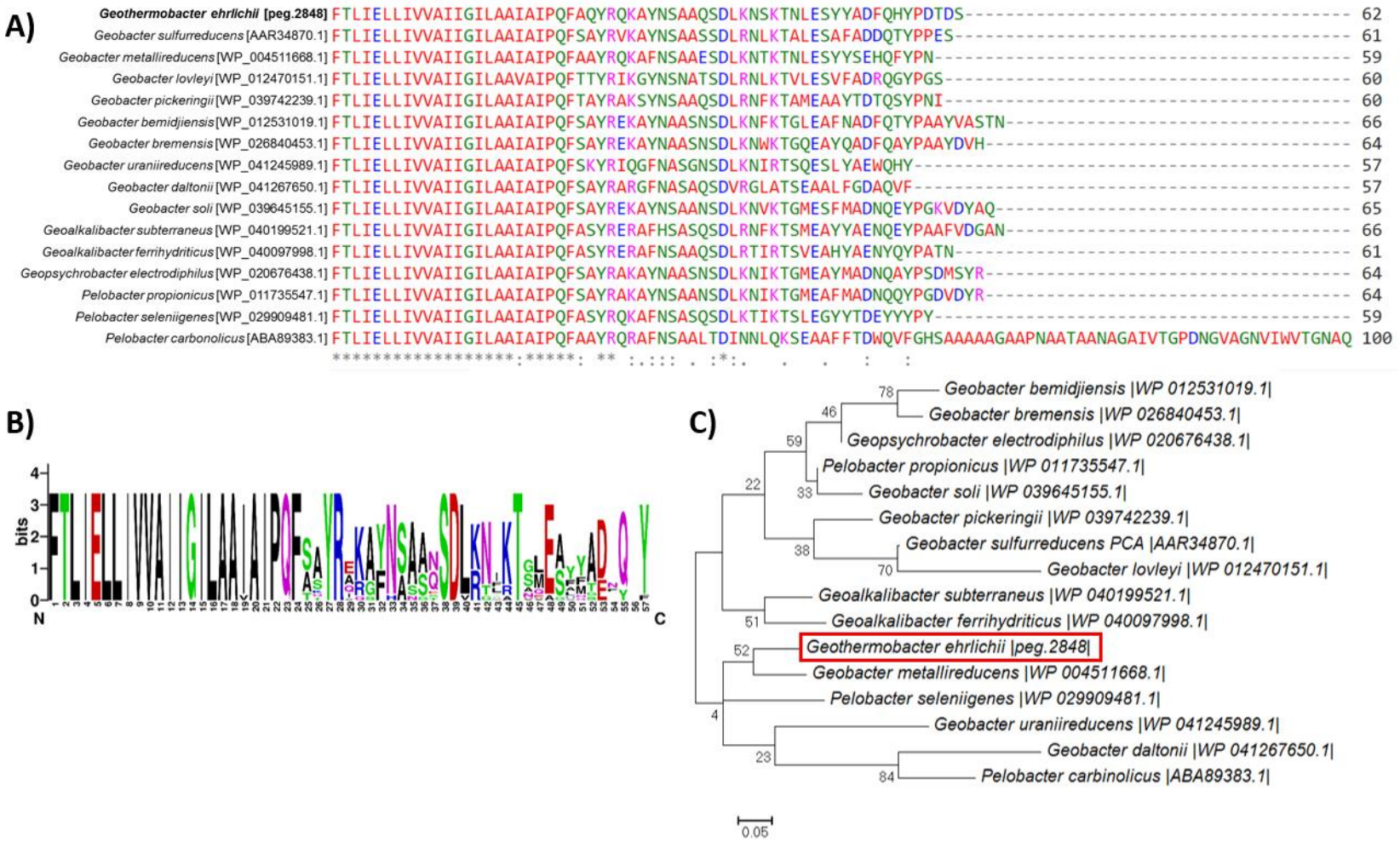

Figure 2.6 (cont'd)

(A) Alignment of the pilin subunit of *G. ehrlichii* strain SS015 to members of the *Geobacteraceae* and *Desulfuromonadaceae* generated using the Muscle alignment tool (167) within MEGA 6.0 (168). (B) Graphical representation (169) of the multiple sequence alignment highlighting the conserved N-terminus region. (C) Phylogenetic tree derived from the multiple sequence alignment created using the Maximum Likelihood algorithm within MEGA 6.0 (168) and bootstrap values represent 100 replicates.

Figure 2.7. SDS-PAGE gel of sheared proteins stained with the TMBZ protocol

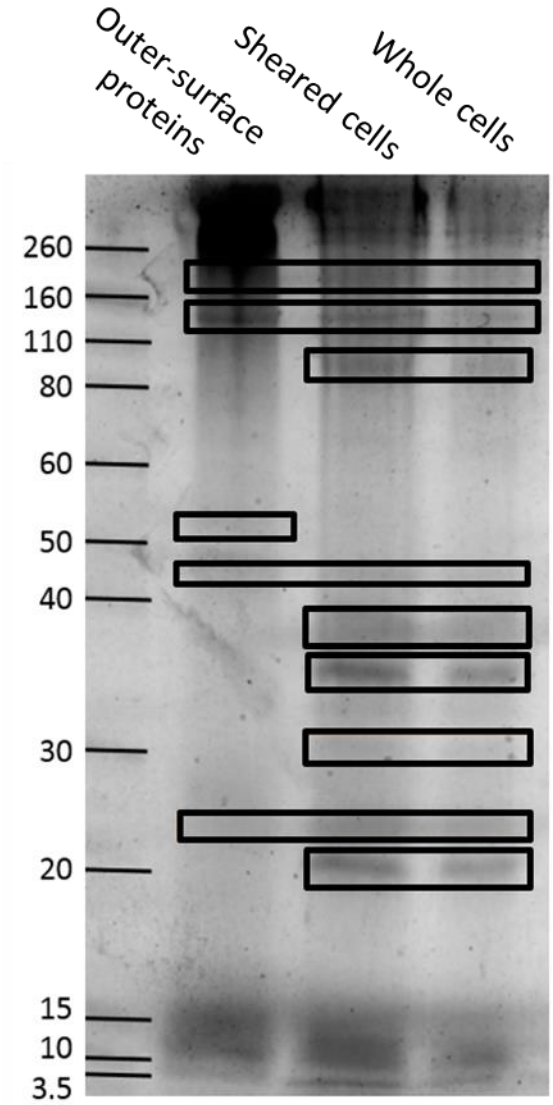

Heme-stained SDS-PAGE of outer-surface proteins sheared from the cell surface (lane 2), sheared cells (lane 3), and whole-cell extracts from *G. ehrlichii* (lane 4). Lane 1 shows protein markers and numbers at left show their corresponding molecular weights in kDa. The Novex molecular weight marker used is shown (left). Black boxes indicate identified cytochromes

Figure 3.1. Phylogenetic tree of *G. ahangari*

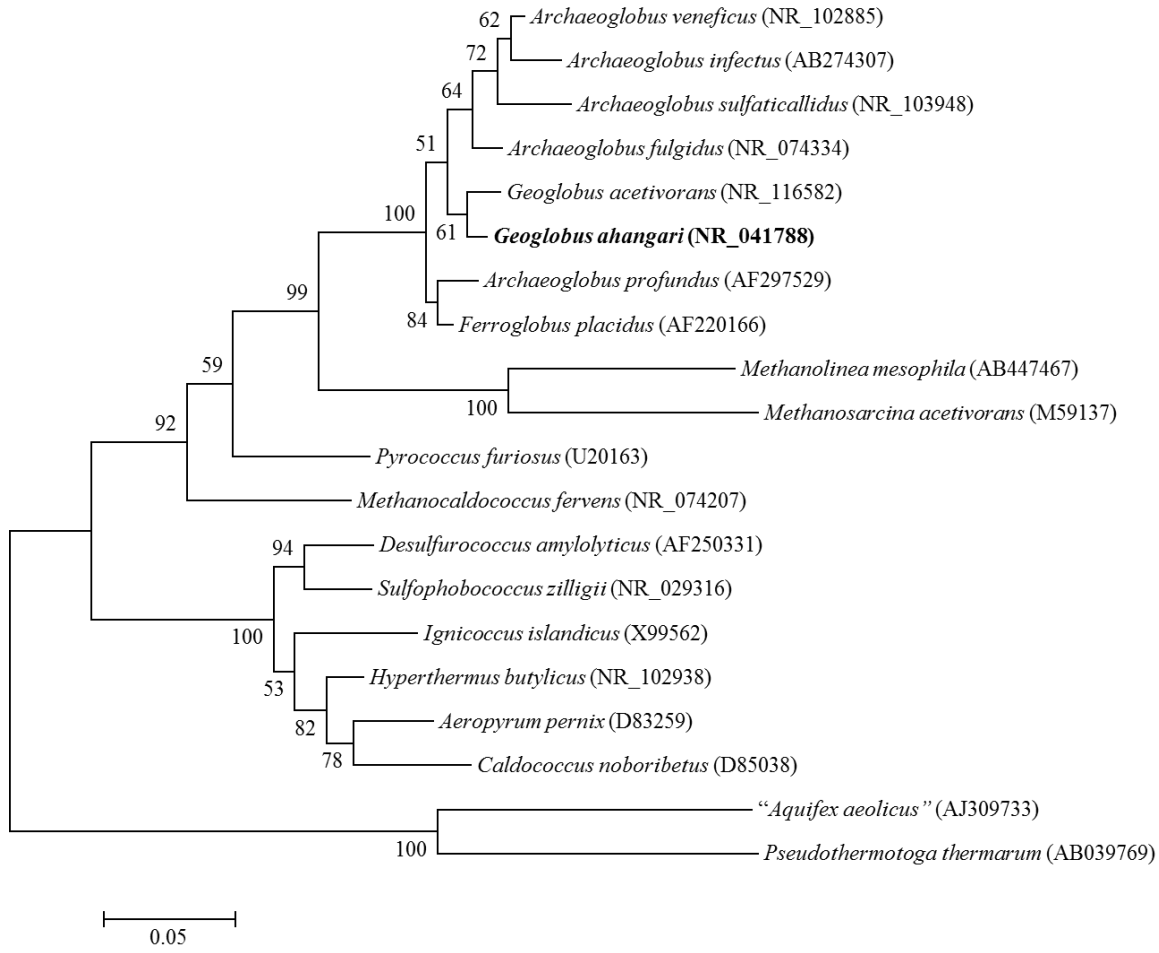

The phylogenetic tree was constructed with the maximum likelihood algorithm comparing the 16S rRNA gene sequence from *G. ahangari* to other hyperthermophilic archaea. Bootstrap values were determined from 100 replicates and "*Aquifex aeolicus*" and *Pseudothermotoga thermarum* were used as outgroups.

Figure 3.2**.** Scanning electron micrograph of cells of *G. ahangari*

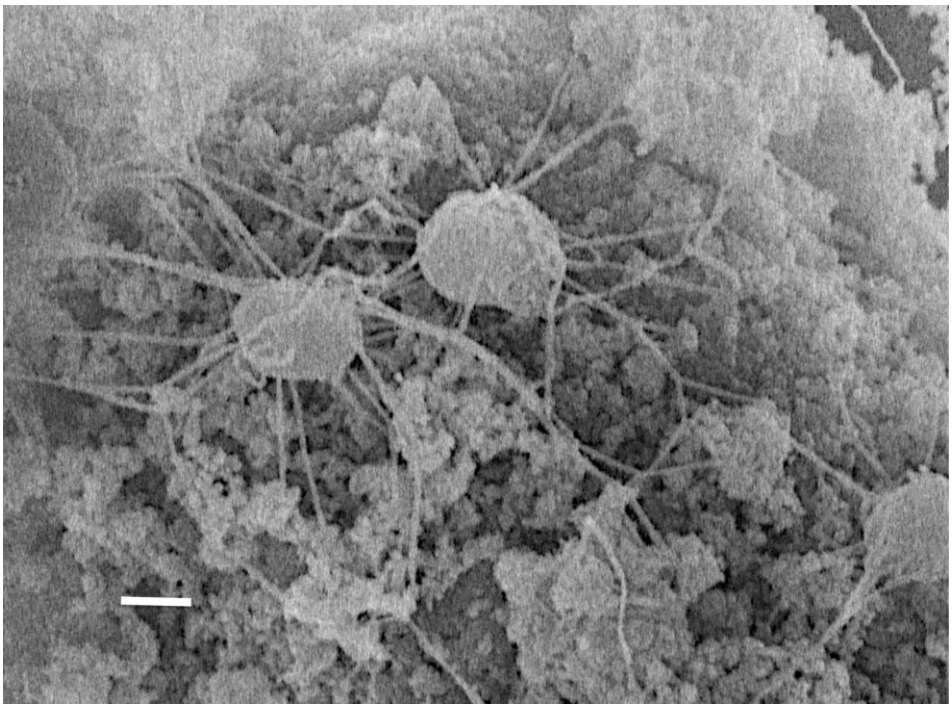

Cells were grown on insoluble Fe(III) oxides. Bar, 100 nm.

Figure 3.3. Graphical circular map of the *G. ahangari* genome

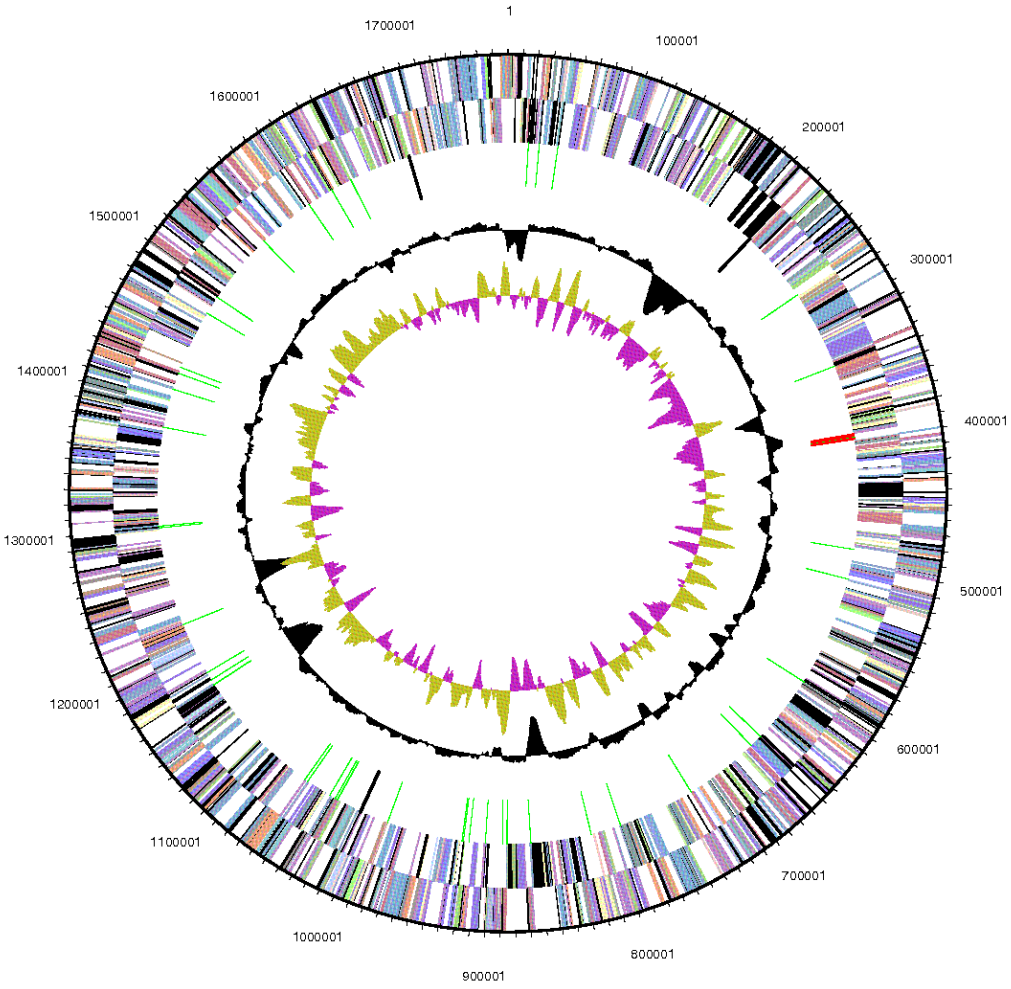

From outside to the center: Genes on forward strand (colored by COG categories), genes on reverse strand (colored by COG categories), RNA genes (tRNAs green, rRNAs red, other RNAs black), GC content, and GC skew.

Figure 3.4. Central metabolism in *G. ahangari*

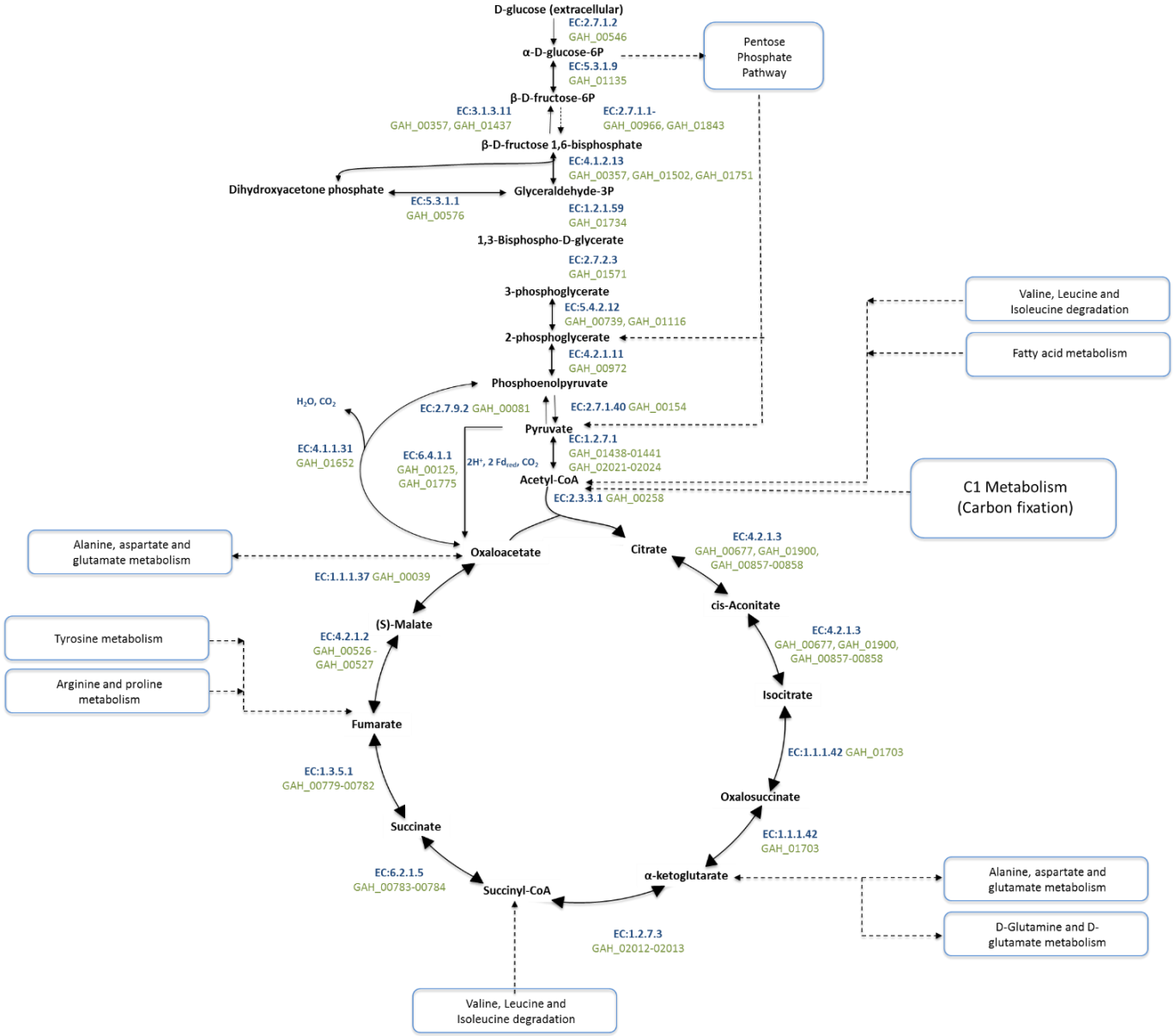

Figure 4.1. Effect of electron shuttles or metal chelators on the reduction of Fe(III) oxides by *G. ahangari*

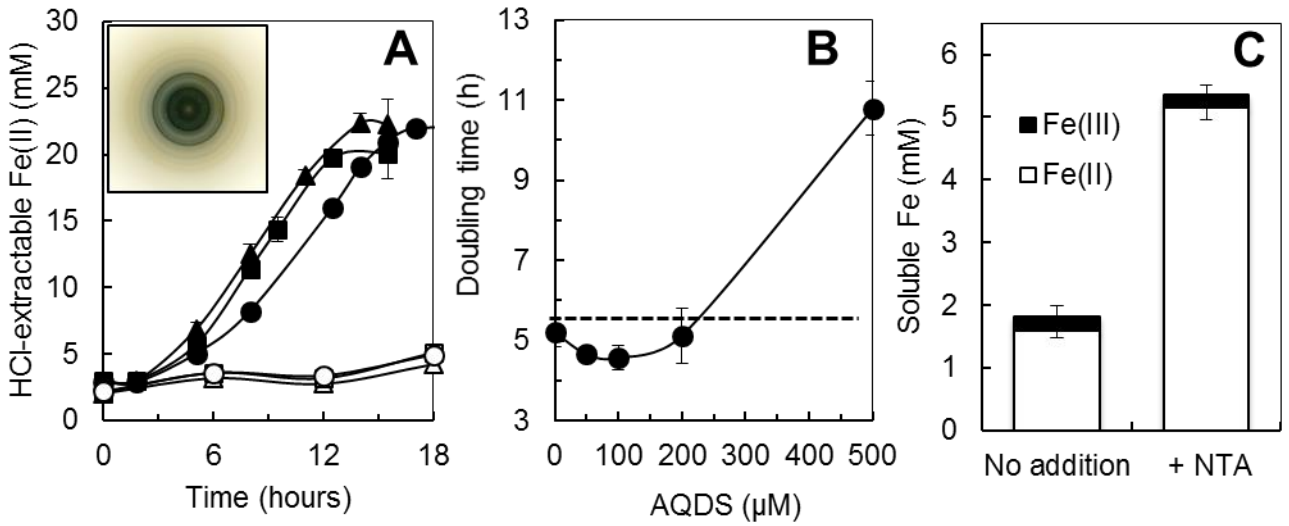

(A) Stimulation of Fe(III) oxide reduction (calculated as HCl-extractable Fe(II)) with 50 μM of the electron shuttle AQDS (squares) and 4 mM of the metal chelator NTA (triangles) in reference to cultures with no additions (circles). Controls lacking electron donor (pyruvate, 10 mM) are also shown (open symbols). Inset shows electron diffraction pattern of the reduced mineral, which is consistent with magnetite. (B) Doubling times (calculated from the rates of HCl-extractable Fe(II) production) as a function of the AQDS concentration present in the medium. Horizontal dashed line marks the doubling time in cultures without AQDS. (C) Soluble Fe(II) and Fe(III) in filtered supernatant fluids from stationary phase (ca. 17 mM of HCl-extractable Fe(II)) cultures with no additions or supplemented with NTA). All data points show averages and standard deviations of five replicates.

Figure 4.2. *G. ahangari* lacks the ability to produce endogenous electron shuttles

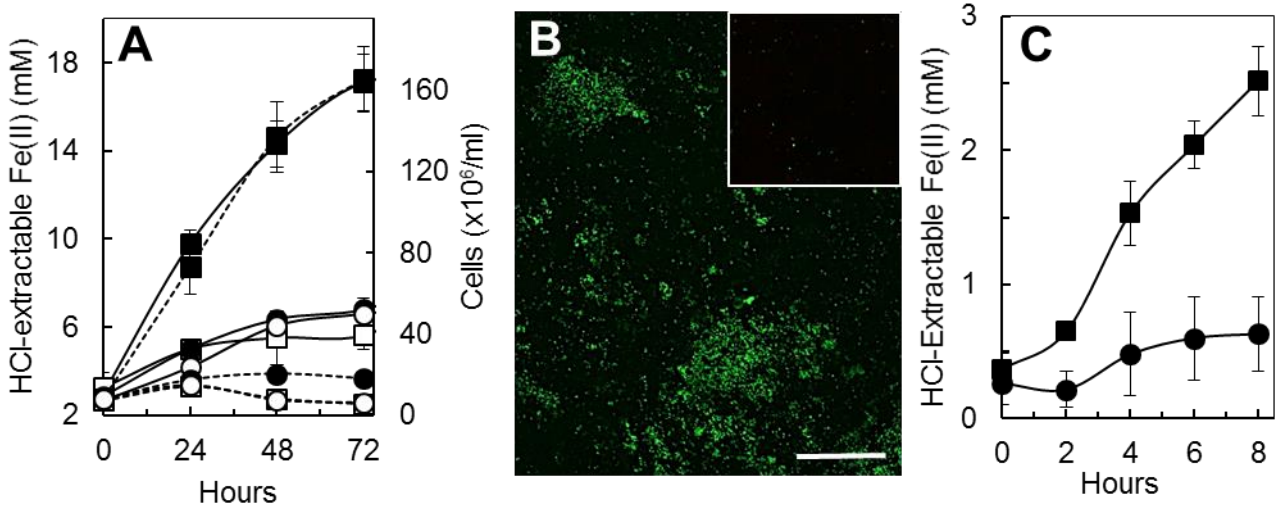

(A) Growth (dashed lines) and Fe(III) reduction (solid lines) of *G. ahangari* with entrapped Fe(III) oxides in the presence (squares) or absence (circles) of 50 uM AQDS. Controls lacking electron donor (pyruvate) are also shown (open symbols). The data points represent averages and standard deviations of triplicate cultures. (B) CLSM micrographs of biofilms formed on the Fe(III) oxides exposed on the bead's surface in cultures with (B) or without (inset) AQDS supplementation. Live cells are stained in green and dead cells in red. Bar, 50 µm. (C) Reduction of free Fe(III) oxides (10 mM) by washed cells resuspended in filter-sterilized supernatant fluids with (squares) or without (circles) AQDS.

Figure 4.3. TEM micrographs of negatively-stained cells of *G. ahangari*

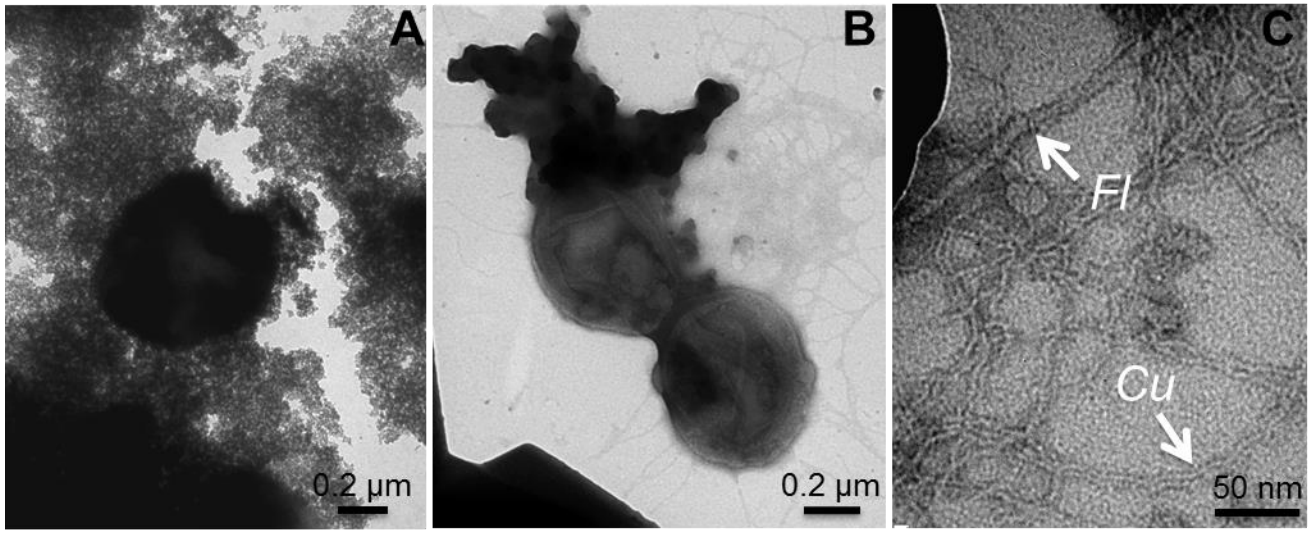

Cultures were grown with free Fe(III) oxides (A) or Fe(III) citrate (B and C). Partial solubilization of cell-associated iron precipitates with oxalate reveals abundant filaments, some still associated with the mineral particles (B). At higher magnification, the cell's archaeal flagellum (arrow labeled *Fl*) and curled filaments (arrow labeled *Cu*) are revealed (C).

Figure 4.4. Surface-exposed *c*-type cytochromes are essential for the reduction of insoluble Fe(III) oxides

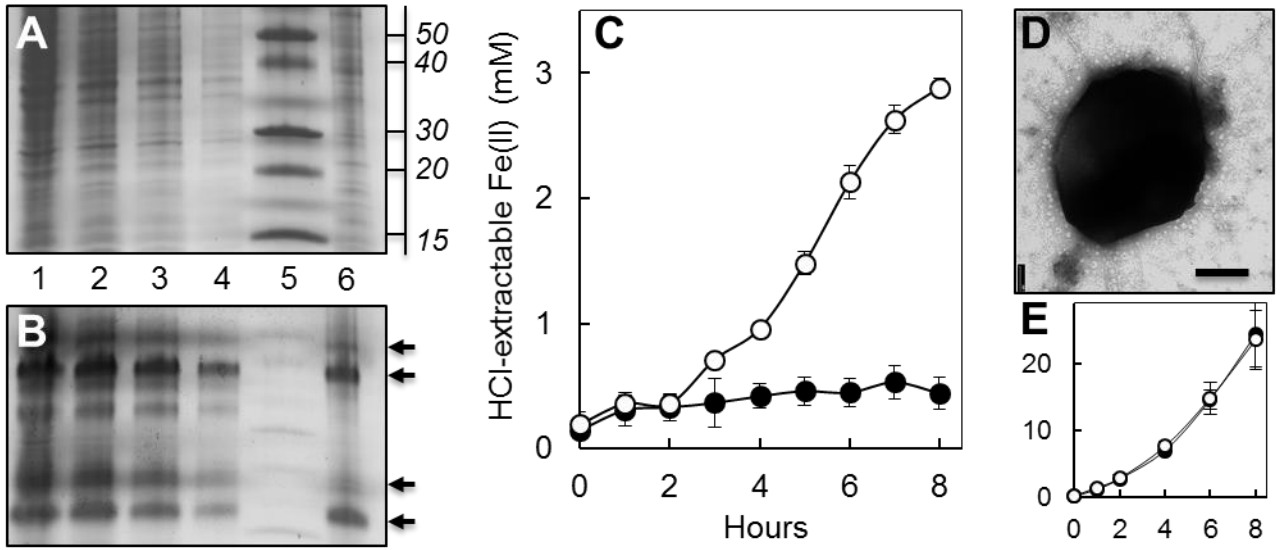

(A-B) Coomassie Blue-stained (A) and heme-stained (B) SDS-PAGE of whole-cell (lanes 1-4, decreasing concentrations of protein) and sheared outer surface (lane 6) protein extracted from *G. ahangari*. Lane 5 shows protein markers and numbers at right (top) show their corresponding molecular weights in kDa. Arrows in B point at 4 discreet heme-containing proteins sheared from the outer surface. (C-E) Effect of shearing on the reduction of Fe(III) oxides (10 mM) (C), production of extracellular appendages, which are visible after dissolving the cell-associated Fe(III) oxides with oxalate (D), and growth with Fe(III) citrate (E); Y and X axes are as in panel C. Closed circles indicate sheared cultures while open circles indicate unsheared cultures. Scale bar in panel D is 100 µm.

Figure 5.1. Transmission electron micrographs of *G. ahangari* filaments

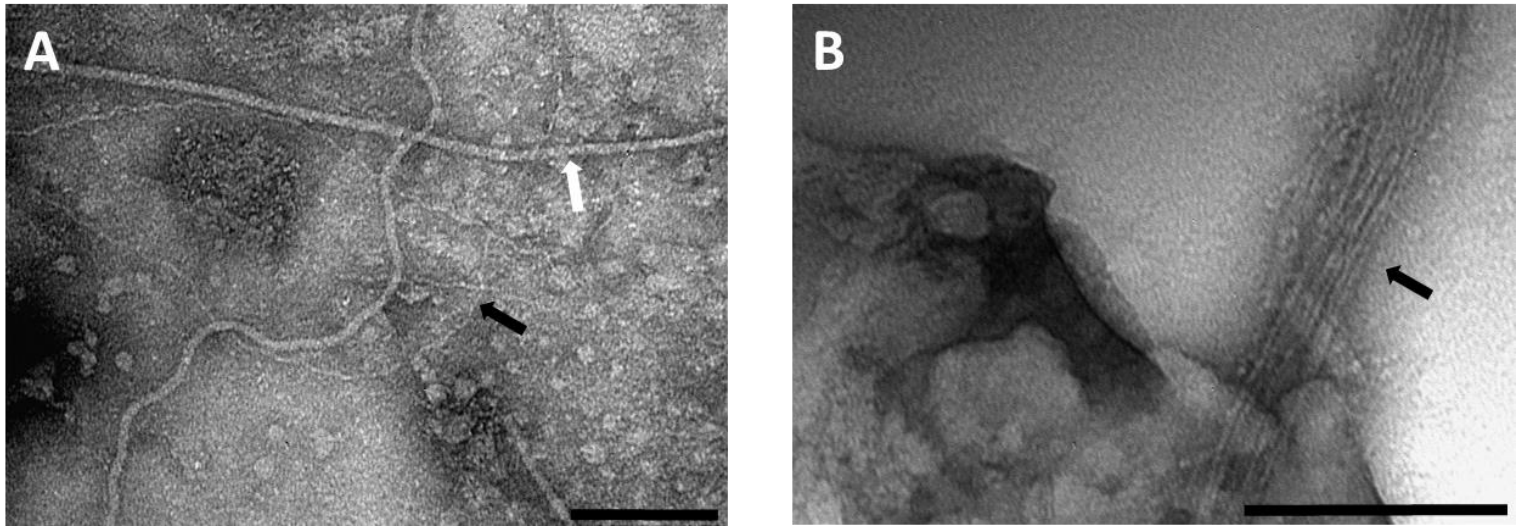

Transmission electron micrographs of the sheared (A) and prep-cell (B) preparations of *G. ahangari* filaments. Archaellar structures (black arrow) and pilus-like filaments (white arrow) are indicated as noted. Scale bars are at 100 nm.

Figure 5.2. Transmission electron micrographs of *G. ehrlichii* filaments

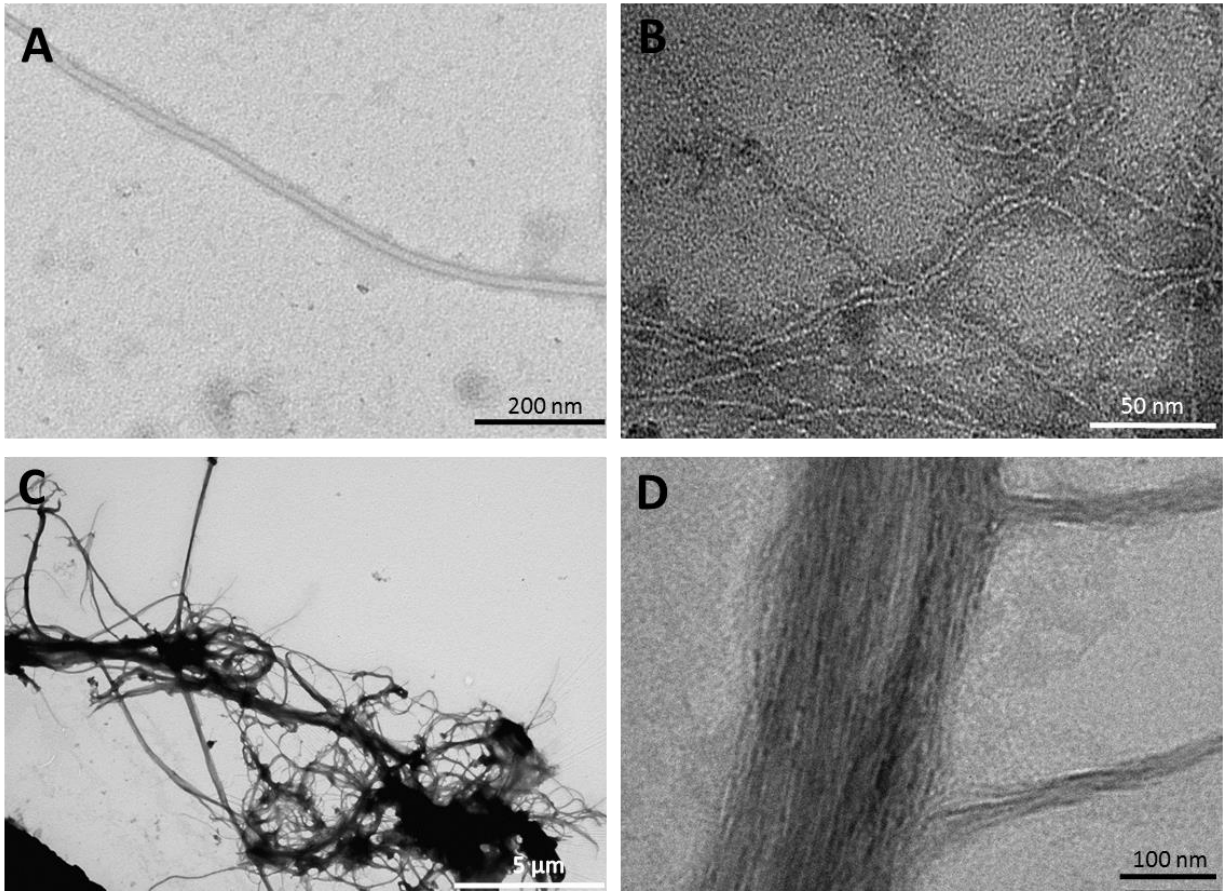

TEM micrographs of the sheared flagella (A) and pili (B) and prep-cell preparations (C and D) of *G. ehrlichii* filaments. Scale bars are as labelled.

Figure 5.3. Preliminary AFM data on *G. ehrlichii*

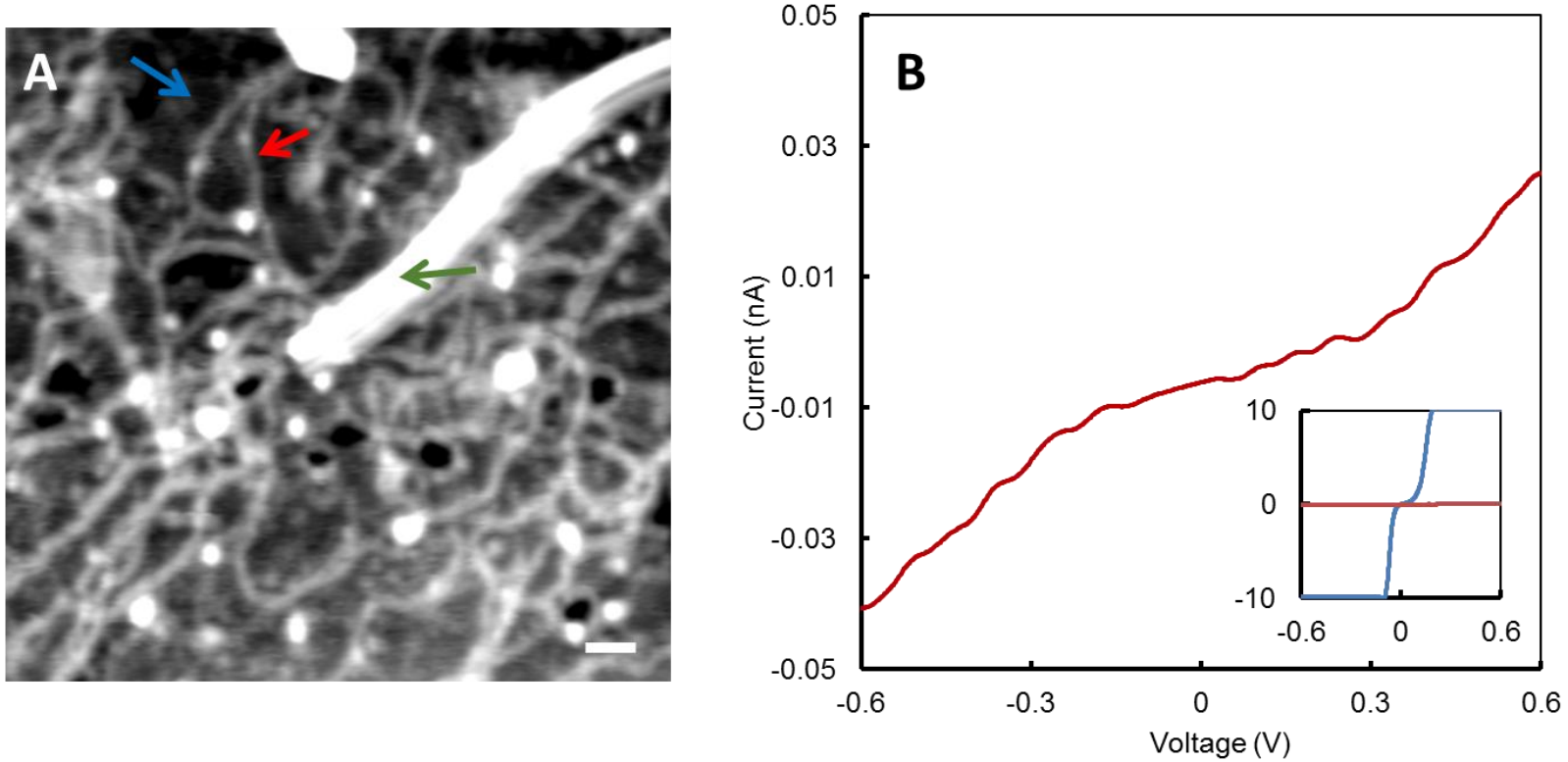

AFM micrograph (A) of *G. ehrlichii* strain SS015 filaments purified from the shearing protocol containing the flagellum (green) and the pili (red) compared to graphite (blue). Panel B contains representative I/V curves for the pili (red) and the insert shows the conductivity of the pili compared to the HOPG surface (blue).

Figure 5.4. Atomic force microscopy on *G. ehrlichii* purified pili

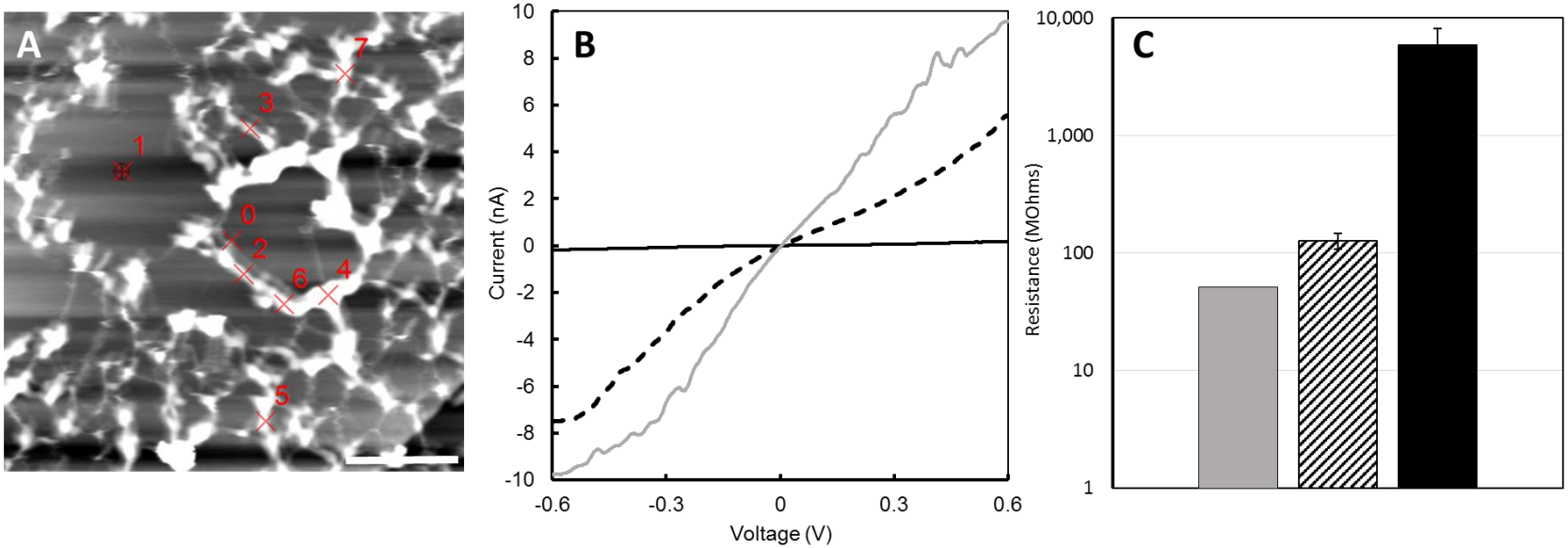

(a) AFM micrograph of *G. ehrlichii* strain SS015 pili purified by the prep-cell protocol containing pure pili which appear as bundles of wires. Panel B contains representative I/V curves for graphite (gray) and the pilus filaments (Positions 3, 6, and 7 represented as dashed black and Position 4 as solid black) across a 0.6 V bias voltage sweep. Panel C contains averaged resistivity for the pilus filaments across both sites and graphite as a control (colors as in B). Scale bar in A is 200 nm.

Figure 5.5. Preliminary AFM data on *G. ahangari*

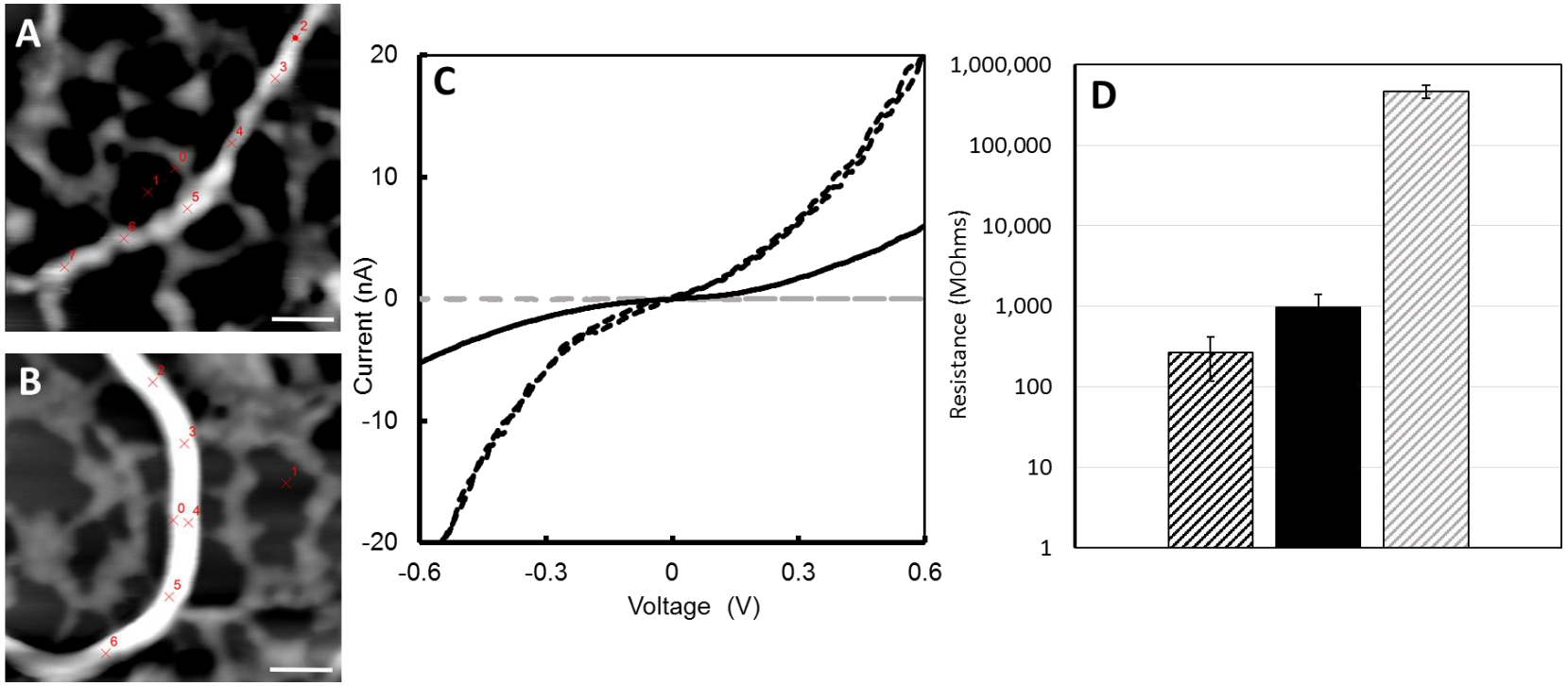

AFM micrographs of *G. ahangari* strain 234^{T} filaments purified from the shearing protocol containing the pilus-like filaments (A) and the archaella (B). Panel C contains representative I/V curves for sheared pilus-like filaments (dashed black), prep-cell purified pilus-like filaments (solid black) and the archaella (dashed gray). Panel D contains averaged resistivity for the pilus-like filaments at a bias voltage of 0.6 V (colors are as in (C)).

Figure 5.6. Atomic force microscopy on *G. ahangari* purified pilus-like filaments

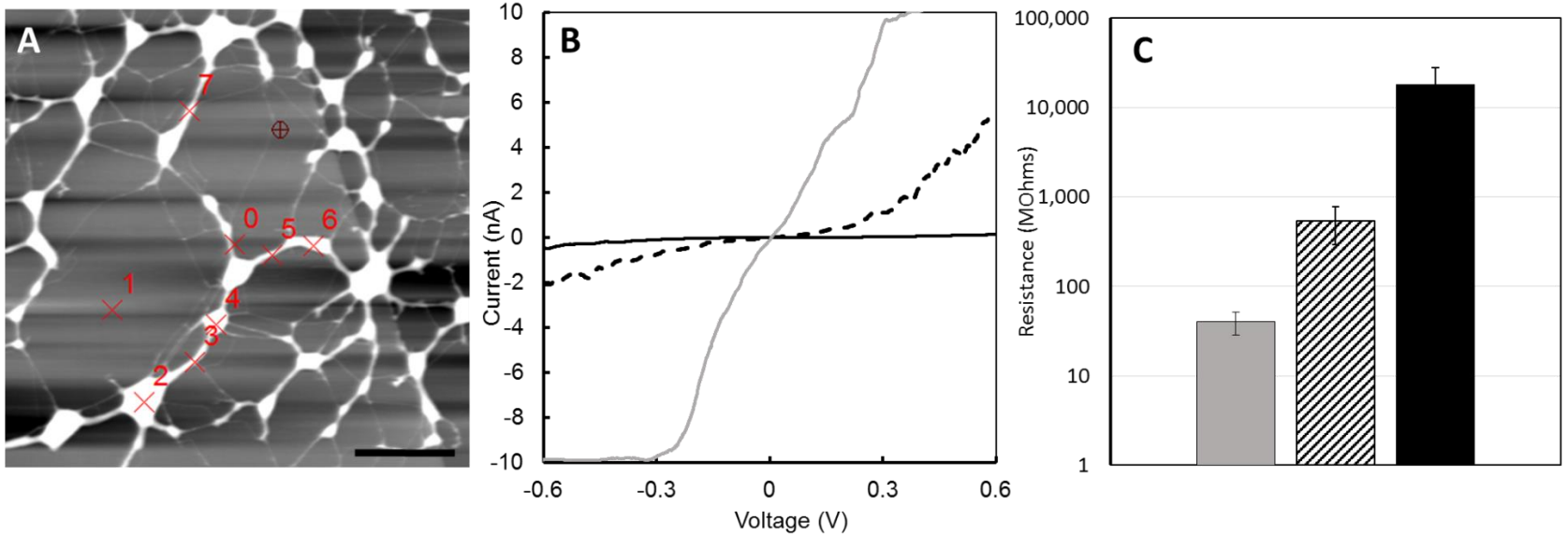

AFM micrograph of *G. ahangari* strain 234^{T} filaments purified from the prep-cell protocol containing only the pilus-like filaments (A). Panel B contains representative I/V curves for graphite (gray) and both the less conductive (solid black) and more conductive (dashed black) measurements. Panel C contains averaged resistivity for the pilus-like filaments at a bias voltage of 0.6 V both before and after removal of the insulating layer (colors as in C). Scale bar in (A) is 200 nm.

Figure 5.7. Sypro Orange thermal shift assays on soluble protein extracts

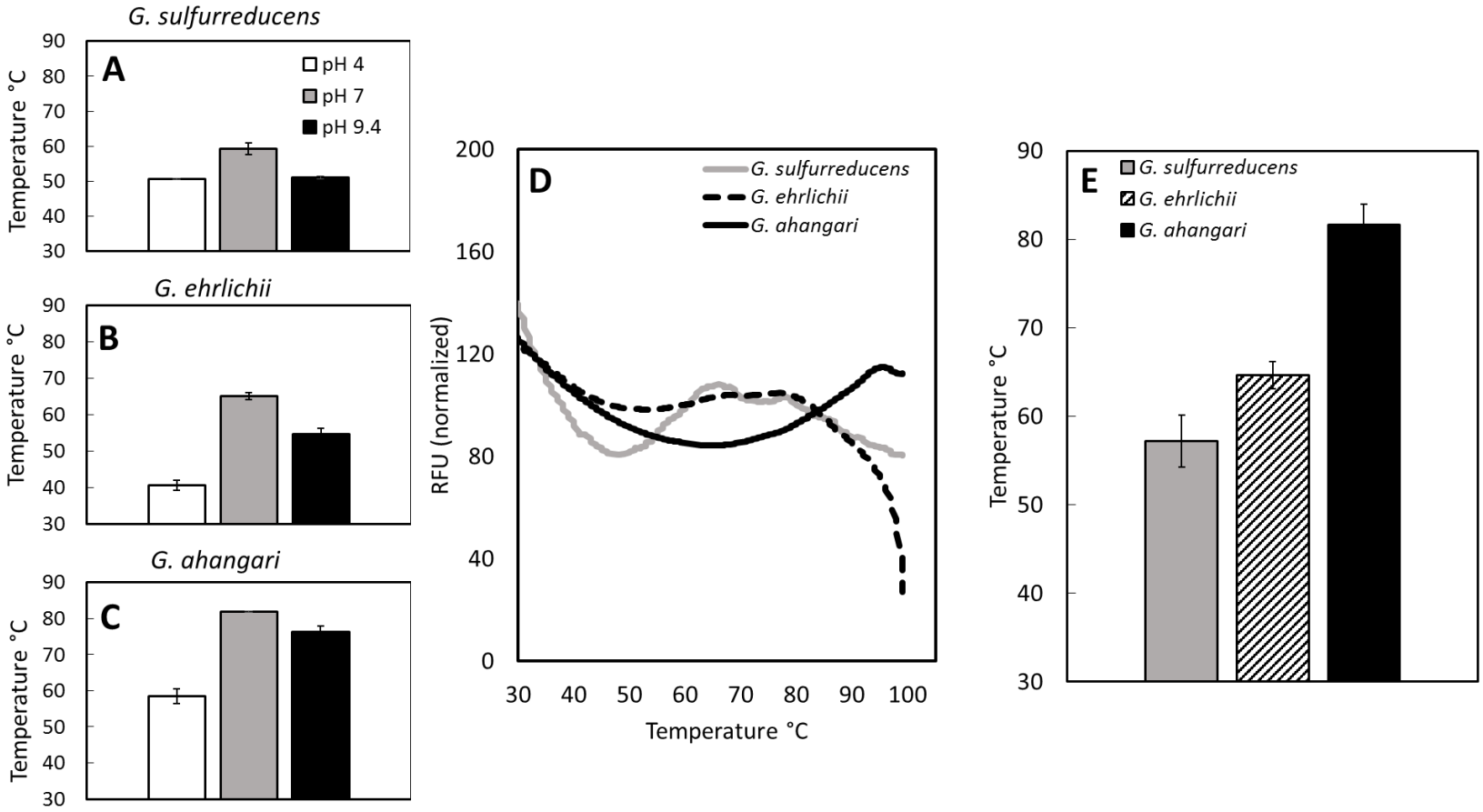

Effect of pH on the T_m of *G.* sulfurreducens, *G. ehrlichii,* and *G. ahangari* (A-C, respectively). Representative thermal shift assay output (D) of *G. sulfurreducens* (gray), *G. ehrlichii* (dashed black), and *G. ahangari* (black) soluble proteins at pH 7.0. (E) Averaged thermal shift data represented as a column chart (labels are as above).

Figure 5.8. Failure of the Sypro Orange thermal shift assay to characterize the T_m of prep-cell purified filaments

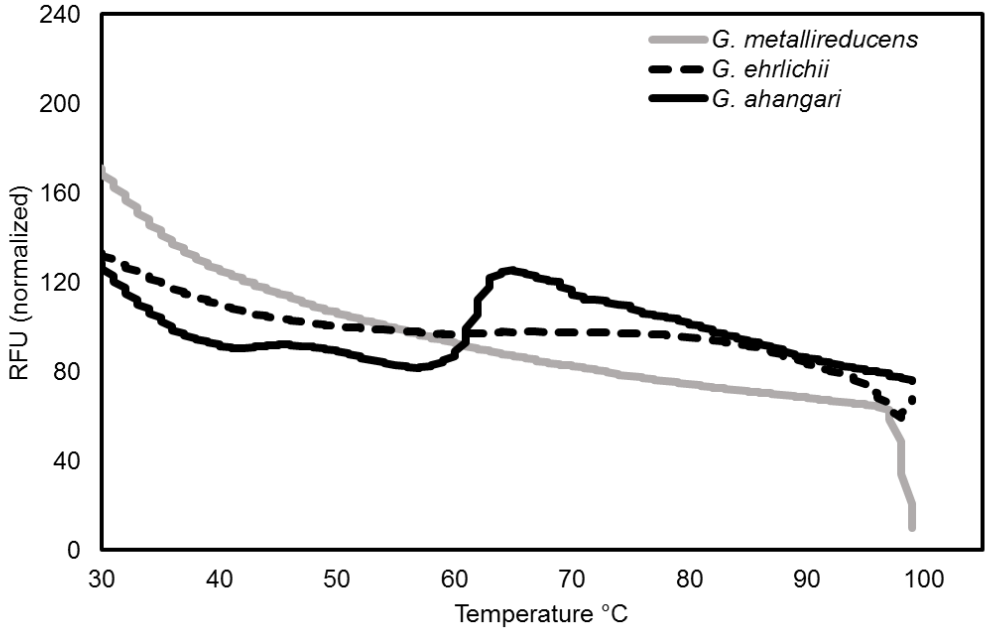

Figure 5.9. Effect of 72 h incubation on the pilus-like filaments of *G. ahangari*

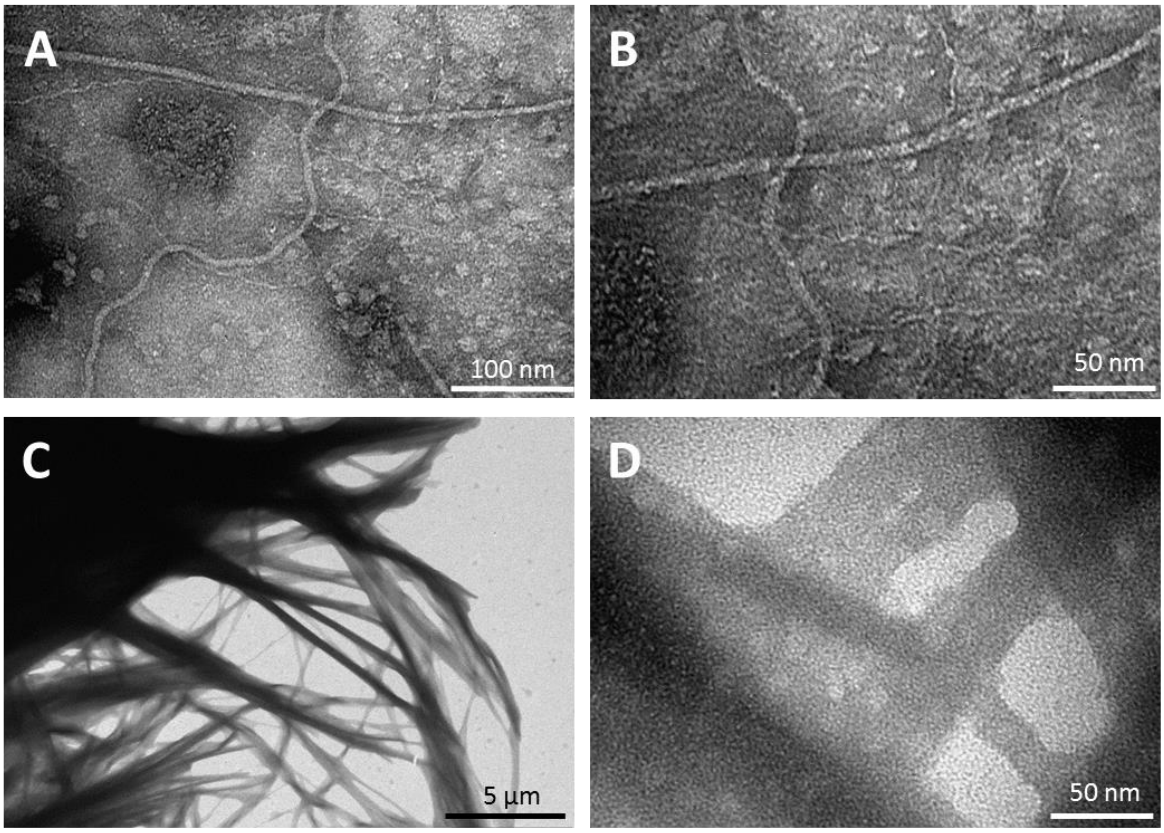

Transmission electron micrographs of the sheared *G. ahangari* strain 234^T filaments before (A and B) and after (C and D) incubation in pH 7.0 buffer showing the increase in the number of bundles and aggregates formed. Scale bars are as indicated.

REFERENCES

REFERENCES

1. **Nisbet EG, Fowler CMR**. 1996. Some liked it hot. Nature **382**:404–405.

2. **Oró J, Miller SL, Lazcano A**. 1990. The origin and early evolution of life on Earth. Annu. Rev. Earth Planet. Sci. **18**:317–356.

3. **Schopf JW**. 1993. Microfossils of the Early Archean Apex chert: new evidence of the antiquity of life. Science **260**:640–646.

4. **Schopf JW**. 2006. Fossil evidence of Archaean life. Philos. Trans. R. Soc. Lond. B. Biol. Sci. **361**:869–885.

5. **Baross JA, Hoffman SE**. 1985. Submarine hydrothermal vents and associated gradient environments as sites for the origin and evolution of life. Orig. Life Evol. Biosph. **15**:327–345.

6. **Miller SL, Lazcano A**. 1995. The origin of life--did it occur at high temperatures? J. Mol. Evol. **41**:689–692.

7. **Pace NR**. 1991. Origin of life - Facing up to the physical setting. Cell **65**:531–533.

8. **Weiner AM, Maizels N**. 1987. tRNA-like structures tag the 3’ ends of genomic RNA molecules for replication: Implications for the origin of protein synthesis. Proc. Natl. Acad. Sci. U. S. A. **84**:7383–7387.

9. **Gilbert W**. 1986. Origin of life: The RNA world. Nature.

10. **Awramik SM, Schopf JW, Walter MR**. 1983. Filamentous fossil bacteria from the Archean of Western Australia. Dev. Precambrian Geol. **7**:249–266.

11. **Hofmann HJ, Grey K, Hickman AH, Thorpe RI**. 1999. Origin of 3.45 Ga coniform stromatolites in Warrawoona Group, Western Australia. Geol. Soc. Am. Bull. **111**:1256–1262.

12. **Knoll AH, Barghoorn ES**. 1977. Archean microfossils showing cell division from the Swaziland system of South Africa. Science **198**:396–398.

13. **Schidlowski M**. 1987. Application of stable carbon isotopes to early biochemical evolution on Earth. Annu. Rev. Earth Planet. Sci. **15**:47–72.

14. **Nisbet EG, Sleep NH**. 2001. The habitat and nature of early life. Nature **409**:1083–1091.

15. **Harvey RB**. 1924. Enzymes of thermal algae. Science **60**:481–482.

16. **Stribling R, Miller SL**. 1987. Energy yields for hydrogen cyanide and formaldehyde syntheses: The HCN and amino acid concentrations in the primitive ocean. Orig. Life Evol. Biosph. **17**:261–273.

17. **Vieille C, Zeikus G**. 2001. Hyperthermophilic enzymes: Sources, uses, and molecular mechanisms for thermostability. Microbiol. Mol. Biol. **65**:1–43.

18. **Woese CR, Kandler O, Wheelis ML**. 1990. Towards a natural system of organisms: Proposal for the domains *Archaea*, *Bacteria*, and *Eucarya*. Proc. Natl. Acad. Sci. U. S. A. **87**:4576–4579.

19. **Woese CR, Fox GE**. 1977. Phylogenetic structure of the prokaryotic domain: The primary kingdoms. Proc. Natl. Acad. Sci. U. S. A. **74**:5088–5090.

20. **Stetter KO**. 1996. Hyperthermophiles in the history of life. Ciba Found. Symp. **202**:1–10; discussion 11–18.

21. **Klenk HP, Palm P, Zillig W**. 1994. DNA-dependent RNA-polymerases as phylogenetic marker molecules. Syst. Appl. Microbiol. **16**:638–647.

22. **Forterre P, Benachenhou-Lahfa N, Confalonieri F, Duguet M, Elie C, Labedan B**. 1992. The nature of the last universal ancestor and the root of the tree of life, still open questions. Biosystems. **28**:15–32.

23. **Richter K, Haslbeck M, Buchner J**. 2010. The heat shock response: Life on the verge of death. Mol. Cell **40**:253–66.

24. **Nisbet EG**. 1995. Archaean ecology: A review of evidence for the early development of bacterial biomes, and speculations on the development of a global-scale biosphere. Geol. Soc. London, Spec. Publ. **95**:27–51.

25. **Cockell CS, Raven JA**. 2007. Ozone and life on the Archaean Earth. Philos. Trans. R. Soc. A Math. Phys. Eng. Sci. **365**:1889–1901.

26. **Cockell CS**. 2000. Ultraviolet radiation and the photobiology of earth's early oceans. Orig. Life Evol. Biosph. **30**:467–499.

27. **Baross JA, Lilley MD, Gordon LI**. 1982. Is the CH_4, H_2 and CO venting from submarine hydrothermal systems produced by thermophilic bacteria? Nature **298**:366–368.

28. **Opatkiewicz AD, Butterfield DA, Baross JA**. 2009. Individual hydrothermal vents at Axial Seamount harbor distinct subseafloor microbial communities. FEMS Microbiol. Ecol. **70**:413–424.

29. **Schrenk MO, Kelley DS, Delaney JR, Baross JA**. 2003. Incidence and diversity of microorganisms within the walls of an active deep-sea sulfide chimney. Appl. Environ. Microbiol. **69**:3580–3592.

30. **Cai W-J, Reimers CE**. 1995. Benthic oxygen flux, bottom water oxygen concentration and core top organic carbon content in the deep northeast Pacific Ocean. Deep Sea Res. Part I Oceanogr. Res. Pap. **42**:1681–1699.

31. **Martin W, Baross J, Kelley D, Russell MJ**. 2008. Hydrothermal vents and the origin of life. Nat. Rev. Microbiol. **6**:805–14.

32. **Vargas M, Kashefi K, Blunt-Harris EL, Lovley DR**. 1998. Microbiological evidence for Fe (III) reduction on early Earth. Nature **395**:65–67.

33. **Delaney JR, Kelley DS, Mathez EA, Yoerger DR, Baross JA, Schrenk MO, Tivey MK, Kaye J, Robigou V**. 2001. "Edifice rex" sulfide recovery project: Analysis of submarine hydrothermal, microbial habitat. Eos (Washington. DC). **82**:67–73.

34. **Harmsen HJM, Prieur D, Jeanthon C**. 1997. Distribution of microorganisms in deep-sea hydrothermal vent chimneys investigated by whole-cell hybridization and enrichment culture of thermophilic subpopulations. Appl. Environ. Microbiol. **63**:2876–2883.

35. **Takai K, Horikoshi K**. 1999. Genetic diversity of archaea in deep-sea hydrothermal vent environments. Genetics **152**:1285–1297.

36. **Takai K, Komatsu T, Inagaki F, Horikoshi K**. 2001. Distribution of archaea in a black smoker chimney structure. Appl. Environ. Microbiol. **67**:3618–3629.

37. **Reysenbach A, Longnecker K**. 2000. Novel bacterial and archaeal lineages from an *in situ* growth chamber deployed at a mid-Atlantic ridge hydrothermal vent. Appl. Environ. Microbiol. **66**:3768–3806.

38. **Takai K, Sako Y**. 1999. A molecular view of archaeal diversity in marine and terrestrial hot water environments. FEMS Microbiol. Ecol. **28**:177–188.

39. **Longnecker K, Reysenbach A**. 2001. Expansion of the geographic distribution of a novel lineage of ε-*Proteobacteria* to a hydrothermal vent site on the Southern East Pacific Rise. FEMS Microbiol. Ecol. **35**:287–293.

40. **Moyer CL, Tiedje JM, Dobbs FC, Karl DM**. 1998. Diversity of deep-sea hydrothermal vent archaea from Loihi Seamount, Hawaii. Deep. Res. Part II Top. Stud. Oceanogr. **45**:303–317.

41. **Xie W, Wang F, Guo L, Chen Z, Sievert SM, Meng J, Huang G, Li Y, Yan Q, Wu S, Wang X, Chen S, He G, Xiao X, Xu A**. 2011. Comparative metagenomics of microbial communities inhabiting deep-sea hydrothermal vent chimneys with contrasting chemistries. ISME J. **5**:414–426.

42. **Jeanthon C**. 2000. Molecular ecology of hydrothermal vent microbial communities. Antonie Van Leeuwenhoek **77**:117–133.

43. **Jollivet D**. 1996. Specific and genetic diversity at deep-sea hydrothermal vents: an overview. Biodivers. Conserv. **5**:1619–1653.

44. **Cragg BA, Parkes RJ**. 1994. Bacterial profiles in hydrothermally active deep sediment layers from Middle Valley (NE Pacific), Sites 857 and 858Proceedings of the Ocean Drilling Program, 139 Scientific Results. Ocean Drilling Program.

45. **Parkes RJ, Cragg BA, Bale SJ, Getlifff JM, Goodman K, Rochelle PA, Fry JC, Weightman AJ, Harvey SM**. 1994. Deep bacterial biosphere in Pacific Ocean sediments. Nature **371**:410–413.

46. **Summit M, Peacock A, Ringelberg D, White D, Baross JA**. 2000. Phospholipid fatty acid-derived microbial biomass and community dynamics in hot, hydrothermally influenced sediments from Middle Valley, Juan De Fuca Ridge. Proc. Ocean Drill. Prog. Sci. Results **169**:1–19.

47. **Delaney JR, Kelley DS, Lilley MD, Butterfield DA, Baross JA, Wilcock WS, Embley RW, Summit M**. 1998. The quantum event of oceanic crustal accretion: Impacts of diking at mid-ocean ridges. Science **281**:222–230.

48. **Holden J, Summit M, Baross JA**. 1998. Thermophilic and hyperthermophilic microorganisms in 3–30°C hydrothermal fluids following a deep-sea volcanic eruption. FEMS Microbiol. Ecol. **25**:33–41.

49. **Huber R, Stotters P, Cheminee JL, Richnow HH, Stetter KO**. 1990. Hyperthermophilic archaebacteria within the crater and open-sea plume of erupting Macdonald Seamount. Nature.

50. **Summit M, Baross JA**. 1998. Thermophilic subseafloor microorganisms from the 1996 north Gorda Ridge eruption. Deep. Res. Part II Top. Stud. Oceanogr. **45**:2751–2766.

51. **Karl DM, Taylor GT, Novitsky JA, Jannasch HW, Wirsen CO, Pace NR, Lane DJ, Olsen GJ, Giovannoni SJ**. 1988. A microbiological study of Guaymas Basin high temperature hydrothermal vents. Deep Sea Res. Part A. Oceanogr. Res. Pap. **35**:777–791.

52. **Kashefi K, Tor JM, Holmes DE, Gaw Van Praagh C V, Reysenbach A-L, Lovley DR**. 2002. *Geoglobus ahangari* gen. nov., sp. nov., a novel hyperthermophilic archaeon capable of oxidizing organic acids and growing autotrophically on hydrogen with Fe(III) serving as the sole electron acceptor. Int. J. Syst. Evol. Microbiol. **52**:719–28.

53. **Huber H, Jannasch H, Rachel R, Fuchs T, Stetter KO**. 1997. *Archaeoglobus veneficus* sp. nov., a novel facultative chemolithoautotrophic hyperthermophilic sulfite reducer, isolated from abyssal black smokers. Syst. Appl. Microbiol. **20**:374–380.

54. **Kristall B, Kelley DS, Hannington MD, Delaney JR**. 2006. Growth history of a diffusely venting sulfide structure from the Juan de Fuca Ridge: A petrological and geochemical study. Geochemistry, Geophys. Geosystems **7**.

55. **Summit M, Baross JA**. 2001. A novel microbial habitat in the mid-ocean ridge subseafloor. Proc. Natl. Acad. Sci. U. S. A. **98**:2158–2163.

56. **Chapelle FH, O'Neill K, Bradley PM, Methé BA, Ciufo SA, Knobel LL, Lovley DR**. 2002. A hydrogen-based subsurface microbial community dominated by methanogens. Nature **415**:312–315.

57. **Huber JA, Butterfield DA, Baross JA**. 2002. Temporal changes in archaeal diversity and chemistry in a mid-ocean ridge subseafloor habitat. Appl. Environ. Microbiol. **68**:1585–1594.

58. **Fisk MR, Giovannoni SJ, Thorseth IH**. 1998. Alteration of oceanic volcanic glass: Textural evidence of microbial activity. Science (80-.). **281**:978–980.

59. **Marchesi JR, Weightman AJ, Cragg BA, John Parkes R, Fry JC**. 2000. Methanogen and bacterial diversity and distribution in deep gas hydrate sediments from the Cascadia Margin as revealed by 16S rRNA molecular analysis. FEMS Microbiol. Ecol. **34**:221–228.

60. **Karl DM, Wirsen COO, Jannasch HW**. 1980. Deep-sea primary production at the Galapagos hydrothermal vents. Science (80-.). **207**:1345–1347.

61. **Harmsen HJM, Prieur D, Jeanthon C**. 1997. Group-specific 16S rRNA-targeted oligonucleotide probes to identify thermophilic bacteria in marine hydrothermal vents. Appl. Environ. Microbiol. **63**:4061–4068.

62. **Nakagawa S, Takai K, Inagaki F, Chiba H, Ishibashi JI, Kataoka S, Hirayama H, Nunoura T, Horikoshi K, Sako Y**. 2005. Variability in microbial community and venting chemistry in a sediment-hosted backarc hydrothermal system: Impacts of subseafloor phase-separation. FEMS Microbiol. Ecol. **54**:141–155.

63. **Huber JA, Welch DM, Morrison HG, Huse SM, Neal PR, Butterfield DA, Sogin ML, Mark Welch DB**. 2007. Microbial population structures in the deep marine biosphere. Science **318**:97–100.

64. **Jannasch HW**. 1995. Microbial interactions with hydrothermal fluids, p. 273–296. *In* Seafloor Hydrothermal Systems: Physical, Chemical, Biological, and Geological Interactions.

65. **Kashefi K, Holmes DE, Reysenbach A-L, Lovley DR**. 2002. Use of Fe(III) as an electron acceptor to recover previously uncultured hyperthermophiles: Isolation and characterization of *Geothermobacterium ferrireducens* gen. nov., sp. nov. Appl. Environ. Microbiol. **68**:1735–1742.

66. **Kashefi K, Holmes DE, Baross JA, Lovley DR**. 2003. Thermophily in the *Geobacteraceae*: *Geothermobacter ehrlichii* gen. nov., sp. nov., a novel thermophilic member of the *Geobacteraceae* from the "Bag City" hydrothermal vent. Appl. Environ. Microbiol. **69**:2985.

67. **Moyer CL, Dobbs FC, Karl DM**. 1995. Phylogenetic diversity of the bacterial community from a microbial mat at an active, hydrothermal vent system, Loihi seamount, Hawaii. Appl. Environ. Microbiol. **61**:1555–1562.

68. **Reysenbach A-L, Shock E**. 2002. Merging genomes with geochemistry in hydrothermal ecosystems. Science **296**:1077–1082.

69. **Acinas SG, Sarma-Rupavtarm R, Klepac-Ceraj V, Polz MF**. 2005. PCR-induced sequence artifacts and bias: Insights from comparison of two 16s rRNA clone libraries constructed from the same sample. Appl. Environ. Microbiol. **71**:8966–8969.

70. **Lam P, Cowen JP, Jones RD**. 2004. Autotrophic ammonia oxidation in a deep-sea hydrothermal plume. FEMS Microbiol. Ecol. **47**:191–196.

71. **Lovley DR, Holmes DE, Nevin KP**. 2004. Dissimilatory Fe(III) and Mn(IV) reduction. Adv. Microb. Physiol. **55**:220–286.

72. **Thöny-Meyer L, Alerts C**. 1997. Biogenesis of respiratory cytochromes in bacteria. Microbiol. Mol. Biol. Rev. **61**:337–376.

73. **Röling WFM**. 2014. The family *Geobacteraceae*, p. 157–172. *In* The Prokaryotes.

74. **Caccavo F, Lonergan DJ, Lovley DR, Davis M, Stolz JF, McInerney MJ**. 1994. *Geobacter sulfurreducens* sp. nov., a hydrogen- and acetate-oxidizing dissimilatory metal-reducing microorganism. Appl. Environ. Microbiol. **60**:3752–3759.

75. **Lovley DR, Giovannoni SJ, White DC, Champine JE, Phillips EJ, Gorby YA, Goodwin S**. 1993. *Geobacter metallireducens* gen. nov. sp. nov., a microorganism capable of coupling the complete oxidation of organic compounds to the reduction of iron and other metals. Arch. Microbiol. **159**:336–344.

76. **Methé BA, Nelson KE, Eisen JA, Paulsen IT, Nelson W, Heidelberg JF, Wu D, Wu M, Ward N, Beanan MJ, Dodson RJ, Madupu R, Brinkac LM, Daugherty SC, DeBoy RT, Durkin AS, Gwinn M, Kolonay JF, Sullivan SA, Haft DH, Selengut J, Davidsen TM, Zafar N, White O, Tran B, Romero C, Forberger HA, Weidman J, Khouri H, Feldblyum T V, Utterback TR, Van Aken SE, Lovley DR, Fraser CM**. 2003. Genome of *Geobacter sulfurreducens*: Metal reduction in subsurface environments. Science **302**:1967–1969.

77. **Aklujkar M, Krushkal J, DiBartolo G, Lapidus A, Land ML, Lovley DR**. 2009. The genome sequence of *Geobacter metallireducens*: features of metabolism, physiology and regulation common and dissimilar to *Geobacter sulfurreducens*. BMC Microbiol. **9**:109.

78. **Badalamenti JP, Bond DR**. 2015. Complete genome of *Geobacter pickeringii* G13^{T}, a metal-reducing isolate from sedimentary kaolin deposits. Genome Announc. **3**:e00038–15.

79. **Ehara A, Suzuki H, Amachi S**. 2015. Draft genome sequence of *Geobacter sp.* strain OR-1, an arsenate-respiring bacterium isolated from Japanese paddy soil. Genome Announc. **3**:e01478–14.

80. **Aklujkar M, Young ND, Holmes DE, Chavan M, Risso C, Kiss HE, Han CS, Land ML, Lovley DR**. 2010. The genome of *Geobacter bemidjiensis*, exemplar for the subsurface clade of *Geobacter* species that predominate in Fe(III)-reducing subsurface environments. BMC Genomics **11**:490.

81. **Coppi MV, Leang C, Sandler SJ, Lovley DR**. 2001. Development of a genetic system for *Geobacter sulfurreducens*. Appl. Environ. Microbiol. **67**:3180.

82. **Tremblay P-LL, Aklujkar M, Leang C, Nevin KP, Lovley DR**. 2012. A genetic system for *Geobacter metallireducens*: Role of the flagellin and pilin in the reduction of Fe(III) oxide. Environ. Microbiol. Rep. **4**:82–88.

83. **Butler JE, Young ND, Lovley DR**. 2010. Evolution of electron transfer out of the cell: Comparative genomics of six *Geobacter* genomes. BMC Genomics **11**:40.

84. **Weber KA, Achenbach LA, Coates JD**. 2006. Microorganisms pumping iron: Anaerobic microbial iron oxidation and reduction. Nat. Rev. Microbiol. **4**:752–64.

85. **Sanders C, Turkarslan S, Lee D-W, Daldal F**. 2010. Cytochrome *c* biogenesis: the Ccm system. Trends Microbiol. **18**:266–74.

86. **Bewley KD, Ellis KE, Firer-Sherwood MA, Elliott SJ**. 2013. Multi-heme proteins: Nature's electronic multi-purpose tool. Biochim. Biophys. Acta - Bioenerg. Elsevier B.V.

87. **Allen JW, Daltrop O, Stevens JM, Ferguson SJ**. 2003. *C*-type cytochromes: Diverse structures and biogenesis systems pose evolutionary problems. Philos. Trans. R. Soc. Lond. B. Biol. Sci. **358**:255–66.

88. **Mavridou DAI, Ferguson SJ, Stevens JM**. 2013. Cytochrome *c* assembly. IUBMB Life **65**:209–16.

89. **Allen JW, Harvat EM, Stevens JM, Ferguson SJ**. 2006. A variant System I for cytochrome c biogenesis in archaea and some bacteria has a novel CcmE and no CcmH. FEBS Lett. **580**:4827–34.

90. **Rollefson JB, Stephen CS, Tien M, Bond DR**. 2011. Identification of an extracellular polysaccharide network essential for cytochrome anchoring and biofilm formation in *Geobacter sulfurreducens*. J. Bacteriol. **193**:1023–1033.

91. **Reguera G, McCarthy KD, Mehta T, Nicoll JS, Tuominen MT, Lovley DR**. 2005. Extracellular electron transfer via microbial nanowires. Nature **435**:1098–1101.

92. **Cologgi DL, Lampa-Pastirk S, Speers AM, Kelly SD, Reguera G**. 2011. Extracellular reduction of uranium via *Geobacter* conductive pili as a protective cellular mechanism. Proc. Natl. Acad. Sci. U. S. A. **108**:15248–15252.

93. **Li Y, Li H**. 2014. Type IV pili of *Acidithiobacillus ferrooxidans* can transfer electrons from extracellular electron donors. J. Basic Microbiol. **54**:226–231.

94. **El-Naggar MY, Wanger G, Leung KM, Yuzvinsky TD, Southam G, Yang J, Lau WM, Nealson KH, Gorby YA**. 2010. Electrical transport along bacterial nanowires from *Shewanella oneidensis* MR-1. Proc. Natl. Acad. Sci. U. S. A. **107**:18127–31.

95. **Pirbadian S, Barchinger SE, Leung KM, Byun HS, Jangir Y, Bouhenni RA, Reed SB, Romine MF, Saffarini DA, Shi L, Gorby YA, Golbeck JH, El-Naggar MY**. 2014. *Shewanella oneidensis* MR-1 nanowires are outer membrane and periplasmic extensions of the extracellular electron transport components. Proc. Natl. Acad. Sci. **111**:1–6.

96. **Lovley DR, Woodward JC**. 1996. Mechanisms for chelator stimulation of microbial Fe(III)-oxide reduction. Chem. Geol. **132**:19–24.

97. **Nevin KP, Lovley DR**. 2002. Mechanisms for accessing insoluble Fe(III) oxide during dissimilatory Fe(III) reduction by *Geothrix fermentans*. Appl. Environ. Microbiol. **68**:2294–2299.

98. **Nevin KP, Lovley DR**. 2000. Lack of production of electron-shuttling compounds or solubilization of Fe(III) during reduction of insoluble Fe(III) oxide by *Geobacter metallireducens*. Appl. Environ. Microbiol. **66**:2248–51.

99. **Hernandez M, Newman D**. 2001. Extracellular electron transfer. Cell. Mol. Life Sci. **58**:1562–1571.

100. **Brutinel ED, Gralnick JA**. 2011. Shuttling happens: Soluble flavin mediators of extracellular electron transfer in *Shewanella*. Appl. Microbiol. Biotechnol. **93**:41–48.

101. **Mehta-Kolte MG, Bond DR**. 2012. *Geothrix fermentans* secretes two different redox-active compounds to utilize electron acceptors across a wide range of redox potentials. Appl. Environ. Microbiol. **78**:6987–6995.

102. **Childers SE, Ciufo S, Lovley DR**. 2002. *Geobacter metallireducens* accesses insoluble Fe(III) oxide by chemotaxis. Nature **416**:767–9.

103. **Levar CE, Rollefson JB, Bond DR**. 2013. Energetic and molecular constraints on the mechanism of environmental Fe(III) reduction by *Geobacter*, p. 29–48. *In* Gescher, J, Kappler, A (eds.), Microbial Metal Respiration. Springer Berlin Heidelberg, Berlin, Heidelberg.

104. **Leang C, Qian X, Mester T, Lovley DR**. 2010. Alignment of the c-type cytochrome OmcS along pili of *Geobacter sulfurreducens*. Appl. Environ. Microbiol. **76**:4080–4084.

105. **Smith JA, Tremblay P-L, Shrestha PM, Snoeyenbos-West OL, Franks AE, Nevin KP, Lovley DR**. 2014. Going wireless: Fe(III) oxide reduction without pili by *Geobacter sulfurreducens* strain JS-1. Appl. Environ. Microbiol. **80**:4331–40.

106. **Johnson HP, Embley RW**. 1990. Axial seamount: An active ridge axis volcano on the Central Juan De Fuca Ridge. J. Geophys. Res. **95**:12689.

107. **Greene AC**. 2014. The family *Desulfuromonadaceae*, p. 143–155. *In* The Prokaryotes.

108. **Greene AC, Patel BKC, Yacob S**. 2009. *Geoalkalibacter subterraneus* sp. nov., an anaerobic Fe(III)- and Mn(IV)-reducing bacterium from a petroleum reservoir, and emended descriptions of the family *Desulfuromonadaceae* and the genus *Geoalkalibacter*. Int. J. Syst. Evol. Microbiol. **59**:781–785.

109. **Lonsdale P, Becker K**. 1985. Hydrothermal plumes, hot springs, and conductive heat flow in the Southern Trough of Guaymas Basin. Earth Planet. Sci. Lett. **73**:211–225.

110. **Jørgensen BB, Zawacki LX, Jannasch HW**. 1990. Thermophilic bacterial sulfate reduction in deep-sea sediments at the Guaymas Basin hydrothermal vent site (Gulf of California). Deep Sea Res. Part A. Oceanogr. Res. Pap. **37**:695–710.

111. **Brune A**. 2013. The ProkaryotesThe Prokaryotes - Prokaryotic biology and symbiotic associations. Springer Berlin Heidelberg, Berlin, Heidelberg.

112. **Tor JM, Kashefi K, Lovley DR**. 2001. Acetate oxidation coupled to Fe(III) reduction in hyperthermophilic microorganisms. Appl. Environ. Microbiol. **67**:1363–5.

113. **Smith JA, Aklujkar M, Risso C, Leang C, Giloteaux L, Holmes DE**. 2015. Insight into mechanisms involved in Fe(III) respiration by the hyperthermophilic archaeon, *Ferroglobus placidus*. Appl. Environ. Microbiol. **81**:AEM.04038–14.

114. **Gavrilov SN, Lloyd JR, Kostrikina NA, Slobodkin AI**. 2012. Fe(III) oxide reduction by a Gram-positive thermophile: Physiological mechanisms for dissimilatory reduction of poorly crystalline Fe(III) oxide by a thermophilic Gram-positive bacterium *Carboxydothermus ferrireducens*. Geomicrobiol. J. **29**:804–819.

115. **Nevin KP, Holmes DE, Woodard TL, Hinlein ES, Ostendorf DW, Lovley DR**. 2005. *Geobacter bemidjiensis* sp. nov. and *Geobacter psychrophilus* sp. nov., two novel Fe(III)-reducing subsurface isolates. Int. J. Syst. Evol. Microbiol. **55**:1667–1674.

116. **Holmes DE, Nicoll JJ, Bond DR, Lovley DR**. 2004. Potential role of a novel psychrotolerant member of the family *Geobacteraceae*, *Geopsychrobacter electrodiphilus* gen. nov., sp. nov., in electricity production by a marine sediment fuel cell. App Env. Microbiol **70**:6023–6030.

117. **Mahadevan R, Bond DR, Butler JE, Coppi V, Palsson BO, Schilling CH, Lovley DR**. 2006. Characterization of metabolism in the Fe(III)-reducing organism *Geobacter sulfurreducens* by constraint-based modeling. Appl. Environ. Microbiol. **72**:1558–1568.

118. **Feliciano GT, da Silva AJR, Reguera G, Artacho E**. 2012. Molecular and electronic structure of the peptide subunit of *Geobacter sulfurreducens* conductive pili from first principles. J. Phys. Chem. A **116**:8023–8030.

119. **Quast C, Pruesse E, Yilmaz P, Gerken J, Schweer T, Yarza P, Peplies J, Glöckner FO**. 2013. The SILVA ribosomal RNA gene database project: Improved data processing and web-based tools. Nucleic Acids Res. **41**:590–596.

120. **Field D**. 2008. The minimum information about a genome sequence (MIGS) specification. Nat. Biotechnol. **26**:541–547.

121. **Garrity GM, Holt JG**. 2001. The road map to the manual, p. 119–166. *In* Bergeys Manual of Systematic Bacteriology The Archaea and the Deeply Branching and Phototrophic Bacteria.

122. **Kuever J, Rainey FA, Widdel F**. 2005. Class IV. *Deltaproteobacteria* class nov., p. 922–1144. *In* Bergey's Manual® of Systematic Bacteriology.

123. **Oren A, Garrity GM**. 2014. List of new names and new combinations previously effectively, but not validly, published. Int. J. Syst. Evol. Microbiol. **64**:2184–2187.

124. **Ashburner M, Ball CA, Blake JA, Botstein D, Butler H, Cherry JM, Davis AP, Dolinski K, Dwight SS, Eppig JT, Harris MA, Hill DP, Issel-Tarver L, Kasarskis A, Lewis S, Matese JC, Richardson JE, Ringwald M, Rubin GM, Sherlock G**. 2000. Gene ontology: Tool for the unification of biology. Nat. Genet. **25**:25–29.

125. **Hungate RE**. 1950. The anaerobic mesophilic cellulolytic bacteria. Bacteriol. Rev. **14**:1–49.

126. **Manzella MP, Holmes DE, Rochelea JM, Chung A, Reguera G, Kashefi K**. 2015. The complete genome sequence and emendation of the hyperthermophilic, obligate iron-reducing archaeon "*Geoglobus ahangari*" strain 234^{T}. Stand. Genomic Sci.

127. **Bennett S**. 2004. Solexa Ltd. Pharmacogenomics **5**:433–438.

128. **Chevreux B, Wetter T, Suhai S**. 1999. Genome sequence assembly using trace signals and additional sequence information. Comput. Sci. Biol. Proc. Ger. Conf. Bioinforma. 45–56.

129. **Chin C-S, Alexander DH, Marks P, Klammer AA, Drake J, Heiner C, Clum A, Copeland A, Huddleston J, Eichler EE, Turner SW, Korlach J**. 2013. Nonhybrid, finished microbial genome assemblies from long-read SMRT sequencing data. Nat. Methods **10**:563–9.

130. **Sommer DD, Delcher AL, Salzberg SL, Pop M**. 2007. Minimus: A fast, lightweight genome assembler. BMC Bioinformatics **8**:64.

131. **Aziz RK, Bartels D, Best AA, DeJongh M, Disz T, Edwards RA, Formsma K, Gerdes S, Glass EM, Kubal M, Meyer F, Olsen GJ, Olson R, Osterman AL, Overbeek R a, McNeil LK, Paarmann D, Paczian T, Parrello B, Pusch GD, Reich C, Stevens R, Vassieva O, Vonstein V, Wilke A, Zagnitko O**. 2008. The RAST Server: Rapid annotations using subsystems technology. BMC Genomics **9**:75.

132. **Pati A, Ivanova NN, Mikhailova N, Ovchinnikova G, Hooper SD, Lykidis A, Kyrpides NC**. 2010. GenePRIMP: A gene prediction improvement pipeline for prokaryotic genomes. Nat. Methods **7**:455–7.

133. **Finn RD, Bateman A, Clements J, Coggill P, Eberhardt RY, Eddy SR, Heger A, Hetherington K, Holm L, Mistry J, Sonnhammer ELL, Tate J, Punta M**. 2014. Pfam: The protein families database. Nucleic Acids Res. **42**:222–230.

134. **Petersen TN, Brunak S, von Heijne G, Nielsen H**. 2011. SignalP 4.0: Discriminating signal peptides from transmembrane regions. Nat. Methods.

135. **Krogh A, Larsson B, von Heijne G, Sonnhammer EL**. 2001. Predicting transmembrane protein topology with a hidden Markov model: Application to complete genomes. J. Mol. Biol. **305**:567–80.

136. **Grissa I, Vergnaud G, Pourcel C**. 2007. CRISPRFinder: A web tool to identify clustered regularly interspaced short palindromic repeats. Nucleic Acids Res. **35**:W52–W57.

137. **Gasteiger E, Hoogland C, Gattiker A, Duvaud S, Wilkins MR, Appel RD, Bairoch A**. 2005. Protein identification and analysis tools on the ExPASy server, p. 571–607. *In* The Proteomics Protocols Handbook.

138. **Thomas PE, Ryan D, Levin W**. 1976. An improved staining procedure for the detection of the peroxidase activity of cytochrome P-450 on sodium dodecyl sulfate polyacrylamide gels. Anal. Biochem. **75**:168–76.

139. **Manzella MP, Reguera G, Kashefi K**. 2013. Extracellular electron transfer to Fe(III) oxides by the hyperthermophilic archaeon *Geoglobus ahangari* via a direct contact mechanism. Appl. Environ. Microbiol. **79**:4694–700.

140. **Gao F, Zhang C-T**. 2008. Ori-Finder: A web-based system for finding OriCs in unannotated bacterial genomes. BMC Bioinformatics **9**:79.

141. **Aklujkar M, Haveman SA, DiDonato R, Chertkov O, Han CS, Land ML, Brown P, Lovley DR**. 2012. The genome of *Pelobacter carbinolicus* reveals surprising metabolic capabilities and physiological features. BMC Genomics **13**:690.

142. **Kumar S, Tsai CJ, Nussinov R**. 2000. Factors enhancing protein thermostability. Protein Eng. **13**:179–91.

143. **Farias ST, Bonato MCM**. 2003. Preferred amino acids and thermostability. Genet. Mol. Res. **2**:383–93.

144. **Nosoh Y, Sekiguchi T**. 1990. Protein engineering for thermostability. Trends Biotechnol. **8**:16–20.

145. **Lehmann M, Wyss M**. 2001. Engineering proteins for thermostability: The use of sequence alignments versus rational design and directed evolution. Curr. Opin. Biotechnol. **12**:371–375.

146. **Ebrahimi M, Lakizadeh A, Agha-Golzadeh P, Ebrahimie E, Ebrahimi M**. 2011. Prediction of thermostability from amino acid attributes by combination of clustering with attribute weighting: A new vista in engineering enzymes. PLoS One **6**:e23146.

147. **Zavarzina DG, Kolganova T V, Bulygina ES, Kostrikina NA, Turova TP, Zavarzin GA**. 2006. *Geoalkalibacter ferrihydriticus* gen. nov., sp. nov., the first alkaliphilic representative of the family *Geobacteraceae*, isolated from a soda lake. Mikrobiologiia **75**:775–785.

148. **Cambillau C, Claverie JM**. 2000. Structural and genomic correlates of hyperthermostability. J. Biol. Chem. **275**:32383–6.

149. **Suhre K, Claverie JM**. 2003. Genomic correlates of hyperthermostability, an update. J. Biol. Chem. **278**:17198–17202.

150. **Nakamura T, Kashima Y, Mine S, Oku T, Uegaki K**. 2012. Characterization and crystal structure of the thermophilic ROK hexokinase from *Thermus thermophilus*. J. Biosci. Bioeng. **114**:150–154.

151. **Bertoldo C, Antranikian G**. 2002. Starch-hydrolyzing enzymes from thermophilic archaea and bacteria. Curr. Opin. Chem. Biol. **6**:151–160.

152. **Lévêque E, Janeček Š, Haye B, Belarbi A**. 2000. Thermophilic archaeal amylolytic enzymes. Enzyme Microb. Technol. **26**:3–14.

153. **Svensson E, Skoog A, Amend JP**. 2004. Concentration and distribution of dissolved amino acids in a shallow hydrothermal system, Vulcano Island (Italy). Org. Geochem. **35**:1001–1014.

154. **Haberstroh P, Karl D**. 1989. Dissolved free amino acids in hydrothermal vent habitats of the Guaymas Basin. Geochim. Cosmochim. Acta **53**:2937–2945.

155. **Barker HA**. 1981. Amino acid degradation by anaerobic bacteria. Annu. Rev. Biochem. **50**:23–40.

156. **Bond DR, Master T, Nesbø CL, Izquierdo-Lopez A V., Collart FL, Lovley DR**. 2005. Characterization of citrate synthase from *Geobacter sulfurreducens* and evidence for a family of citrate synthases similar to those of eukaryotes throughout the *Geobacteraceae* . Appl. Environ. Microbiol. **71**:3858–3865.

157. **Berndt C, Lillig CH, Wollenberg M, Bill E, Mansilla MC, De Mendoza D, Seidler A, Schwenn JD**. 2004. Characterization and reconstitution of a 4Fe-4S adenylyl sulfate/phosphoadenylyl sulfate reductase from *Bacillus subtilis*. J. Biol. Chem. **279**:7850–7855.

158. **Painter H.** 1970. A review of literature on inorganic nitrogen metabolism in microorganisms. Water Res. **4**:393–450.

159. **Lin JT, Stewart V**. 1998. Nitrate assimilation by bacteria. Adv. Microb. Physiol. **39**:1–30, 379.

160. **Cruz-García C, Murray AE, Klappenbach JA, Stewart V, Tiedje JM**. 2007. Respiratory nitrate ammonification by *Shewanella oneidensis* MR-1. J. Bacteriol. **189**:656–662.

161. **Martínez Murillo F, Gugliuzza T, Senko J, Basu P, Stolz JF**. 1999. A heme-C-containing enzyme complex that exhibits nitrate and nitrite reductase activity from the dissimilatory iron-reducing bacterium *Geobacter metallireducens*. Arch. Microbiol. **172**:313–320.

162. **Tran HT, Krushkal J, Antommattei FM, Lovley DR, Weis RM**. 2008. Comparative genomics of *Geobacter* chemotaxis genes reveals diverse signaling function. BMC Genomics **9**:471.

163. **Cannon GA, Pashinski DJ**. 1990. Circulation near Axial Seamount. J. Geophys. Res. **95**:12823.

164. **Lloyd JR, Blunt-Harris EL, Lovley DR**. 1999. The periplasmic 9.6-kilodalton *c*-type cytochrome of *Geobacter sulfurreducens* is not an electron shuttle to Fe(III). J. Bacteriol. **181**:7647–7649.

165. **Leang C, Coppi M, Lovley D**. 2003. OmcB, a c-type polyheme cytochrome, involved in Fe (III) reduction in Geobacter sulfurreducens. J. Bacteriol. **185**:2096.

166. **Mehta T, Coppi M V, Childers SE, Lovley DR**. 2005. Outer membrane *c*-type cytochromes required for Fe(III) and Mn(IV) oxide reduction in *Geobacter sulfurreducens*. Appl. Environ. Microbiol. **71**:8634–8641.

167. **Edgar RC**. 2004. MUSCLE: Multiple sequence alignment with high accuracy and high throughput. Nucleic Acids Res. **32**:1792–1797.

168. **Tamura K, Stecher G, Peterson D, Filipski A, Kumar S**. 2013. MEGA6: Molecular evolutionary genetics analysis version 6.0. Mol. Biol. Evol. **30**:2725–2729.

169. **Crooks GE, Hon G, Chandonia JM, Brenner SE**. 2004. WebLogo: A sequence logo generator. Genome Res. **14**:1188–1190.

170. **Inoue K, Qian X, Morgado L, Kim B-C, Mester T, Izallalen M, Salgueiro CA, Lovley DR**. 2010. Purification and characterization of OmcZ, an outer-surface, octaheme *c*-type

cytochrome essential for optimal current production by *Geobacter sulfurreducens*. Appl. Environ. Microbiol. **76**:3999–4007.

171. **Qian X, Mester T, Morgado L, Arakawa T, Sharma ML, Inoue K, Joseph C, Salgueiro C a, Maroney MJ, Lovley DR**. 2011. Biochemical characterization of purified OmcS, a *c*-type cytochrome required for insoluble Fe(III) reduction in *Geobacter sulfurreducens*. Biochim. Biophys. Acta - Bioenerg. **1807**:404–412.

172. **Liu X, Tremblay PL, Malvankar NS, Nevin KP, Lovley DR, Vargas M**. 2014. A *Geobacter sulfurreducens* strain expressing *Pseudomonas aeruginosa* type IV pili localizes OmcS on pili but is deficient in Fe(III) oxide reduction and current production. Appl. Environ. Microbiol. **80**:1219–1224.

173. **Lloyd JR, Leang C, Hodges Myerson AL, Coppi M V, Cuifo S, Methe B, Sandler SJ, Lovley DR**. 2003. Biochemical and genetic characterization of PpcA, a periplasmic *c*-type cytochrome in *Geobacter sulfurreducens*. Biochem. J. **369**:153–161.

174. **Esteve-Núñez A, Sosnik J, Visconti P, Lovley DR**. 2008. Fluorescent properties of *c*-type cytochromes reveal their potential role as an extracytoplasmic electron sink in *Geobacter sulfurreducens*. Environ. Microbiol. **10**:497–505.

175. **Morgado L, Bruix M, Pessanha M, Londer YY, Salgueiro CA**. 2010. Thermodynamic characterization of a triheme cytochrome family from *Geobacter sulfurreducens* reveals mechanistic and functional diversity. Biophys. J. **99**:293–301.

176. **Kashefi K, Shelobolina ES, Elliott WC, Lovley DR**. 2008. Growth of thermophilic and hyperthermophilic Fe(III)-reducing microorganisms on a ferruginous smectite as the sole electron acceptor. Appl. Environ. Microbiol. **74**:251–8.

177. **Kashefi K**. 2012. Hyperthermophiles: Metabolic diversity and biotechnological applications, p. . *In* Anitori, RP (ed.), Extremophiles: Microbiology and Biotechnology.

178. **Slobodkina GB, Kolganova T V, Querellou J, Bonch-Osmolovskaya EA, Slobodkin AI**. 2009. *Geoglobus acetivorans* sp. nov., an iron(III)-reducing archaeon from a deep-sea hydrothermal vent. Int. J. Syst. Evol. Microbiol. **59**:2880–3.

179. **Hafenbradl D, Keller M, Dirmeier R, Rachel R, Roßnagel P, Burggraf S, Huber H, Stetter KO**. 1996. *Ferroglobus placidus* gen. nov., sp. nov., a novel hyperthermophilic archaeum that oxidizes Fe2+ at neutral pH under anoxic conditions. Arch. Microbiol. **166**:308–314.

180. **Beeder J, Nilsen RK, Rosnes JT, Torsvik T, Lien T**. 1994. *Archaeoglobus fulgidus* isolated from hot North Sea oil field waters. Appl. Environ. Microbiol. **60**:1227–31.

181. **Mori K, Maruyama A, Urabe T, Suzuki K-I, Hanada S**. 2008. *Archaeoglobus infectus* sp. nov., a novel thermophilic, chemolithoheterotrophic archaeon isolated from a deep-sea rock collected at Suiyo Seamount, Izu-Bonin Arc, western Pacific Ocean. Int. J. Syst. Evol. Microbiol. **58**:810–6.

182. **Steinsbu BO, Thorseth IH, Nakagawa S, Inagaki F, Lever MA, Engelen B, Øvreås L, Pedersen RB**. 2010. *Archaeoglobus sulfaticallidus* sp. nov., a thermophilic and facultatively lithoautotrophic sulfate-reducer isolated from black rust exposed to hot ridge flank crustal fluids. Int. J. Syst. Evol. Microbiol. **60**:2745–52.

183. **Burggraf S, Jannasch HW, Nicolaus B, Stetter KO**. 1990. *Archaeoglobus profundus* sp. nov., represents a new species within the sulfate-reducing archaeobacteria. Syst. Appl. Microbiol. **13**:24–28.

184. **Mardanov A V, Slododkina GB, Slobodkin AI, Beletsk A V, Gavrilov SN, Kublanov I V, Bonch-Osmolovskaya EA, Skryabin KG, Ravin N V**. 2015. The *Geoglobus acetivorans* genome: Fe(III) reduction, acetate utilization, autotrophic growth, and degradation of aromatic compounds in a hyperthermophilic archaeon. Appl. Environ. Microbiol. **81**:1003–1012.

185. **Wrighton KC, Thrash JC, Melnyk RA, Bigi JP, Byrne-Bailey KG, Remis JP, Schichnes D, Auer M, Chang CJ, Coates JD**. 2011. Evidence for direct electron transfer by a gram-positive bacterium isolated from a microbial fuel cell. Appl. Environ. Microbiol. **77**:7633–9.

186. **Carlson HK, Iavarone AT, Gorur A, Yeo BS, Tran R, Melnyk RA, Mathies RA, Auer M, Coates JD**. 2012. Surface multiheme c-type cytochromes from *Thermincola potens* and implications for respiratory metal reduction by Gram-positive bacteria. Proc. Natl. Acad. Sci. U. S. A. **109**:1702–7.

187. **Lovley DR, Coates JD, Blunt-Harris EL, Phillips EJ, Woodward JC**. 1996. Humic substances as electron acceptors for microbial respiration. Nature **382**:445–448.

188. **Roden EE, Kappler A, Bauer I, Jiang J, Paul A, Stoesser R, Konishi H, Xu H**. 2010. Extracellular electron transfer through microbial reduction of solid-phase humic substances. Nat. Geosci. **3**:417–421.

189. **Pagani I, Liolios K, Jansson J, Chen IMA, Smirnova T, Nosrat B, Markowitz VM, Kyrpides NC**. 2012. The Genomes OnLine Database (GOLD) v.4: Status of genomic and metagenomic projects and their associated metadata. Nucleic Acids Res. **40**:571–579.

190. **Anderson I, Risso C, Holmes D, Lucas S, Copeland A, Lapidus A, Cheng J-F, Bruce D, Goodwin L, Pitluck S, Saunders E, Brettin T, Detter JC, Han C, Tapia R, Larimer F, Land M, Hauser L, Woyke T, Lovley D, Kyrpides N, Ivanova N**. 2011. Complete genome sequence of *Ferroglobus placidus* AEDII12DO. Stand. Genomic Sci. **5**:50–60.

191. **Zerbino DR, Birney E**. 2008. Velvet: algorithms for de novo short read assembly using de Bruijn graphs. Genome Res. **18**:821–9.

192. **Rogers YC, Munk AC, Meincke LJ, Han CS**. 2005. Closing bacterial genomic sequence gaps with adaptor-PCR. Biotechniques **39**:31–2, 34.

193. **Aronesty E**. 2011. ea-utils: Command-line tools for processing biological sequencing data.

194. **Smeds L, Künstner A**. 2011. ConDeTri--a content dependent read trimmer for Illumina data. PLoS One **6**:e26314.

195. **Galens K, Orvis J, Daugherty S, Creasy HH, Angiuoli S, White O, Wortman J, Mahurkar A, Giglio MG**. 2011. The IGS standard operating procedure for automated prokaryotic annotation. Stand. Genomic Sci. **4**:244–51.

196. **Markowitz VM, Chen I-MA, Palaniappan K, Chu K, Szeto E, Pillay M, Ratner A, Huang J, Woyke T, Huntemann M, Anderson I, Billis K, Varghese N, Mavromatis K, Pati A, Ivanova NN, Kyrpides NC**. 2014. IMG 4 version of the integrated microbial genomes comparative analysis system. Nucleic Acids Res. **42**:D560–7.

197. **Delcher AL, Bratke KA, Powers EC, Salzberg SL**. 2007. Identifying bacterial genes and endosymbiont DNA with Glimmer. Bioinformatics **23**:673–9.

198. **Yu NY, Wagner JR, Laird MR, Melli G, Rey S, Lo R, Dao P, Sahinalp SC, Ester M, Foster LJ, Brinkman FSL**. 2010. PSORTb 3.0: Improved protein subcellular localization prediction with refined localization subcategories and predictive capabilities for all prokaryotes. Bioinformatics **26**:1608–15.

199. **Bagos PG, Nikolaou EP, Liakopoulos TD, Tsirigos KD**. 2010. Combined prediction of Tat and Sec signal peptides with hidden Markov models. Bioinformatics **26**:2811–7.

200. **Hofmann K, Stoffel W**. 1993. TMbase-A database of membrane spanning protein segments. Biol. Chem. Hoppe-Seyler 35.

201. **Klenk HP, Clayton RA, Tomb JF, White O, Nelson KE, Ketchum KA, Dodson RJ, Gwinn M, Hickey EK, Peterson JD, Richardson DL, Kerlavage AR, Graham DE, Kyrpides NC, Fleischmann RD, Quackenbush J, Lee NH, Sutton GG, Gill S, Kirkness EF, Dougherty B a, McKenney K, Adams MD, Loftus B, Peterson S, Reich CI, McNeil LK, Badger JH, Glodek A, Zhou L, Overbeek R, Gocayne JD, Weidman JF, McDonald L, Utterback T, Cotton MD, Spriggs T, Artiach P, Kaine BP, Sykes SM, Sadow PW, D'Andrea KP, Bowman C, Fujii C, Garland SA, Mason TM, Olsen GJ, Fraser CM, Smith HO, Woese CR, Venter JC**. 1997. The complete genome sequence of the hyperthermophilic, sulphate-reducing archaeon *Archaeoglobus fulgidus*. Nature **390**:364–70.

202. **Von Jan M, Lapidus A, Del Rio TG, Copeland A, Tice H, Cheng J-F, Lucas S, Chen F, Nolan M, Goodwin L, Han C, Pitluck S, Liolios K, Ivanova N, Mavromatis K, Ovchinnikova G, Chertkov O, Pati A, Chen A, Palaniappan K, Land M, Hauser L, Chang Y-J, Jeffries CD, Saunders E, Brettin T, Detter JC, Chain P, Eichinger K, Huber H, Spring S, Rohde M, Göker M, Wirth R, Woyke T, Bristow J, Eisen J a, Markowitz V, Hugenholtz P, Kyrpides NC, Klenk H-P**. 2010. Complete genome sequence of *Archaeoglobus profundus* type strain (AV18). Stand. Genomic Sci. **2**:327–46.

203. **Stokke R, Hocking WP, Steinsbu BO, Steen IH**. 2013. Complete genome sequence of the thermophilic and facultatively chemolithoautotrophic sulfate reducer *Archaeoglobus sulfaticallidus*. Genome Announc. **1**:4–5.

204. **Grabowski B, Kelman Z**. 2003. Archeal DNA replication: eukaryal proteins in a bacterial context. Annu. Rev. Microbiol. **57**:487–516.

205. **Wu Z, Liu J, Yang H, Xiang H**. 2014. DNA replication origins in archaea. Front. Microbiol. **5**:179.

206. **Gao F, Zhang C-T**. 2007. DoriC: a database of *oriC* regions in bacterial genomes. Bioinformatics **23**:1866–7.

207. **Wu Z, Liu J, Yang H, Liu H, Xiang H**. 2014. Multiple replication origins with diverse control mechanisms in *Haloarcula hispanica*. Nucleic Acids Res. **42**:2282–94.

208. **Wood HG**. 1991. Life with CO or CO_2 and H_2 as a source of carbon and energy. FASEB J. **5**:156–63.

209. **Drake HL, Gössner AS, Daniel SL**. 2008. Old acetogens, new light. Ann. N. Y. Acad. Sci. **1125**:100–28.

210. **Ragsdale SW**. 2008. Enzymology of the Wood-Ljungdahl pathway of acetogenesis. Ann. N. Y. Acad. Sci. **1125**:129–36.

211. **Ljungdahl LG**. 1986. The autotrophic pathway of acetate synthesis in acetogenic bacteria. Annu. Rev. Microbiol. **40**:415–50.

212. **Berg IA, Kockelkorn D, Ramos-Vera WH, Say RF, Zarzycki J, Hügler M, Alber BE, Fuchs G**. 2010. Autotrophic carbon fixation in archaea. Nat. Rev. Microbiol. **8**:447–60.

213. **Vornolt J, Kunow J, Stetter KO, Thauer RK**. 1995. Enzymes and coenzymes of the carbon monoxide dehydrogenase pathway for autotrophic CO_2 fixation in *Archaeoglobus lithotrophicus* and the lack of carbon monoxide dehydrogenase in the heterotrophic *A. profundus*. Arch. Microbiol. **163**:112–118.

214. **Estelmann S, Ramos-Vera WH, Gad'on N, Huber H, Berg IA, Fuchs G**. 2011. Carbon dioxide fixation in *"Archaeoglobus lithotrophicus"*: are there multiple autotrophic pathways? FEMS Microbiol. Lett. **319**:65–72.

215. **Vorholt J, Hafenbradl D, Stetter K, Thauer R**. 1997. Pathways of autotrophic CO_2 fixation and of dissimilatory nitrate reduction to N_2O in *Ferroglobus placidus*. Arch. Microbiol. **167**:19–23.

216. **Möller-Zinkhan D, Börner G, Thauer RK**. 1989. Function of methanofuran, tetrahydromethanopterin, and coenzyme F_{420} in *Archaeoglobus fulgidus*. Arch. Microbiol. **152**:362–368.

217. **Wood H**. 1986. The acetyl-CoA pathway of autotrophic growth. FEMS Microbiol. Lett. **39**:345–362.

218. **Kunow J, Schwörer B, Setzke E, Thauer RK**. 1993. Si-face stereospecificity at C5 of coenzyme F_{420} for F_{420}-dependent N^5,N^{10}-methylenetetrahydromethanopterin dehydrogenase, F_{420}-dependent N^5,N^{10}-methylenetetrahydromethanopterin reductase and $F_{420}H_2$:dimethylnaphthoquinone oxidoreductase. Eur. J. Biochem. **214**:641–646.

219. **Möller-Zinkhan D, Thauer RK**. 1990. Anaerobic lactate oxidation to 3 CO_2 by *Archaeoglobus fulgidus* via the carbon monoxide dehydrogenase pathway: demonstration of the acetyl-CoA carbon-carbon cleavage reaction in cell extracts. Arch. Microbiol. **153**:215–218.

220. **Schmitz RA, Linder D, Stetter KO, Thauer RK**. 1991. N_5,N_{10}-Methylenetetrahydromethanopterin reductase (coenzyme $_{F420}$-dependent) and formylmethanofuran dehydrogenase from the hyperthermophile *Archaeoglobus fulgidus*. Arch. Microbiol. **156**:427–434.

221. **Coppi M V**. 2005. The hydrogenases of *Geobacter sulfurreducens*: a comparative genomic perspective. Microbiology **151**:1239–54.

222. **Deppenmeier U**. 2002. Redox-driven proton translocation in methanogenic archaea. Cell. Mol. Life Sci. **59**:1513–1533.

223. **Graham DE, Xu H, White RH**. 2003. Identification of the 7,8-didemethyl-8-hydroxy-5-deazariboflavin synthase required for coenzyme F_{420} biosynthesis. Arch. Microbiol. **180**:455–64.

224. **Bräsen C, Esser D, Rauch B, Siebers B**. 2014. Carbohydrate metabolism in *Archaea*: Current insights into unusual enzymes and pathways and their regulation. Microbiol. Mol. Biol. Rev. **78**:89–175.

225. **Hansen T, Schönheit P**. 2004. ADP-dependent 6-phosphofructokinase, an extremely thermophilic, non-allosteric enzyme from the hyperthermophilic, sulfate-reducing archaeon *Archaeoglobus fulgidus* strain 7324. Extremophiles **8**:29–35.

226. **Hansen T, Schönheit P**. 2000. Purification and properties of the first-identified, archaeal, ATP- dependent 6-phosphofructokinase, an extremely thermophilic non-allosteric enzyme, from the hyperthermophile *Desulfurococcus amylolyticus*. Arch. Microbiol. **173**:103–109.

227. **Hansen T, Schönheit P**. 2002. Sequence, expression, and characterization of the first archaeal ATP-dependent 6-phosphofructokinase, a non-allosteric enzyme related to the phosphofructokinase-B sugar kinase family, from the hyperthermophilic crenarchaeote *Aeropyrum pernix*. Arch. Microbiol. **177**:62–69.

228. **Say RF, Fuchs G**. 2010. Fructose 1,6-bisphosphate aldolase/phosphatase may be an ancestral gluconeogenic enzyme. Nature **464**:1077–81.

229. **Johnsen U, Schönheit P**. 2007. Characterization of cofactor-dependent and cofactor-independent phosphoglycerate mutases from Archaea. Extremophiles **11**:647–657.

230. **Johnsen U, Hansen T, Schonheit P**. 2003. Comparative analysis of pyruvate kinases from the hyperthermophilic archaea *Archaeoglobus fulgidus, Aeropyrum pernix*, and *Pyrobaculum aerophilum* and the hyperthermophilic bacterium *Thermotoga maritima*: Unusual regulatory properties in. J. Biol. Chem. **278**:25417–25427.

231. **Orita I, Sato T, Yurimoto H, Kato N, Atomi H, Imanaka T, Sakai Y**. 2006. The ribulose monophosphate pathway substitutes for the missing pentose phosphate pathway in the archaeon *Thermococcus kodakaraensis*. J. Bacteriol. **188**:4698–704.

232. **Makarova KS, Koonin E V.** 2003. Filling a gap in the central metabolism of archaea: Prediction of a novel aconitase by comparative-genomic analysis. FEMS Microbiol. Lett. **227**:17–23.

233. **Zwolinski, Harris RF, Hickey WJ**. 2000. Microbial consortia involved in the anaerobic degradation of hydrocarbons. Biodegradation **11**:141–58.

234. **So CM, Phelps CD, Young LY**. 2003. Anaerobic transformation of alkanes to fatty acids by a sulfate-reducing bacterium, Strain Hxd3. Appl. Environ. Microbiol. **69**:3892–3900.

235. **Atlas RM**. 1981. Microbial degradation of petroleum hydrocarbons: An environmental perspective. Microbiol. Rev. **45**:180–209.

236. **Mbadinga SM, Li K-P, Zhou L, Wang L-Y, Yang S-Z, Liu J-F, Gu J-D, Mu B-Z**. 2012. Analysis of alkane-dependent methanogenic community derived from production water of a high-temperature petroleum reservoir. Appl. Microbiol. Biotechnol. **96**:531–42.

237. **Tor JM, Lovley DR**. 2001. Anaerobic degradation of aromatic compounds coupled to Fe(III) reduction by *Ferroglobus placidus*. Environ. Microbiol. **3**:281–7.

238. **Holmes DE, Risso C, Smith JA, Lovley DR**. 2012. Genome-scale analysis of anaerobic benzoate and phenol metabolism in the hyperthermophilic archaeon *Ferroglobus placidus*. ISME J. **6**:146–57.

239. **Holmes DE, Risso C, Smith JA, Lovley DR**. 2011. Anaerobic oxidation of benzene by the hyperthermophilic archaeon *Ferroglobus placidus*. Appl. Environ. Microbiol. **77**:5926–33.

240. **Khelifi N, Grossi V, Hamdi M, Dolla A, Tholozan J-L, Ollivier B, Hirschler-Réa A**. 2010. Anaerobic oxidation of fatty acids and alkenes by the hyperthermophilic sulfate-reducing archaeon *Archaeoglobus fulgidus*. Appl. Environ. Microbiol. **76**:3057–60.

241. **Khelifi N, Amin Ali O, Roche P, Grossi V, Brochier-Armanet C, Valette O, Ollivier B, Dolla A, Hirschler-Réa A**. 2014. Anaerobic oxidation of long-chain n-alkanes by the hyperthermophilic sulfate-reducing archaeon, *Archaeoglobus fulgidus*. ISME J. **8**:3057–60.

242. **Johnson HA, Pelletier DA, Spormann AM**. 2001. Isolation and characterization of anaerobic ethylbenzene dehydrogenase, a novel Mo-Fe-S enzyme. J. Bacteriol. **183**:4536–42.

243. **Rabus R, Kube M, Heider J, Beck A, Heitmann K, Widdel F, Reinhardt R**. 2005. The genome sequence of an anaerobic aromatic-degrading denitrifying bacterium, strain EbN1. Arch. Microbiol. **183**:27–36.

244. **Cabello P, Roldán MD, Moreno-Vivián C**. 2004. Nitrate reduction and the nitrogen cycle in archaea. Microbiology **150**:3527–46.

245. **Mehta MP, Butterfield DA, Baross JA**. 2003. Phylogenetic diversity of nitrogenase (nifH) genes in deep-sea and hydrothermal vent environments of the Juan de Fuca Ridge. Appl. Environ. Microbiol. **69**:960–970.

246. **Charlou JL, Donval JP, Douville E, Jean-Baptiste P, Radford-Knoery J, Fouquet Y, Dapoigny A, Stievenard M**. 2000. Compared geochemical signatures and the evolution of Menez Gwen (37°50′N) and Lucky Strike (37°17′N) hydrothermal fluids, south of the Azores Triple Junction on the Mid-Atlantic Ridge. Chem. Geol. **171**:49–75.

247. **Canfield DE, Kristensen E, Thamdrup B**. 2005. Aquatic geomicrobiology. Adv. Mar. Biol. **48**:1–599.

248. **Bick JA, Leustek T**. 1998. Plant sulfur metabolism — the reduction of sulfate to sulfite. Curr. Opin. Plant Biol. **1**:240–244.

249. **Peck HD**. 1961. Enzymatic basis for assimilatory and dissimilatory sulfate reduction. J. Bacteriol. **82**:933–9.

250. **Postgate J**. 1959. Sulphate reduction by bacteria. Annu. Rev. Microbiol. **13**:505–520.

251. **Fritz G, Einsle O, Rudolf M, Schiffer A, Kroneck PMH**. 2005. Key bacterial multi-centered metal enzymes involved in nitrate and sulfate respiration. J. Mol. Microbiol. Biotechnol. **10**:223–33.

252. **Hansen TA**. 1994. Metabolism of sulfate-reducing prokaryotes. Antonie Van Leeuwenhoek **66**:165–85.

253. **Parey K, Fritz G, Ermler U, Kroneck PMH**. 2013. Conserving energy with sulfate around 100 °C--structure and mechanism of key metal enzymes in hyperthermophilic *Archaeoglobus fulgidus*. Metallomics **5**:302–17.

254. **Jarrell KF, Albers S-V**. 2012. The archaellum: An old motility structure with a new name. Trends Microbiol. **20**:307–12.

255. **Desmond E, Brochier-Armanet C, Gribaldo S**. 2007. Phylogenomics of the archaeal flagellum: Rare horizontal gene transfer in a unique motility structure. BMC Evol. Biol. **7**:106.

256. **Voisin S, Houliston RS, Kelly J, Brisson J-R, Watson D, Bardy SL, Jarrell KF, Logan SM**. 2005. Identification and characterization of the unique N-linked glycan common to the flagellins and S-layer glycoprotein of *Methanococcus voltae*. J. Biol. Chem. **280**:16586–93.

257. **Eichler J**. 2013. Extreme sweetness: Protein glycosylation in archaea. Nat. Rev. Microbiol. **11**:151–6.

258. **Esquivel RN, Xu R, Pohlschroder M**. 2013. Novel archaeal adhesion pilins with a conserved N terminus. J. Bacteriol. **195**:3808–18.

259. **Shi L, Richardson DJ, Wang Z, Kerisit SN, Rosso KM, Zachara JM, Fredrickson JK**. 2009. The roles of outer membrane cytochromes of *Shewanella* and *Geobacter* in extracellular electron transfer. Environ. Microbiol. Rep. **1**:220–227.

260. **Wächtershäuser G**. 1988. Before enzymes and templates: Theory of surface metabolism. Microbiol. Rev. **52**:452–84.

261. **Aono S, Bryant FO, Adams MW**. 1989. A novel and remarkably thermostable ferredoxin from the hyperthermophilic archaebacterium *Pyrococcus furiosus*. J. Bacteriol. **171**:3433–9.

262. **Karl DM**. 1995. Ecology of free-living, hydrothermal vent microbial communities. Microbiol. Deep. hydrothermal Vent. 35–124.

263. **Heimann A, Johnson CM, Beard BL, Valley JW, Roden EE, Spicuzza MJ, Beukes NJ**. 2010. Fe, C, and O isotope compositions of banded iron formation carbonates demonstrate a major role for dissimilatory iron reduction in ~2.5Ga marine environments. Earth Planet. Sci. Lett. **294**:8–18.

264. **Johnson CM, Beard BL, Roden EE**. 2008. The iron isotope fingerprints of redox and biogeochemical cycling in modern and ancient Earth. Annu. Rev. Earth Planet. Sci. **36**:457–493.

265. **Johnson CM, Beard BL, Klein C, Beukes NJ, Roden EE**. 2008. Iron isotopes constrain biologic and abiologic processes in banded iron formation genesis. Geochim. Cosmochim. Acta **72**:151–169.

266. **Tangalos GE, Beard BL, Johnson CM, Alpers CN, Shelobolina ES, Xu H, Konishi H, Roden EE**. 2010. Microbial production of isotopically light iron(II) in a modern chemically precipitated sediment and implications for isotopic variations in ancient rocks. Geobiology **8**:197–208.

267. **Shi L, Squier TC, Zachara JM, Fredrickson JK**. 2007. Respiration of metal (hydr)oxides by *Shewanella* and *Geobacter*: a key role for multihaem *c*-type cytochromes. Mol. Microbiol. **65**:12–20.

268. **Nevin KP, Lovley DR**. 2000. Potential for nonenzymatic reduction of Fe(III) via electron shuttling in subsurface sediments. Environ. Sci. Technol. **34**:2472–2478.

269. **Gorby YA, Yanina S, McLean JS, Rosso KM, Moyles D, Dohnalkova A, Beveridge TJ, Chang IS, Kim BH, Kim KS**. 2006. Microarray and genetic analysis of electron transfer to electrodes in *Geobacter sulfurreducens*. Proc. Natl. Acad. Sci. **103**:11358.

270. **Roling WFM, van Breukelen BM, Braster M, Lin B, van Verseveld HW**. 2001. Relationships between microbial community structure and hydrochemistry in a landfill leachate-polluted aquifer. Appl. Environ. Microbiol. **67**:4619–4629.

271. **Rooney-Varga JN, Anderson RT, Fraga JL, Ringelberg D, Lovley DR**. 1999. Microbial communities associated with anaerobic benzene degradation in a petroleum-contaminated aquifer. Appl. Environ. Microbiol. **65**:3056–63.

272. **Snoeyenbos-West O, Nevin K, Anderson R, Lovley D**. 2000. Enrichment of *Geobacter* species in response to stimulation of Fe(III) reduction in sandy aquifer sediments. Microb. Ecol. **39**:153–167.

273. **Stein LY, La Duc MT, Grundl TJ, Nealson KH**. 2001. Bacterial and archaeal populations associated with freshwater ferromanganous micronodules and sediments. Environ. Microbiol. **3**:10–18.

274. **Lovley DR, Phillips EJ**. 1986. Organic matter mineralization with reduction of ferric iron in anaerobic sediments. Appl. Environ. Microbiol. **51**:683–9.

275. **Stookey LL**. 1970. Ferrozine---a new spectrophotometric reagent for iron. Anal. Chem. **42**:779–781.

276. **Phillips EJ, Lovley DR**. 1987. Determination of Fe (III) and Fe (II) in oxalate extracts of sediment. Soil Sci. Soc. Am. J. 938–941.

277. **Birnbaum S, Pendleton R, Larsson PO, Mosbach K**. 1981. Covalent stabilization of alginate gel for the entrapment of living whole cells. Biotechnol. Lett. **3**:393–400.

278. **Cheetham PSJ, Blunt KW, Bocke C**. 1979. Physical studies on cell immobilization using calcium alginate gels. Biotechnol. Bioeng. **21**:2155–2168.

279. **Hobbie JE, Daley RJ, Jasper S**. 1977. Use of nuclepore filters for counting bacteria by fluorescence microscopy. Appl. Environ. Microbiol. **33**:1225–8.

280. **Zhang L-M, Liu F, Tan W-F, Feng X-H, Zhu Y-G, He J**. 2008. Microbial DNA extraction and analyses of soil iron–manganese nodules. Soil Biol. Biochem. **40**:1364–1369.

281. 1967. National Bureau of Standards.Natl. Bureau Stand. Monogr.

282. **Lovley D, Fraga J, Hayes L, Phillips E, Coates J**. 1998. Humic substances as a mediator for microbially catalyzed metal reduction. Water Resour. **26**:152–157.

283. **Shyu JBH, Lies DP, Newman DK**. 2002. Protective role of tolC in efflux of the electron shuttle anthraquinone-2, 6-disulfonate. J. Bacteriol. **184**:1806.

284. **Kashefi K, Lovley DR**. 2000. Reduction of Fe(III), Mn(IV), and toxic metals at 100 degrees C by *Pyrobaculum islandicum*. Appl. Environ. Microbiol. **66**:1050–6.

285. **Lovley, Derek R., Woodward, Joan C., Chapelle FH**. 1994. Stimulated anoxic biodegradation of aromatic hydrocarbons usanother paper down, blamo ing Fe(III) ligands. Lett. to Nat. **370**.

286. **Lanthier M, Gregory KB, Lovley DR**. 2008. Growth with high planktonic biomass in *Shewanella oneidensis* fuel cells. FEMS Microbiol. Lett. **278**:29–35.

287. **Oda K, Kodama R, Yoshidome T, Yamanaka M, Sambongi Y, Kinoshita M**. 2011. Effects of heme on the thermal stability of mesophilic and thermophilic cytochromes c: comparison between experimental and theoretical results. J. Chem. Phys. **134**:025101.

288. **Schink B**. 1984. Fermentation of 2, 3-butanediol by *Pelobacter carbinolicus* sp. nov. and Pelobacter propionicus sp. nov., and evidence for propionate formation from C2 compounds. Arch. Microbiol. 33–41.

289. **Schink B**. 1982. Fermentation of trihydroxybenzenes by *Pelobacter acidigallici* gen. nov. sp. nov., a new strictly anaerobic, non-sporeforming bacterium. Arch. Microbiol. 195–201.

290. **Schink B**. 1983. Fermentative degradation of polyethylene glycol by a strictly anaerobic, Gram-negative, nonsporeforming bacterium, *Pelobacter venetianus* sp. nov. Appl. Environ. Microbiol. **45**:54505.

291. **Haveman SA, Holmes DE, Ding Y-HR, Ward JE, Didonato RJ, Lovley DR**. 2006. *C*-type cytochromes in *Pelobacter carbinolicus*. Appl. Environ. Microbiol. **72**:6980–5.

292. **Page CC, Moser CC, Chen X, Dutton PL**. 1999. Natural engineering principles of electron tunnelling in biological oxidation-reduction. Nature **402**:47–52.

293. **Kashefi K, Lovley DR**. 2003. Extending the upper temperature limit for life. Science **301**:934.

294. **Kashefi K, Moskowitz BM, Lovley DR**. 2008. Characterization of extracellular minerals produced during dissimilatory Fe(III) and U(VI) reduction at 100 degrees C by *Pyrobaculum islandicum*. Geobiology **6**:147–54.

295. **Macnab RM**. 1992. Genetics and biogenesis of bacterial flagella. Annu. Rev. Genet. **26**:131–58.

296. **Zhao K, Liu M, Burgess RR**. 2007. Adaptation in bacterial flagellar and motility systems: from regulon members to “foraging”-like behavior in *E. coli*. Nucleic Acids Res. **35**:4441–52.

297. **Venkateswaran K, Moser DP, Dollhopf ME, Lies DP, Saffarini DA, MacGregor BJ, Ringelberg DB, White DC, Nishijima M, Sano H, Burghardt J, Stackebrandt E, Nealson KH**. 1999. Polyphasic taxonomy of the genus *Shewanella* and description of *Shewanella oneidensis* sp. nov. Int. J. Syst. Bacteriol. **49**:705–724.

298. **Jiang X, Hu J, Fitzgerald LA, Biffinger JC, Xie P, Ringeisen BR, Lieber CM**. 2010. Probing electron transfer mechanisms in *Shewanella oneidensis* MR-1 using a nanoelectrode platform and single-cell imaging. Proc. Natl. Acad. Sci. U. S. A. 1–5.

299. **Marsili E, Baron DB, Shikhare ID, Coursolle D, Gralnick JA, Bond DR**. 2008. *Shewanella* secretes flavins that mediate extracellular electron transfer. Proc. Natl. Acad. Sci. U. S. A. **105**:3968–73.

300. **Coursolle D, Baron DB, Bond DR, Gralnick JA**. 2010. The Mtr respiratory pathway is essential for reducing flavins and electrodes in *Shewanella oneidensis*. J. Bacteriol. **192**:467–474.

301. **Bond DR, Lovley DR**. 2003. Electricity production by *Geobacter sulfurreducens* attached to electrodes. Appl. Environ. Microbiol. **69**:1548.

302. **Srikanth S, Marsili E, Flickinger MC, Bond DR**. 2008. Electrochemical characterization of *Geobacter sulfurreducens* cells immobilized on graphite paper electrodes. Biotechnol. Bioeng. **99**:1065–1073.

303. **Beliaev AS, Saffarini DA, McLaughlin JL, Hunnicutt D**. 2001. MtrC, an outer membrane decahaem *c* cytochrome required for metal reduction in *Shewanella putrefaciens* MR-1. Mol. Microbiol. **39**:722–730.

304. **Myers JM, Myers CR**. 2001. Role for outer membrane cytochromes OmcA and OmcB of *Shewanella putrefaciens* MR-1 in reduction of manganese dioxide. Appl. Environ. Microbiol. **67**:260–269.

305. **Byrne-Bailey KG, Wrighton KC, Melnyk RA, Agbo P, Hazen TC, Coates JD**. 2010. Complete genome sequence of the electricity-producing "*Thermincola potens*" strain JR. J. Bacteriol. **192**:4078–4079.

306. **Slobodkin AI, Sokolova TG, Lysenko AM, Wiegel J**. 2006. Reclassification of *Thermoterrabacterium ferrireducens* as *Carboxydothermus ferrireducens* comb. nov., and emended description of the genus *Carboxydothermus*. Int. J. Syst. Evol. Microbiol. **56**:2349–51.

307. **Malvankar NS, Lovley DR**. 2012. Microbial nanowires: A new paradigm for biological electron transfer and bioelectronics. ChemSusChem **5**:1039–1046.

308. **Phillips K, de la Peña AH**. 2011. The combined use of the thermofluor assay and thermoQ analytical software for the determination of protein stability and buffer optimization as an aid in protein crystallization. Curr. Protoc. Mol. Biol. 1–15.

309. **Ericsson UB, Hallberg BM, DeTitta GT, Dekker N, Nordlund P**. 2006. Thermofluor-based high-throughput stability optimization of proteins for structural studies. Anal. Biochem. **357**:289–298.

310. **Lavinder JJ, Hari SB, Sullivan BJ, Magliery TJ**. 2009. High-throughput thermal scanning: A general, rapid dye-binding thermal shift screen for protein engineering. J. Am. Chem. Soc. **131**:3794–5.

311. **Savitzky A, Golay MJE**. 1964. Smoothing and differentiation of data by simplified least squares procedures. Anal. Chem. **36**:1627–1639.

312. **Nilsson MR**. 2004. Techniques to study amyloid fibril formation *in vitro*. Methods **34**:151–160.

313. **LeVine H**. 1995. Thioflavine T interaction with amyloid β-sheet structures. Amyloid **2**:1–6.

314. **Zhou S, Yang G, Lu Q, Wu M**. 2014. *Geobacter soli* sp. nov., a dissimilatory Fe(III)-reducing bacterium isolated from forest soil. Int. J. Syst. Evol. Microbiol. **64**:3786–3791.

315. **Shelobolina ES, Nevin KP, Blakeney-Hayward JD, Johnsen C V, Plaia TW, Krader P, Woodard T, Holmes DE, VanPraagh CG, Lovley DR**. 2007. *Geobacter pickeringii* sp. nov., *Geobacter argillaceus* sp. nov. and *Pelosinus fermentans* gen. nov., sp. nov., isolated from subsurface kaolin lenses. Int. J. Syst. Evol. Microbiol. **57**:126–135.

316. **Barnhart MM, Chapman MR**. 2006. Curli biogenesis and function. Annu. Rev. Microbiol. **60**:131.

317. **Blanco LP, Evans ML, Smith DR, Badtke MP, Chapman MR**. 2012. Diversity, biogenesis and function of microbial amyloids. Trends Microbiol. **20**:66–73.

318. **Ng SYM, Chaban B, Jarrell KF**. 2006. Archaeal flagella, bacterial flagella and type IV pili: A comparison of genes and posttranslational modifications. J. Mol. Microbiol. Biotechnol. **11**:167–91.

319. **Malvankar NS, Lovley DR**. 2014. Microbial nanowires for bioenergy applications. Curr. Opin. Biotechnol. **27**:88–95.

320. **France RM, Grossman SH**. 2000. Acrylamide quenching of apo- and holo-alpha-lactalbumin in guanidine hydrochloride. Biochem. Biophys. Res. Commun. **269**:709–712.

321. **Eftink MR, Jameson DM**. 1982. Acrylamide and oxygen fluorescence quenching studies with liver alcohol dehydrogenase using steady-state and phase fluorometry. Biochemistry **21**:4443–4449.

322. **Eftink MR, Selvidge LA**. 1982. Fluorescence quenching of liver alcohol dehydrogenase by acrylamide. Biochemistry **21**:117–125.

323. **Khurana R, Coleman C, Ionescu-Zanetti C, Carter SA, Krishna V, Grover RK, Roy R, Singh S**. 2005. Mechanism of thioflavin T binding to amyloid fibrils. J. Struct. Biol. **151**:229–238.

324. **Vassar PS, Culling CF**. 1959. Fluorescent stains, with special reference to amyloid and connective tissues. Arch. Pathol. **68**:487–498.

325. **Chimileski S, Franklin MJ, Papke R**. 2014. Biofilms formed by the archaeon *Haloferax volcanii* exhibit cellular differentiation and social motility, and facilitate horizontal gene transfer. BMC Biol. **12**:65.

326. **Balba MT, Al-Awadhi N, Al-Daher R**. 1998. Bioremediation of oil-contaminated soil: Microbiological methods for feasibility assessment and field evaluation. J. Microbiol. Methods **32**:155–164.

327. **Brock TD, Freeze H**. 1969. *Thermus aquaticus* gen. n. and sp. n., a nonsporulating extreme thermophile. J. Bacteriol. **98**:289–297.

328. **Kristjansson J**. 1989. Thermophilic organisms as sources of thermostable enzymes. Trends Biotechnol. **7**:349–353.

329. **Chien A, Edgar DB, Trela JM**. 1976. Deoxyribonucleic acid polymerase from the extreme thermophile *Thermus aquaticus*. Org. Geochem. **26**:105–115.

330. **Haki GD, Rakshit SK**. 2003. Developments in industrially important thermostable enzymes: A review. Bioresour. Technol. **89**:17–34.

331. **Egorova K, Antranikian G**. 2005. Industrial relevance of thermophilic *Archaea*. Curr. Opin. Microbiol. **8**:649–55.

332. **Demirjian DC, Morís-Varas F, Cassidy CS**. 2001. Enzymes from extremophiles. Curr. Opin. Chem. Biol. **5**:144–151.

333. **Senko JM, Stolz JF**. 2001. Evidence for iron-dependent nitrate respiration in the dissimilatory iron-reducing bacterium *Geobacter metallireducens* **67**:3750–3752.

334. **Huber H, Stetter KO**. 2001. Family I. *Archaeoglobaceae* fam. nov., 2nd ed. Springer, New York.

335. **Huber H, Stetter KO**. 2001. Order I. *Archaeoglobales* ord. nov., 2nd ed. Springer, New York.

336. **Garrity GM, Holt JG, Whitman WB, Keswani J, Boone DR, Koga Y, Miller TL, Stetter KO, Zellner G, Chong SC, Huber H, Huber G, Ferry JG, Ollivier B, Mah RA, Sowers KR, Zhilina TN, Baker CC, Romesser JA, Grant WD, Patel GB, McGenity TJ, Kamekura M, Ventosa A, Kobayashi T, Oren A, Montalvo-Rodríguez R, Vreeland RH, Tindall BJ, Huber R, Xu Y, Zhou P, Reysenbach A-L, Langworthy TA, Tian X,**

Zillig W, Kobayashi T, Hafenbradl D. 2001. Phylum All. Euryarchaeota phy. nov., p. 211–355. *In* Bergey's Manual® of Systematic Bacteriology.

337. **Garrity GM, Holt JG**. 2001. Class VI. *Archaeoglobi* class. nov., 2nd ed. Springer, New York.